AD NUMBER: AD0150527
CLASSIFICATION CHANGES
TO: Unclassified
FROM: Confidential
LIMITATION CHANGES
TO: Approved for public release; distribution is unlimited.
FROM: Distribution authorized to US Government Agencies and their Contractors; Administrative/Operational Use; 30 Sep 1957. Other requests shall be referred to Wright Air Development Center, Wright-Patterson AFB, OH 45433
AUTHORITY
U per W.A.D.D-W.C.L.S.F.F. ltr dtd 25 Nov 1959; ST-A per AFFDL ltr dtd 2 May 1979

CONFIDENTIAL

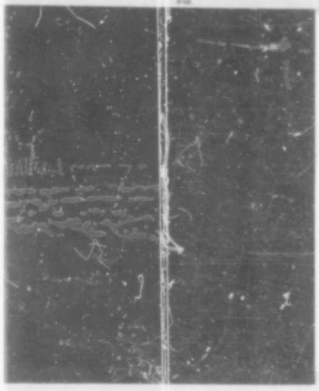

NORTHROP AIRCRAFT, INC., HAWTHORNE, CALIF.

CONFIDENTIAL

NORTHROP AIRCRAFT, INC.
HAWTHORNE — CALIFORNIA

NAI-57-1094

RESEARCH AND REPORTS ON LAMINAR FLOW BOUNDARY LAYER CONTROL SYSTEMS

CONTRACT AF33(616)-3168
Task No. 13618

PROGRESS REPORT FOR PERIOD

1 SEPTEMBER through 30 SEPTEMBER 1957

REPORT TO WRIGHT AIR DEVELOPMENT CENTER

GPO
AD-150 527 (24 Feb 58 jb) CONFIDENTIAL

Northrop Aircraft, Inc., Hawthorne, Calif.
RESEARCH AND REPORTS ON LAMINAR FLOW BOUNDARY LAYER CONTROL SYSTEMS. Progress rept. for 1-30 Sep 57, lv. incl. illus. tables
(Rept. no. NAI-57-1094)
(Contract AF 33(616)3168) Confidential report

Includes AD-150 527 (a), (b), and (c).

FORM 60-136A (R.8-55)

TABLE OF CONTENTS

NORTHROP AIRCRAFT, INC.

PROGRESS REPORT ON CONTRACT AF33(616)-3168

RESEARCH AND REPORTS ON LAMINAR FLOW BOUNDARY LAYER CONTROL SYSTEMS

I. BASIC CONTRACT PURPOSES

To supply the necessary personnel, services, and facilities to investigate laminar boundary layer control on wings and bodies through suction and to develop methods for the design and construction of a laminar boundary layer control airplane.

II. FACILITIES AND EQUIPMENT

There has been no change in the facility and equipment situation during the period covered by this report.

III. ORGANIZATION AND PERSONNEL

A. Organization

There have been no organizational changes during this period.

B. Personnel

The staff now engaged full time on this contract consists of the following:

Engineering

Supervision	2
Clerical and Secretarial	2
Direct Charging	19
	23

Shop

Supervision	1
Direct Charging	11
	12

Flight Test

Direct Charging	1

IV. TECHNICAL PROGRESS

A. Theoretical Investigations

1. Integration of Laminar Boundary Layer Equations

The floating-decimal-point setup of the present integration procedure was completed. Several integrations on a suction body of revolution, being designed for flight testing on the B57 airplane, were undertaken. Work on the general three-dimensional setup on the IBM 704 computer was resumed.

2. Solution of Boundary Layer Stability

a. Iterative Method

These calculations were continued on the profiles $u = e^{-y} - 3/2\, e^{-2y}$ and $u = e^{-y} - 1.6e^{-2y} + 0.6e^{-3y}$. A brief study of the possibility of using multiple-precision on the IBM 704 computer for future calculations was made, showing that a precision of 30 or more significant figures is entirely practicable. With this precision, any profile could be handled easily by this method.

b. Investigation of the Stability Limit Reynolds Number on Swept Laminar Suction Wings for Compressible Flow

The preliminary analytical work has been completed and the coding for the I.B.M. computing machine has started. A highly swept laminar suction wing at supersonic speeds will be chosen as an example. Comparison calculations are planned for incompressible flow with the same suction mass flow as for the compressible case.

c. Three-Dimensional Disturbance Equations for the Rotating Disc

Approximate boundary conditions have been used for the solution of the three-dimensional disturbance equation on the rotating disc. Preliminary I.B.M. calculations indicated a stability limit Reynolds number of the order of 400 (instead of 180 in the previous two-dimensional calculations) which is close to the experimental value.

d. Analysis of the Michigan Swept Laminar Suction Wing Experiments

In order to compare the results of the Michigan experiments on the NAI swept laminar suction wing with theory, an analysis of the stability limit Reynolds number on this wing has been started.

e. Modification of the Michigan Swept Laminar Suction Wing

In order to maintain full laminar flow on swept laminar suction wings at further increased wing chord Reynolds numbers (beyond 10^7) it will be necessary to apply suction practically over the whole wing surface, starting from a position close to the leading edge. The Michigan swept laminar suction wing will be modified accordingly, with the purpose in mind of obtaining full laminar flow at higher Reynolds numbers. Stability calculations have been started for the forward region of the wing.

Most of these stability calculations have been stopped due to the present restriction of funds.

B. Basic Laminar Suction and Transition Experiments

1. Experiments with Suction Through Holes in the 2-inch Tube

Additional experiments have been made to determine the critical suction quantities for two rows of holes with hole centerline spacings of .21 and .63 inch. Previously, the critical suction quantities were measured for a centerline spacing of .32 inch. This range of hole spacings gives nondimensional configuration parameters which correspond to practical full-scale values of the same parameter; in other words, hole spacings of the order of .21 to .63 inch in the tube correspond to full-scale airplane hole spacings of the order of .050 to .075 inch.

Fortunately, the results of the experimental measurements in the 2-inch tube indicate exceptionally high critical suction quantities for certain hole centerline spacing within the .21 to .63 range. Since a high critical suction value is desirable, the experimental work for this range of hole spacings will be continued in an effort to determine why certain hole configurations are superior to others.

Although the full-scale hole spacing corresponding to these experiments is adequate, the corresponding full-scale hole diameters would be quite small. It is desirable therefore, to include experiments for still larger hole diameters. The test rig is currently being modified to permit the installation of larger diameter holes.

2. Pressure Drop Through Suction Holes and Slots

Preparation of the report summarizing the experimental and analytical results of pressure-drop through suction metering holes and slots is continuing.

C. Wind Tunnel Experiments

1. Two-Dimensional Wings at Subsonic Speeds

a. Modification of the Swept Laminar Suction Wing Model

Studies have been initiated to determine the allowables for the thick skin leading edge which has been slotted and drilled with a resulting reduction of cross-section area approaching 50%.

Detail drawings for the extension of suction to the forward portion of the swept laminar suction wing are complete and in the process of being released to the shop for fabrication.

b. 4%-Thick Straight Laminar Suction Model

Polishing of the model to waviness and contour tolerances required for full laminar flow at high Reynolds numbers has continued.

c. Investigation of the Effect of Concave Curvature on a Straight Wing Model with a Concave Surface With and Without Suction

The Report No. BLC-103, "Preliminary Experimental and Analytical Investigations of a Two-Dimensional Wing with Concave Cutout and Auxiliary Airfoil", has been completed and is included with this progress report.

Detail design of the 10-ft chord wing with concave curvature and suction is continuing. Fabrication of the 3-ft chord auxiliary airfoil (to provide the desired pressure distribution along the wing concave surface) has begun.

2. Wings and Bodies at Supersonic Speeds

The suction experiments on the 5%-thick biconvex wing at the Convair OAL tunnel were continued at a Mach number 2.77 . Laminar flow was observed at $R_c = 12.5 \cdot 10^6$ with a 5-tube total head rake at the station 93.75% c over a wide range of suction quantities. The data reduction is in progress.

The final test program at the OAL tunnel will be conducted at the end of October, since tunnel operation will be discontinued in November.

The design of a wedge insert mentioned in the previous report is now complete. The design allows for adjustment fore and aft, and through various angles of attack. This provides a means of controlling the chordwise station at which shock impingement takes place.

Fabrication of the body with the single slot adjustment is 80% complete. The measuring nozzle and metering box for this model is 60% complete.

D. Investigation of Bodies of Revolution and Wing Root Junctures

1. Bodies of Revolution

The final report, BLC-100, on the boundary layer transition measurements for the elliptic, modified Sears Haack, and modified parabolic bodies is submitted with this progress report.

2. Wing Body Combinations with Laminar Flow

a. Wing Leading Edge and Flat Plate Intersection

Analysis of the data for the first experiments exposed two difficulties that needed correction before the experimental work could proceed:

(1) The pressure distributions on the flat plate and on the wing leading edge were not as predicted. The use of filler in a slightly hollow spot on the leading edge corrected the pressure distribution in this region. The difficulty on the flat plate was the result of the necessity to splice the plate (due to its large size) just behind the wing leading edge. Maintaining a precisely flat surface at this splice proved to be difficult without additional stiffening and, as a result, a slightly adverse pressure gradient occurred near the splice. The plate has since been stiffened with "I" beams attached to the rear side, and the undesirable pressure distribution was eliminated.

(2) The second difficulty is a direct result of the fact that the suction requirements are somewhat lower than originally estimated. Due to lower suction requirements, the slot and suction hole losses are less than expected, and the slot designs are therefore somewhat in error. When there is an external pressure gradient along the length of the slot (and this is generally unavoidable for the intersection problem) the slot and hole sizes must be precisely chosen to correspond to the suction requirements. When the slot and hole sizes are incorrect, air is apt to flow out of the slots at the point of minimum external pressure. Such outflow has two undesirable aspects. First, it may cause local transition, and second, it causes an error in the measurement of the suction quantities since any suction air which flows into one end of the slot and out of the other end does not pass through the suction flow measuring nozzle. In order to correct this situation it is necessary to seal all portions of the slots where outflow would otherwise occur. This is being done for the current experiments.

E. F94 Flight Low Drag Suction Experiments

The available flight data on the subject of laminar suction airfoil tolerances have been summarized in Report BLC-101 and are included with this progress report.

As a result of the present restriction of funds, no further suction experiments have been conducted in flight on the F94.

F. Structural Investigations

1. Full-Scale Static Test Panel

Frequently, a misunderstanding of the meaning of certain tolerances leads to excessive cost in tooling, manufacturing, and inspection. Therefore, a tolerance control diagram was made to clarify their meaning.

The design of this panel is completed but because of a shortage of funds, no tooling or fabrication is allowed at this time. However, the following analytical work is being continued.

The derivation of allowables for the honeycomb sandwich spar webs, loaded simultaneously in bending, compression, shear, and crushing, is 60% complete.

2. Stress and Fatigue Studies

Studies of transient thermal stresses are being undertaken to establish design charts for BLC structure with surface temperatures of about 600° F .

Interest in the BLC waviness recorder for measuring initial irregularities in sandwich faces has been evinced by the Structures Research Group. The

difficulty in measuring and interpreting the results by previous techniques has been noted by Forest Products Laboratory at the industry-wide meetings on sandwich construction.

Fatigue studies are being continued.

G. Power Plant Studies

1. Preliminary Design and Model Tests of a Jet Exhaust Duct and Nozzle for a Suction Compressor Drive System Utilizing a Free-Wheeling Turbine Stage

Tests and data reduction of the new duct configuration have been carried to a point where it seems practical to write a preliminary report although more work is needed to obtain quantitative design data for curved ducts and diffusers with boundary layer bleed or suction. However, the results obtained to date show that boundary layer bleed in critical regions of the exhaust nozzle of the engines of a laminar suction airplane can appreciably reduce the losses in curved ducts of a given size or conversely permit the use of more compact ducting for given losses.

2. Design Studies of a High Altitude, Long Range Reconnaissance Airplane Using Liquid Hydrogen as Fuel

Design studies have continued for a laminar suction airplane with an average weight of 40,000 lbs during cruise at $M_o = 0.9$ and $H_o = 90,000$ ft with a cruise range of 10,000 nautical miles.

3. Engine Design Studies of Hypothetical Supersonic Laminar Suction Airplanes

Studies have been conducted on engines suitable for hypothetical supersonic long range laminar suction airplanes.

CONFIDENTIAL

NORTHROP AIRCRAFT, INC.

HAWTHORNE, CALIFORNIA

REPORT NO. NAI-57-1164
REPORT NO. BLC-103

PRELIMINARY EXPERIMENTAL AND ANALYTICAL INVESTIGATIONS OF A TWO-DIMENSIONAL WING WITH CONCAVE CUTOUT AND AUXILIARY AIRFOIL

July 1957

PREPARED BY

Kenneth H Rogers

K. H. Rogers

APPROVED BY

W. Pfenninger

W. Pfenninger

REVISIONS

CHG. NO.	DATE	ENGR.	PAGES AFFECTED	REMARKS

CONFIDENTIAL

FORM 20-S (R.9-54)

GPO
AD-150 527 (a) (24 Feb 58 jb) CONFIDENTIAL

Northrop Aircraft, Inc., Hawthorne, Calif.
PRELIMINARY EXPERIMENTAL AND ANALYTICAL INVESTIGATIONS OF A TWO-DIMENSIONAL WING WITH CONCAVE CUTOUT AND AUXILIARY AIRFOIL, by Kenneth H. Rogers. July 57 [32]p. incl. illus. tables (Rept. no. NAI 57-1164; HLC-103)
(Appendice to Northrop Aircraft, Inc., Contract AF 33(616)3168, Progress rept. for 1-30 Sep 57, AD-150 527)

Confidential re port

I. Author
II. Northrop Aircraft, Inc., Hawthorne, Calif.
III. Contract AF 33(616)3168

TABLE OF CONTENTS

ILLUSTRATIONS

FORM 60-136A (R.8.55)

ILLUSTRATIONS (cont'd.)

K. Rogers
July 1957

SUMMARY

Transition experiments were conducted in the BLC-wind tunnel in the region of a concave curvature on the lower wing surface of a thin cambered airfoil. The surfaces upstream and downstream of the concave region were flat. A uniform chordwise velocity distribution along the lower wing surface was achieved by means of an auxiliary airfoil located opposite to the lower wing concave surface. Transition due to Taylor-Goertler-type vortices generated by the concave surface occurred downstream of the concave region for an amplification factor $\int \beta \, dx \cong 7$. Similar results for strongly accelerated flow on the lower surface of the wing (at high angle of attack) indicate that the transition due to Taylor-Goertler-type vortices is substantially independent of the chordwise velocity and pressure distribution.

I. INTRODUCTION AND PURPOSE OF THE INVESTIGATION

In the design of high speed aircraft, some of the surface areas may include concave curvatures or "cutouts" to provide favorable pressure distribution on the surface (e.g., cutouts on a wing or body at the wing-body juncture, special body shapes for application of the "area rule", and cutouts on the lower surface of a wing near a strut-wing intersection). In many cases the region of concave curvature is followed by a long distance with zero or convex curvature. Considerable work has been done on the Taylor or Goertler-type instability of laminar flow on concave surfaces (References 1 through 8). Very little knowledge, however, is available concerning the further development of the laminar boundary layer downstream of the concave region, or concerning the effect of boundary layer control in regions of concave curvature. As a preliminary step in the investigation of these problems, wind tunnel experiments and theoretical investigations were conducted on a solid two-dimensional wing with a concave region (wing cutout) on the lower surface and an auxiliary airfoil located opposite to the cutout to control the velocity distribution along the wing cutout.

The purpose of the preliminary experiments on the solid wing with a concave region or cutout is (1) to determine the optimum configuration of the cutout and auxiliary wing combination to provide a uniform chordwise pressure distribution on the lower wing surface in the region of the cutout and (2) to investigate transition in the region downstream of the concave surface and the corresponding amplification of Taylor-Goertler-type disturbances.

The Taylor-Goertler-type instability in the region of concave curvature is a function of the radius of curvature, the momentum thickness θ and Reynolds

number R_θ of the boundary layer, and the length of the concave region. All of these effects are included in the stability parameter $\int \beta \, dx$ suggested by A.M.O. Smith (Ref. 6). According to Smith, transition occurs in the region of concave curvature when $\int \beta \, dx$ approaches a value of about 10 .

The experiments were made in Northrop's BLC wind tunnel. The flat plate transition Reynolds number for this tunnel is about three million.

II. NOTATION

a	=	Gap or spacing between the wing and auxiliary airfoil (See Fig. 14)
b	=	Depth of concave cutout in lower surface of wing (See Fig. 14)
c_s	=	chord of auxiliary airfoil or "strut" (see Fig. 14)
C_p	=	Pressure coefficient = $\frac{p}{\frac{\rho}{2} u_o^2}$
ΔC_p	=	Increment of pressure coefficient = $\frac{\Delta p}{\frac{\rho}{2} u_o^2}$
d	=	Half thickness of auxiliary airfoil (see Fig. 14)
i, j, k	=	Successive stations across the channel between the wing and auxiliary airfoil. (See Diagram, Part IV-B-1).
r	=	Radius of curvature
R_x	=	Length Reynolds number = $\frac{\rho u x}{\mu}$
R_θ	=	Momentum thickness Reynolds number = $\frac{\rho u \theta}{\mu}$
T.E.	=	Abbreviation for "trailing edge"
u	=	Local velocity in potential flow
u_o	=	Freestream velocity
U	=	Velocity ratio u/u_o

FORM 60-136A (R.8-55)

NOTATION (cont'd.)

y = Distance measured from the wing lower surface

Δy = Width of a stream tube measured normal to the streamlines (see Diagram, part IV-B-1)

α = Angle of attack of wing

α^* = Spacial frequency of the Taylor-Goertler vortices in the spanwise direction. (Called α rather than α^* in Ref. 6).

β = A measure of stability of Taylor-Goertler vortex, where the strength of the vortex is proportional to $e^{\int \beta \, dx}$ (See Ref. 6).

γ = Goertler parameter = $R_\theta \sqrt{\frac{\theta}{r}}$

θ = Momentum thickness of boundary layer

= $\int_0^1 W(1-W)dy$,

where W is the velocity ratio within the boundary layer

μ = Coefficient of viscosity

ρ = Mass density

τ = Thickness ratio of auxiliary airfoil

= $2d/c_s$ (See Fig. 14)

III. WIND TUNNEL EXPERIMENTS

A. Experimental Setup

The principal dimension of the experimental wing and auxiliary airfoil combination are shown in the accompanying diagram. The wing upper surface, and the auxiliary

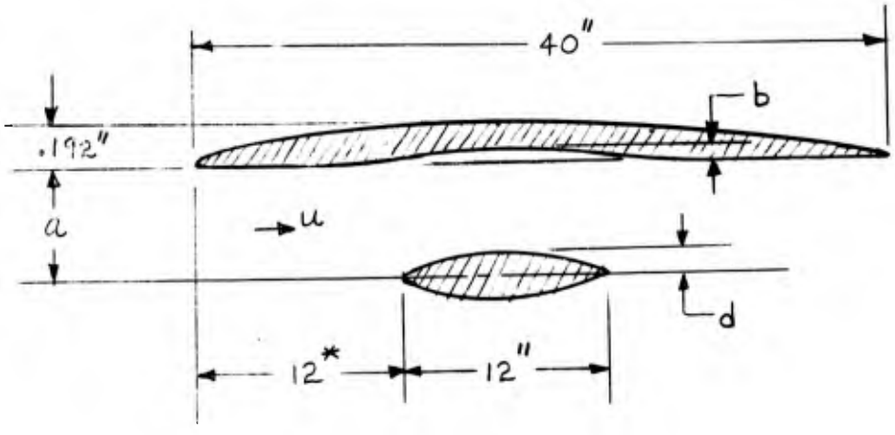

* In Combination No. 4 the stagger was increased to 13.1 and 13.5 inches.

GEOMETRY OF WING AND AUXILIARY AIRFOIL

airfoil profile are modified circular arc sections. The wing lower surface is flat except for the cutout. The auxiliary airfoil is a symmetrical section. The airfoil profiles are plotted in Figure 1. The determination of the concave curvature param-

eter $\int \beta\, dx$ is shown in part IV-A. The cutout depth b, the auxiliary airfoil half thickness d, and the maximum value of $\int \beta\, dx$ for the combinations tested are shown in Table I.

TABLE I. TEST COMBINATIONS

Combination No.	b ~IN.	d ~IN.	b/d	$\left(\int \beta\, dx\right)_{max}$
1	0	0	-	0
2	.40	.60	.67	-
3	.40	.84	.48	-
4	.60	.84	.71	5.7 at q = 6"
5	.77	1.08	.71	7.8 at q = 6"

The wing and auxiliary airfoil were 20 inches long and were mounted between parallel end plates. Photographs of the installation in Northrop's BLC wind tunnel are shown in Figures 15 and 16.

Static pressure orifices of about .022-in. diameter were located at mid span along both sides of the wing and auxiliary airfoil. The frequency of turbulent bursts on the wing lower surface was determined by means of a total-pressure probe connected to a stethoscope.

The angle of attack of the combination could be adjusted over the range of 0^{o} to 3^{o} by shifting the parallel end plates, and the spacing "a" by relocating

either the wing or the auxiliary airfoil.

The test procedure for each configuration or combination was to investigate several different values of the spacing "a" at two or more values of the angle of attack α . For each combination of a and α the static pressure and velocity distributions were determined; and after the tunnel turbulence had stabilized, the state of the boundary layer on the wing and the auxiliary airfoil was observed and recorded.

B. Experimental Results

The chordwise potential flow velocity distributions for various cases are shown in Figures 2 through 12. The results show that the velocity distribution along the cutout can be altered greatly by changing the gap or spacing "a". The velocity distribution along the cutout can be made almost the same as that on a flat plate by proper selection of dimension a . The amount of cutout required for a flat velocity distribution, as a function of the spacing or gap between the airfoils, is shown on the design chart, Fig. 14.

The first experiment showed a pressure peak on the lower side of the wing near the leading edge at zero degrees angle of attack α , but no pressure peak at $\alpha = 1^\circ$; therefore, subsequent tests were made at $\alpha \geq 1^\circ$.

Turbulence diagrams, showing the increase in turbulence as the velocity and chord station increase, are plotted in Figures 2, 9, 10, 11 and 12. The results show that transition due to Taylor-Goertler-type instability first occurred near the trailing edge when the vorticity growth exponent $\int \beta \, dx$ approached a value of about 7 . (See Fig. 11). The critical value of $\int \beta \, dx$ was about the same for strongly accelerated flow as for a uniform velocity distribution. (See Fig. 12).

FORM 60-136A (R.8-55)

IV. THEORETICAL INVESTIGATIONS

A. Determination of $\int \beta \, dx$

1. Diagram

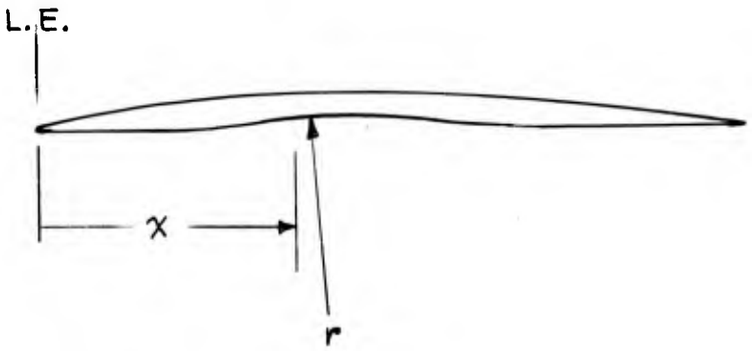

2. Introduction and Assumptions

A. M. O. Smith, in Ref. 6, shows that the Goertler parameter $R_\theta \sqrt{\frac{\theta}{r}}$ alone is inadequate as an indicator of the transition point. Instead, experimental data* indicate that the growth factor $e^{\int \beta \, dx}$ is a much better measure, and that transition will occur in the region of concave curvature when $\int \beta dx$ reaches a value of about 10. Fig. 7 of Ref. 6 shows a stability chart wherein lines of constant $(\beta\theta R_\theta)$ are plotted as a function of ordinates $R_\theta \sqrt{\frac{\theta}{r}}$ and abscissa $\alpha^*\theta$. On this log log chart, straight lines with a slope of 3/2 are lines of constant vortex frequency α^*. Also, for a given value of $R_\theta \sqrt{\frac{\theta}{r}}$ the maximum value of β will occur at the minimum point of the $\beta\theta R_\theta$ curve. Therefore, a line with slope of 3/2, passing near the minimum points of the $\beta\theta R_\theta$ curves, is a logical choice for determining the maximum value of $\int \beta \, dx$ along a concave surface. On the basis of the foregoing, the stability chart has been replotted as the parameter $\beta\theta R_\theta$ vs the Goertler

---

* shown in Ref. 6

parameter $R_\theta \sqrt{\frac{\theta}{r}}$, and is shown in Figure 11.

In the analysis presented, the equations for laminar flow on a flat plate are assumed applicable for the calculation of the momentum thickness θ and the Reynolds number. For the experiment with strongly accelerated flow (Fig. 12) the momentum thickness was calculated by Falkner Skan's method. In the case of the strongly accelerated flow, the momentum thickness was reduced to about 36 per cent of the flat plate value, and the $\int \beta \, dx$ increased to about 106 per cent of the flat plate value. Roughly, a 10% reduction in the momentum thickness θ resulted in a 1% increase in the instability exponent $\int \beta \, dx$.

3. Equations for Laminar Flat Plate

$$\theta = \frac{.664 x}{\sqrt{R_x}} \qquad \text{(Ref. 9, p. 110)} \qquad \text{(A1)}$$

$$R_\theta = .664 \sqrt{R_x} \qquad \text{Derived from (A1)} \qquad \text{(A2)}$$

$$\theta R_\theta = (.664)^2 x = .441x \qquad \text{(A3)}$$

$$R_\theta \sqrt{\theta} = (.664)^{1.5} R_x^{.25} x^{.5} = .541 (x \sqrt{R_x})^{.5} \qquad \text{(A4)}$$

Call Goertler parameter $R_\theta \sqrt{\frac{\theta}{r}} = \gamma$: (A5)

Then $\gamma = .541 \left(\frac{x}{r}\right)^{.5} R_x^{.25}$ (A6)

4. Example

Assume Condition 4: b = .60 inch, q = 6" , and u = 161.7 ft/sec.

FORM 60-136A (R.8.55)

FIG. 1

(1) x ~IN	(2) $1/r$ ~1/IN	(3) x/r = (1)(2)	(4) (3)$^{.5}$	(5) $\gamma/R_x^{.25}$ .541(4)	(6) x ~FT	(7) θR_θ .441(6)	(8) Δx ft
12.7	0	0	0	0	1.06	.468	
							.14
14.4	.0094	.135	.368	.199	1.20	.530	
							.10
15.6	.0150	.234	.484	.262	1.30	.574	
16.8	.0182	.306	.554	.300	1.40	.618	
18.0	.0191	.344	.586	.318	1.50	.662	
19.2	.0182	.349	.590	.320	1.60	.706	
20.4	.0150	.306	.554	.300	1.70	.750	
							.10
21.6	.0094	.203	.451	.245	1.80	.795	
							.14
23.3	0	0	0	0	1.94	.855	

FORM 60-136A (R.8.55)

(9) R_x $= 10^6$ (6)	(10) (9)$^{.25}$	(11) γ $=$ (5)(10)	(12) $\beta\theta R_\theta$ FIG 13	(13) β $=$ (12)/(7)	(14) $\bar{\beta}$	(15) $\bar{\beta}\Delta x$ $=$ (8)(14)	(16) $\Sigma\bar{\beta}\Delta x$ $=\int\beta dx$
106 (10^4)	-	0	0	0			0
					3.2	.45	
120	33.1	6.59	3.10	5.84			.45
					6.9	.69	
130	33.8	8.86	4.47	7.80			1.14
					8.3	.83	
140	34.4	10.31	5.36	8.68			1.97
					8.9	.89	
150	35.0	11.12	5.95	9.00			2.86
					8.8	.88	
160	35.6	11.39	6.06	8.58			3.74
					8.2	.82	
170	36.2	10.86	5.67	7.57			4.56
					6.7	.67	
180	36.7	8.99	4.52	5.69			5.23
					3.2	.45	
194	-	0	0	0			5.68

333 (10^4) at x = 3.33 ft.

Stability Diagram (Column 16 vs Column 9)

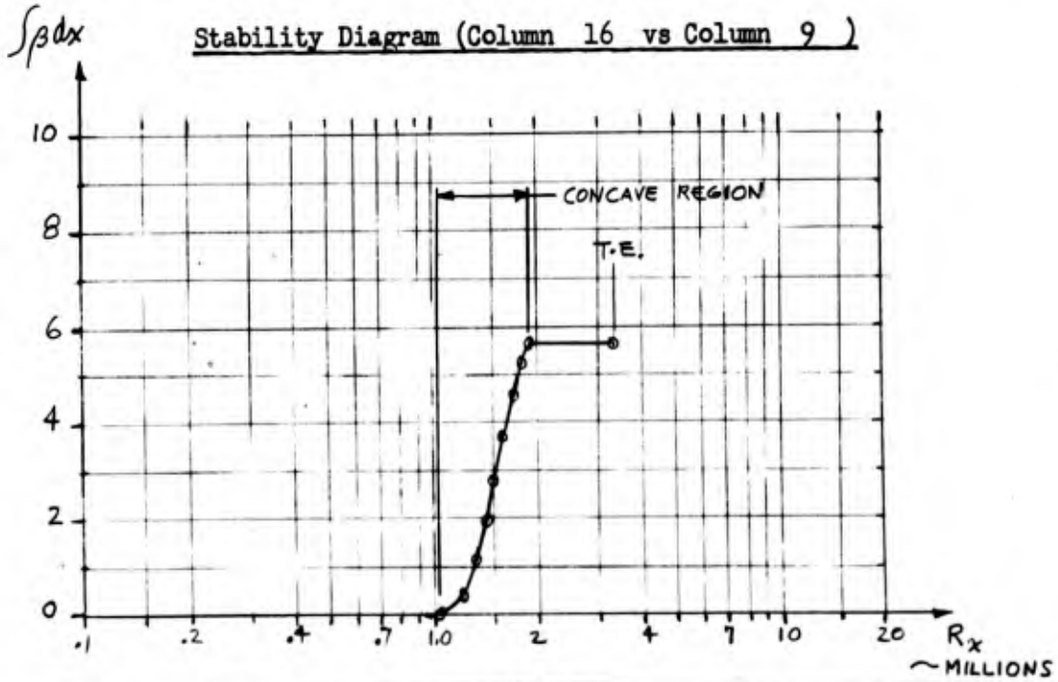

FORM 60-136A (R.8-55)

B. Method for Calculating Velocity Distribution

1. Diagram

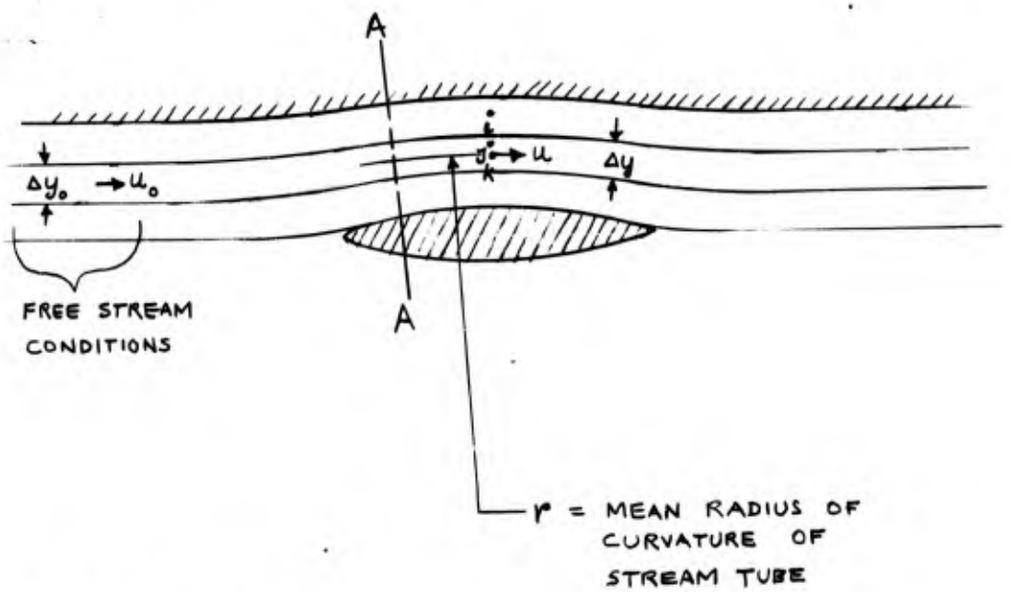

2. Assumptions

Assume incompressible flow.

3. Equations

Pressure gradient in y-direction normal to main flow:

$$dP/dy = \rho u^2/r$$

Divide by reference dynamic pressure $\frac{\rho}{2} u_o^2$,

Call $\Delta C_p = \Delta P / \frac{\rho}{2} u_o^2$, Call $U = u/u_o$

Rewriting,

$$\Delta C_{p_{i-k}} = 2 \left(\Delta y/r\right) U_j^2 \qquad (B1)$$

Bernoulli's Equation:

$$p_o - p_j = \frac{\rho}{2}(u_j^2 - u_o^2)$$

or $$\Delta C_{p_{o-i}} = U_i^2 - 1$$

and $$\Delta C_{p_{o-k}} = U_k^2 - 1$$

From which

$$\Delta C_{p_{i-k}} = U_k^2 - U_i^2 \qquad (B2)$$

Continuity Equation:

$$\Delta y_o = U_j \, \Delta y \qquad (B3)$$

Combining (B1) and (B2)

$$U_k^2 - U_i^2 = 2(\Delta y/r)U_j^2 \qquad (B4)$$

4. Iterative Procedure

(1) construct approximate streamlines

(2) select streamwise station for analysis (e.g., station A-A)

(3) measure mean radius r for each stream tube

(4) complete the following table:

FORM 60-136A (R.8-55)

STATION A-A $\quad \Delta y_o = \_\_\_ .$

① STREAMTUBE No.	② Δy	③ r	④ $\frac{2\Delta y}{r}$ $= 2\text{②}/\text{③}$	⑤ U_j $= \frac{\Delta y_o}{\Delta y}$	⑥ U_j^2 $= \text{⑤}^2$	⑦ ΔU_j^2 $= \Delta\text{⑥}$	⑧ $U_k^2 - U_i^2$ $= \text{④⑥}$	⑨ ΔU_j^2 $= \text{⑧}$ INTERPOLATED
1								
2								
⋮								
n								

(5) In the above table, column 9 will be more accurate than column 7 . Adjust U_j to agree with column 9 and repeat above steps.

REFERENCES

1 Rayleigh, Lord: On the Dynamics of Revolving Fluids, Royal Society Proceedings A, 1916, pp. 148-154.

2 Taylor, G. I.: Stability of a Viscous Liquid Contained Between Two Rotating Cylinders, Phil. Trans. Roy. Soc., London, Series A, v. 223, 1923, pp. 289-343.

3 Goertler, H.: Über eine dreidimensionale Instabilität laminarer Grenzschichten an konkaven Wänden, Nachrichten Gesellschaft der Wissenschaften zu Göttingen, Neue Folge 2, No. 1.

4 Liepmann, Hans W.: Investigation of Boundary Layer Stability and Transition on Curved Boundaries, NACA Wartime Report ACR No. 3H30, August 1943.

5 Liepmann, Hans W.: Investigation of Boundary Layer Transition on Concave Walls, NACA Wartime Report ACR No. 4J28, Febr. 1945.

6 Smith, A.M.O.: On the Growth of Taylor-Goertler Vortices Along Highly Concave Walls, Douglas Report No. E.S. 17110, March, 1953.

7 Meksyn, D.: Stability of Viscous Flow over Concave Cylindrical Surfaces, Proc. Roy. Soc., London, Series A, Sept. 22, 1950, pp. 253-265.

8 Richards, E. J., Walker, W. S., and Greening, J. R.: Tests of a Griffith Aerofoil in the 13 ft x 9 ft Wind Tunnel, British Reports and Memoranda No. 2148, March 1944.

9 Schlichting, Hermann: Boundary Layer Theory, McGraw-Hill, N.Y., 1955

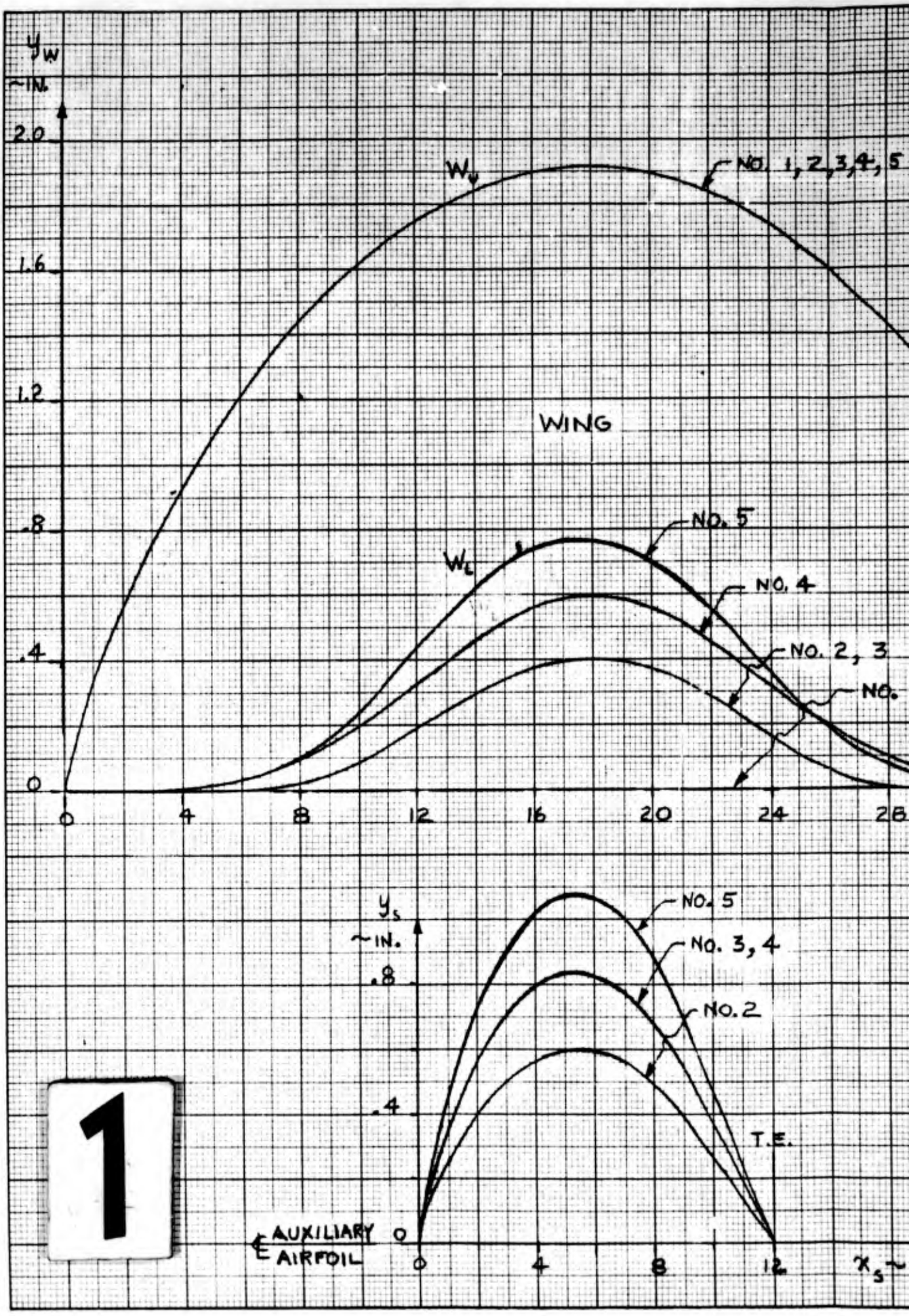
y_w ~IN.
2.0
1.6
1.2
.8
.4
0
W_w
NO. 1, 2, 3, 4, 5
WING
W_L
NO. 5
NO. 4
NO. 2, 3
NO.
0
4
8
12
16
20
24
28
y_s ~IN.
.8
.4
NO. 5
NO. 3, 4
NO. 2
T.E.
AUXILIARY AIRFOIL
0
4
8
12
x_s ~
1

ENGINEER K. Rogers	NORTHROP AIRCRAFT INC.	PAGE 17
CHECKER		REPORT NO. BLC-103
DATE July 1957		MODEL

FIG 1. AIRFOIL COORDINATES

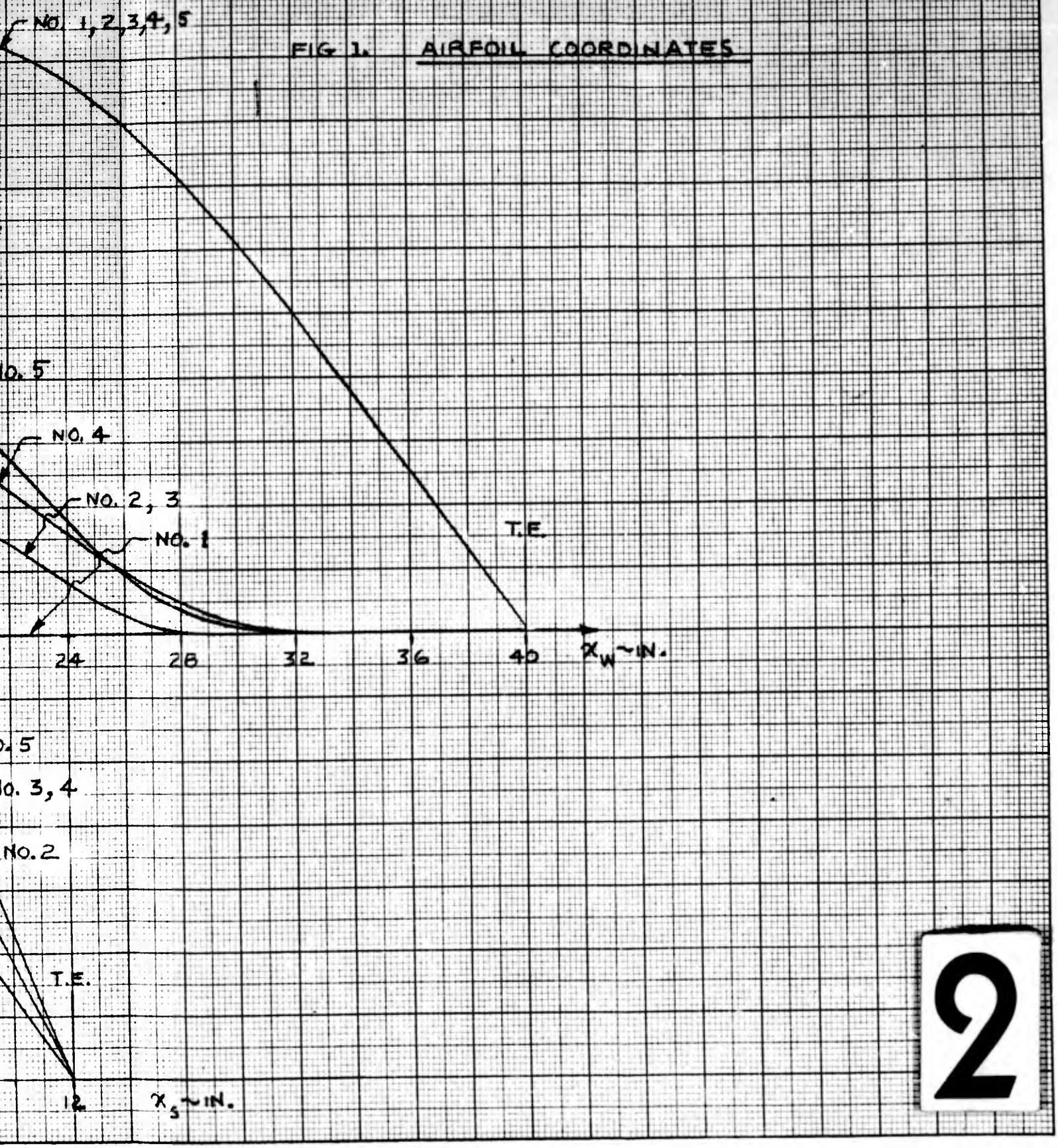

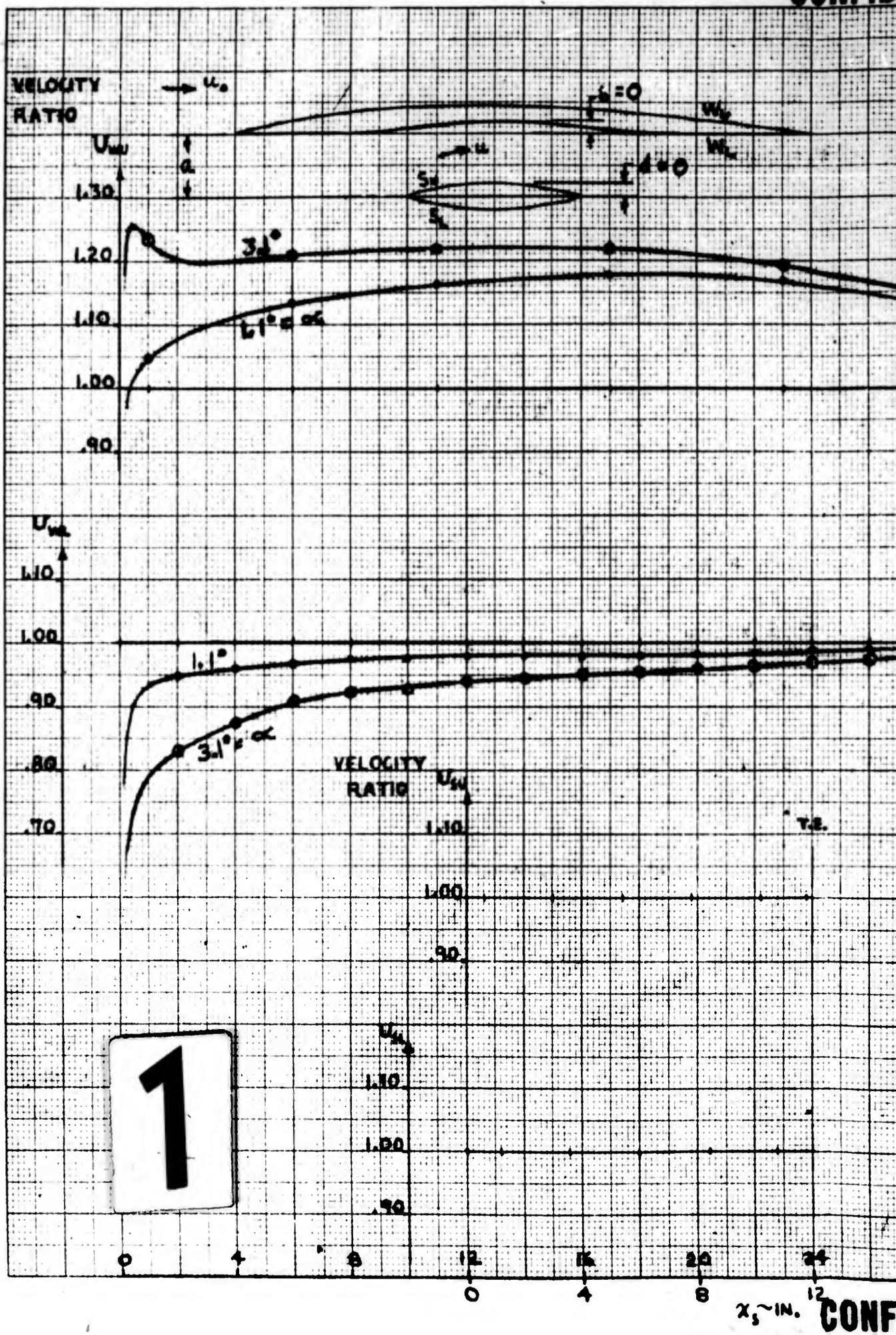

1

CONFIDENTIAL

FORM 20-118 (R. 6-51)

ENGINEER: K. Rogers	Figure 2	PAGE: 18
CHECKER:	NORTHROP AIRCRAFT INC.	REPORT NO.: BLO-103
DATE: July 1957	TEST- RESULTS — TWO DIMENSIONAL WING WITH CUTOUT AND AUXILIARY AIRFOIL IN BLR WIND TUNNEL	MODEL:

COMBINATION NO. 1

NO CUTOUT

NO AUXILIARY AIRFOIL

W_W

W_L

T.E.

T.E.

TURBULENCE ON W_L

- 1 BURST / SEC.
- 5 BURSTS / SEC.
- 10 BURSTS / SEC.

R_{CW} ~MILLIONS

q_o ~IN. H_2O

3.1°

α = 1.1°

X_W ~IN.

20 24 28 32 36 40

8 12

X_S ~IN.

$\left(\frac{x}{c}\right)_W$

.4 .6 .8 1.0

2

CONFIDENTIAL

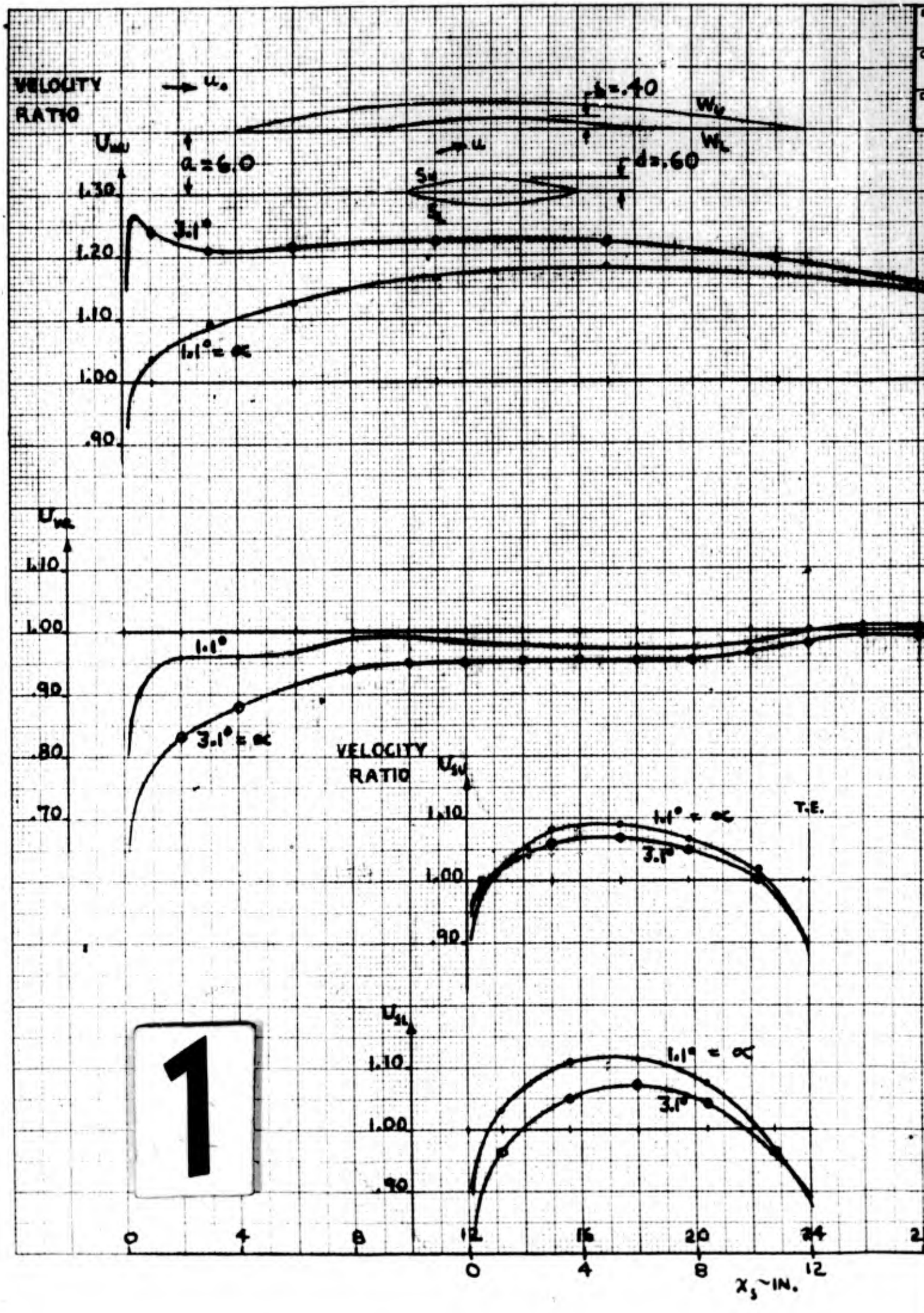
VELOCITY RATIO
u_o
U_{ss}
a = 6.0
h = .40
W_u
W_L
u
S_u
S_L
d = .60
3.1°
1.1° = α
1.30
1.20
1.10
1.00
.90
U_{ss}
1.10
1.00
.90
.80
.70
1.1°
3.1° = α
VELOCITY RATIO
U_{su}
1.10
1.00
.90
1.1° = α
3.1°
T.E.
U_{sL}
1.10
1.00
.90
1.1° = α
3.1°
0
4
8
12
16
20
24
0
4
8
12
X_s - IN.

1

FORM 20-118 (R. 6-51)

ENGINEER: K. Rogers	Figure 3	PAGE: 19
CHECKER:	NORTHROP AIRCRAFT INC.	REPORT NO.: BLC-103
DATE: July 1957	TEST RESULTS — TWO DIMENSIONAL WING WITH CUTOUT AND AUXILIARY AIRFOIL IN BLR WIND TUNNEL	MODEL:

COMBINATION NO. 2

$a = 6.0$

$\alpha = 1.1°, 3.1°$

T.E.

TURBULENCE ON W_L

- 1 BURST / SEC.
- 5 BURSTS / SEC.
- 10 BURSTS / SEC.

R_{CW} ~MILLIONS

~IN. H_2O

X_W ~IN.

$\left(\frac{x}{c}\right)_W$

X_S ~IN.

2

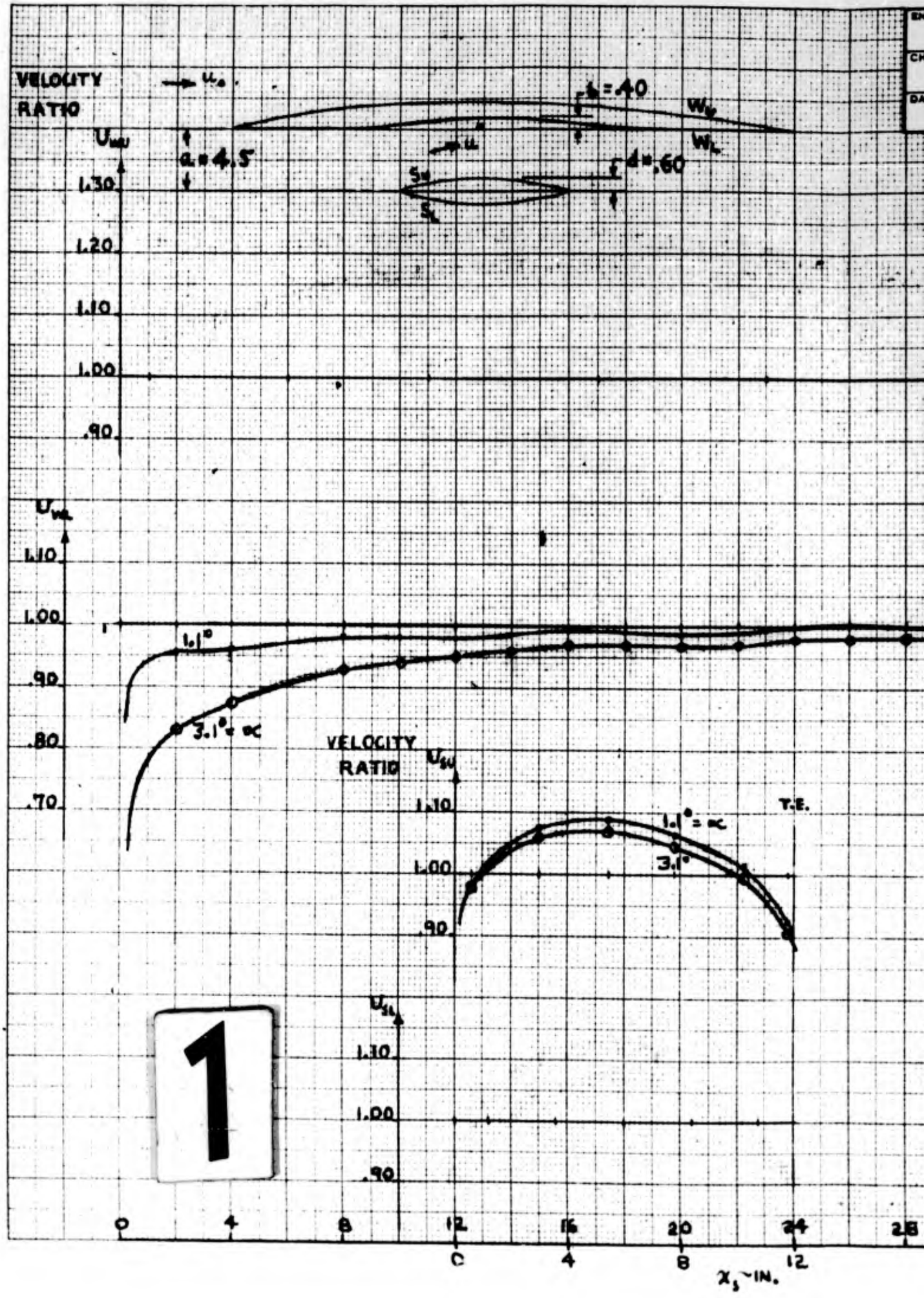
VELOCITY RATIO
U_{WU}
1.30
1.20
1.10
1.00
.90
U_{WL}
1.10
1.00
.90
.80
.70
U_{SU}
1.10
1.00
.90
U_{SL}
1.10
1.00
.90
0
4
8
12
16
20
24
28
C
4
8
12
X_s ~IN.
$\alpha = 4.5$
$\frac{t}{c} = .40$
$\frac{t}{c} = .60$
W_U
W_L
S_U
S_L
U_∞
1.1°
3.1°
1.1° = α_C
3.1°
T.E.
VELOCITY RATIO
1

FORM 20-11B (R. 6-51)

ENGINEER: K. Rogers	Figure 4	PAGE: 20
CHECKER:	NORTHROP AIRCRAFT INC.	REPORT NO.: NAI-103
DATE: July 1957	TEST RESULTS — TWO DIMENSIONAL WING WITH CUTOUT AND AUXILIARY AIRFOIL IN BLR WIND TUNNEL	MODEL:

COMBINATION NO. 2.

$\alpha = 4.5$

T.E.

TURBULENCE ON W_u

- 1 BURST / SEC.
- 5 BURSTS / SEC.
- 10 BURSTS / SEC.

R_{CW} ~MILLIONS

q_o ~IN. H_2O

$\alpha = \alpha_c$

T.E.

X_W ~IN.

X_s ~IN.

$\left(\frac{x}{c}\right)_W$

2

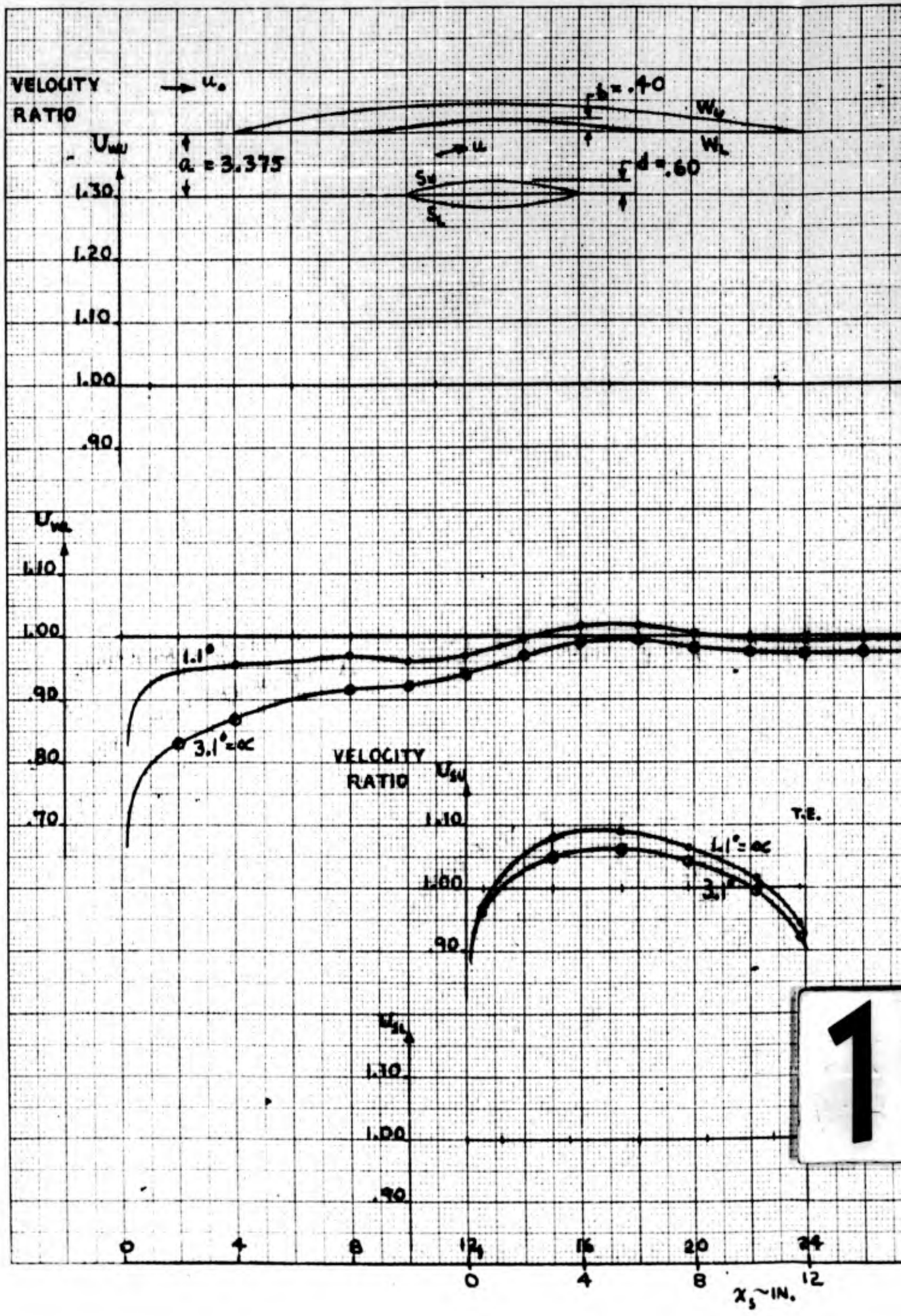
VELOCITY RATIO
u_∞
$h = .40$
W_u
W_L
$a = 3.375$
u
S_u
S_L
$d = .60$
U_{wu}
1.30
1.20
1.10
1.00
.90
U_{wL}
1.10
1.00
.90
.80
.70
1.1°
3.1° = α
VELOCITY RATIO
U_{su}
1.10
1.00
.90
T.E.
1.1° = α
3.1°
U_{sL}
1.30
1.00
.90
0
4
8
12
16
20
24
0
4
8
12
x_s ~ IN.

1

FORM 20-118 (R. 6-51)

ENGINEER	Figure 5	PAGE
K. Rogers	NORTHROP AIRCRAFT INC.	21
CHECKER		REPORT NO. BLC-103
DATE July 1957	TEST RESULTS — TWO DIMENSIONAL WING WITH CUTOUT AND AUXILIARY AIRFOIL IN BLR WIND TUNNEL	MODEL

COMBINATION NO. 2

$a = 3.375$

T.E.

TURBULENCE ON W_L

- 1 BURST / SEC.
- 5 BURSTS/SEC.
- 10 BURSTS/SEC.

R_{CW} ~MILLIONS

~IN. H_2O

T.E.

$L.I° = \alpha_c$

3.1°

X_W ~IN.

X_3 ~IN.

$\left(\frac{x}{c}\right)_W$

2

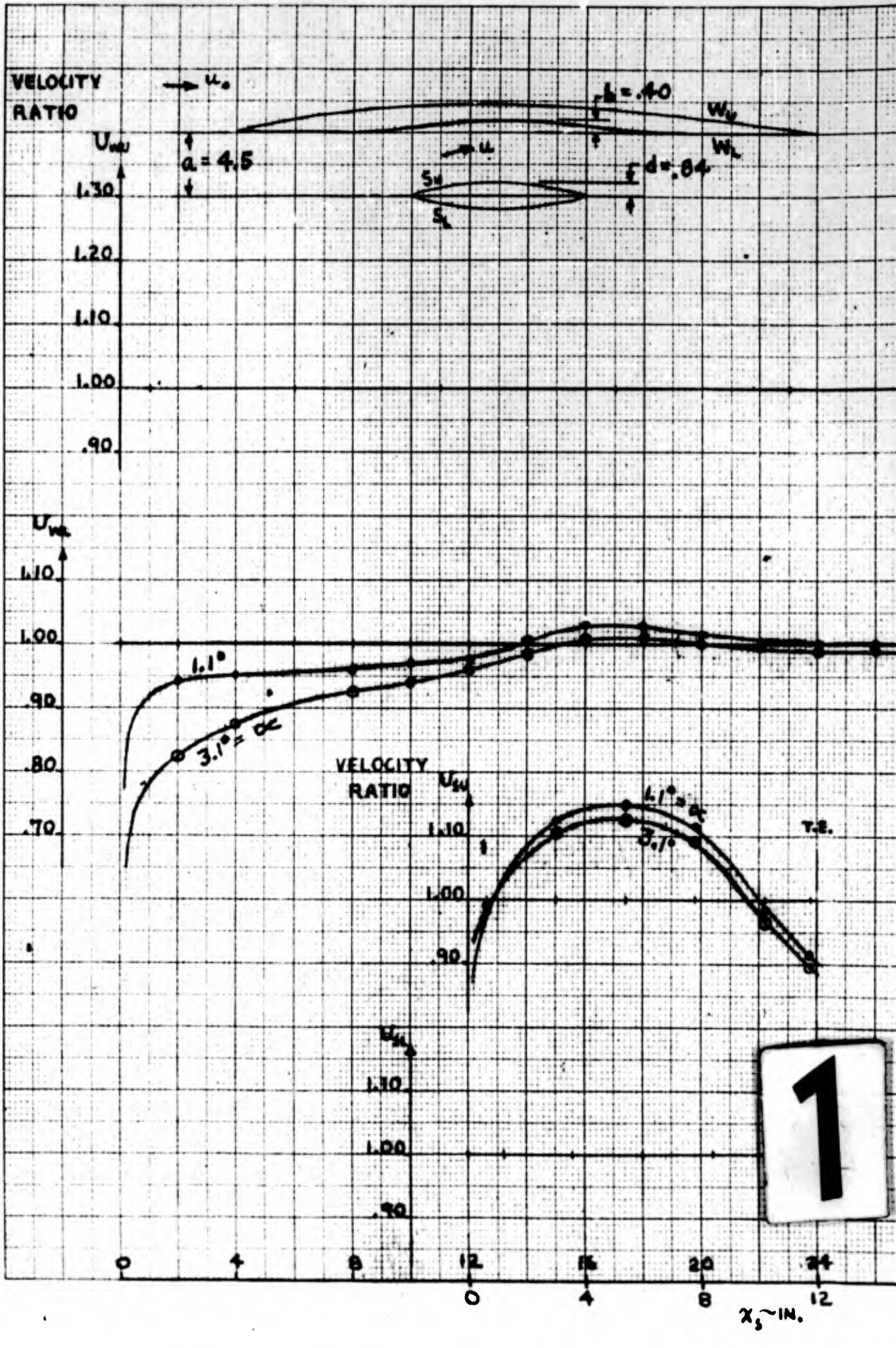
VELOCITY RATIO
U_{wu}
u_o
a = 4.5
h = .40
W_u
W_L
d = .84
S_u
S_L
u
1.30
1.20
1.10
1.00
.90
U_{wL}
1.10
1.00
.90
.80
.70
1.1°
3.1° = α
VELOCITY RATIO
U_{su}
1.1° = α
3.1°
T.E.
U_{sL}
1.10
1.00
.90
1.30
1.00
.90
0
4
8
12
16
20
24
0
4
8
12
x_s ~ IN.
1

FORM 20-118 (R. 6-51)

ENGINEER: K. Rogers	Figure 6	PAGE: 22
CHECKER:	NORTHROP AIRCRAFT INC.	REPORT NO.: BLO-103
DATE: July 1957	TEST RESULTS — TWO DIMENSIONAL WING WITH CUTOUT AND AUXILIARY AIRFOIL IN BLR WIND TUNNEL	MODEL:

COMBINATION NO. 3

$\alpha = 4.5$

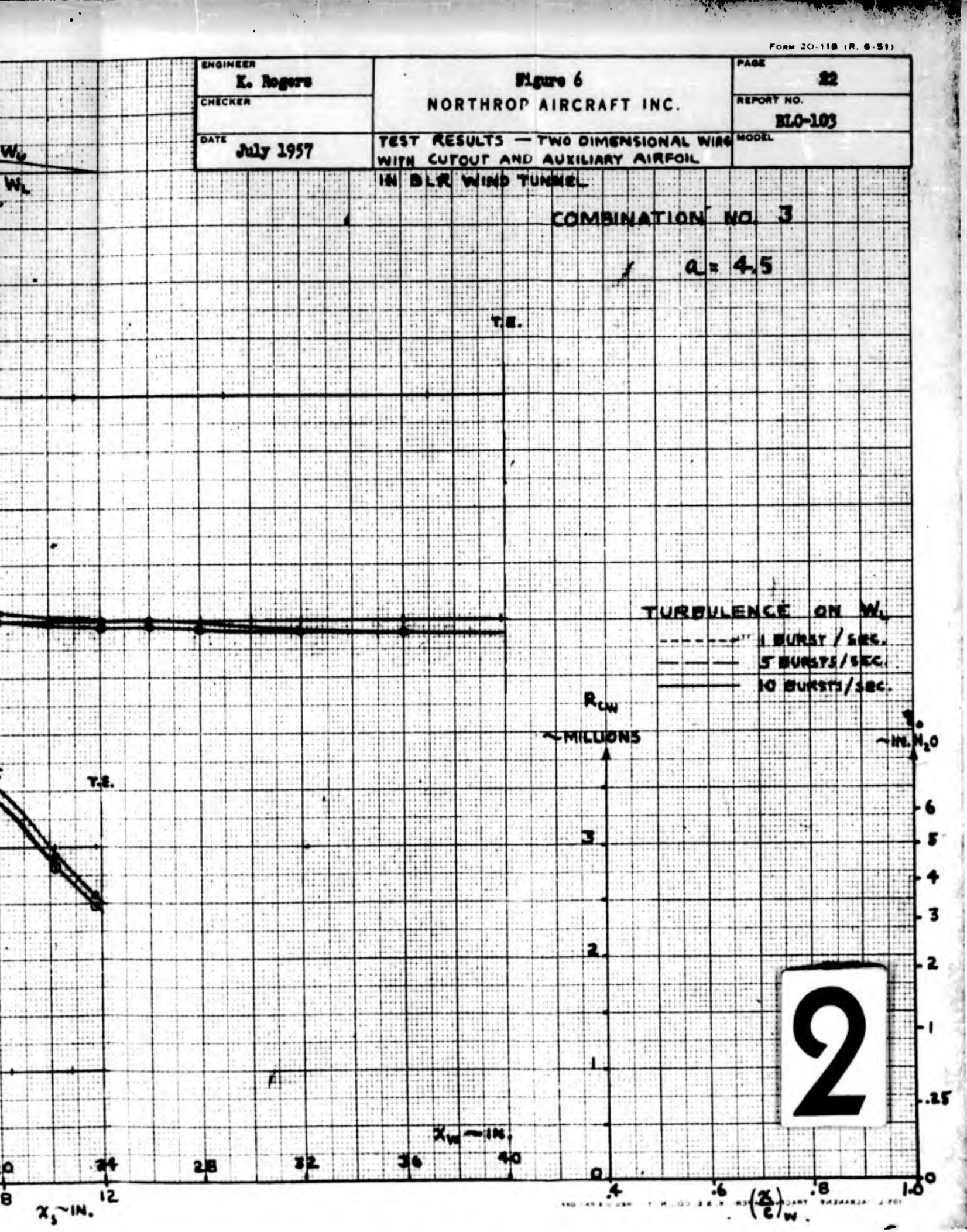

2

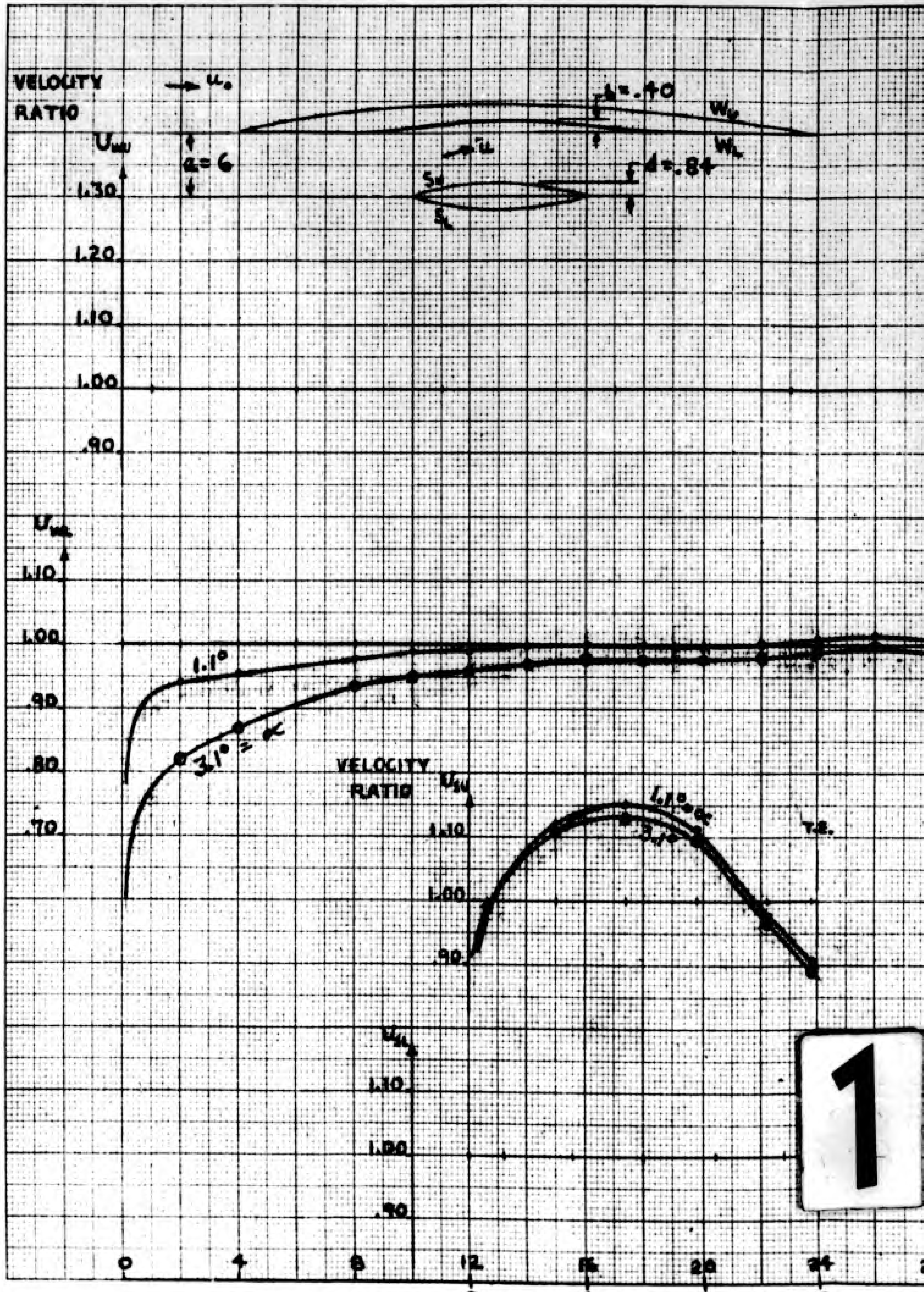

VELOCITY RATIO
u_o
$t = .40$
W_U
W_L
U_{WU}
$a = 6$
S_U
S_L
$t = .84$
1.30
1.20
1.10
1.00
.90
U_{WL}
1.10
1.00
.90
.80
.70
1.1°
3.1° = α
VELOCITY RATIO
U_{SU}
1.10
1.00
.90
T.E.
U_{SL}
1.10
1.00
.90
0
4
8
12
16
20
24
0
4
8
12
X_S ~ IN.

1

FORM 20-11B (R. 6-51)

ENGINEER: K. Rogers	Figure 7 NORTHROP AIRCRAFT INC.	PAGE: 23
CHECKER:		REPORT NO.: BLO-103
DATE: July 1957	TEST RESULTS — TWO DIMENSIONAL WING WITH CUTOUT AND AUXILIARY AIRFOIL IN BLR WIND TUNNEL	MODEL:

COMBINATION NO. 3

$\alpha = 6$

T.E.

TURBULENCE ON W_L

- 1 BURST / SEC.
- 5 BURSTS / SEC.
- 10 BURSTS / SEC.

R_{CW} ~MILLIONS

~IN. H_2O

6
5
4
3
2
1
.25

3
2
1

T.E.

X_W ~IN.

24 28 32 36 40

0 .4 .6 .8 1.0

$\left(\frac{x}{c}\right)_W$

8 12

X_S ~IN.

2

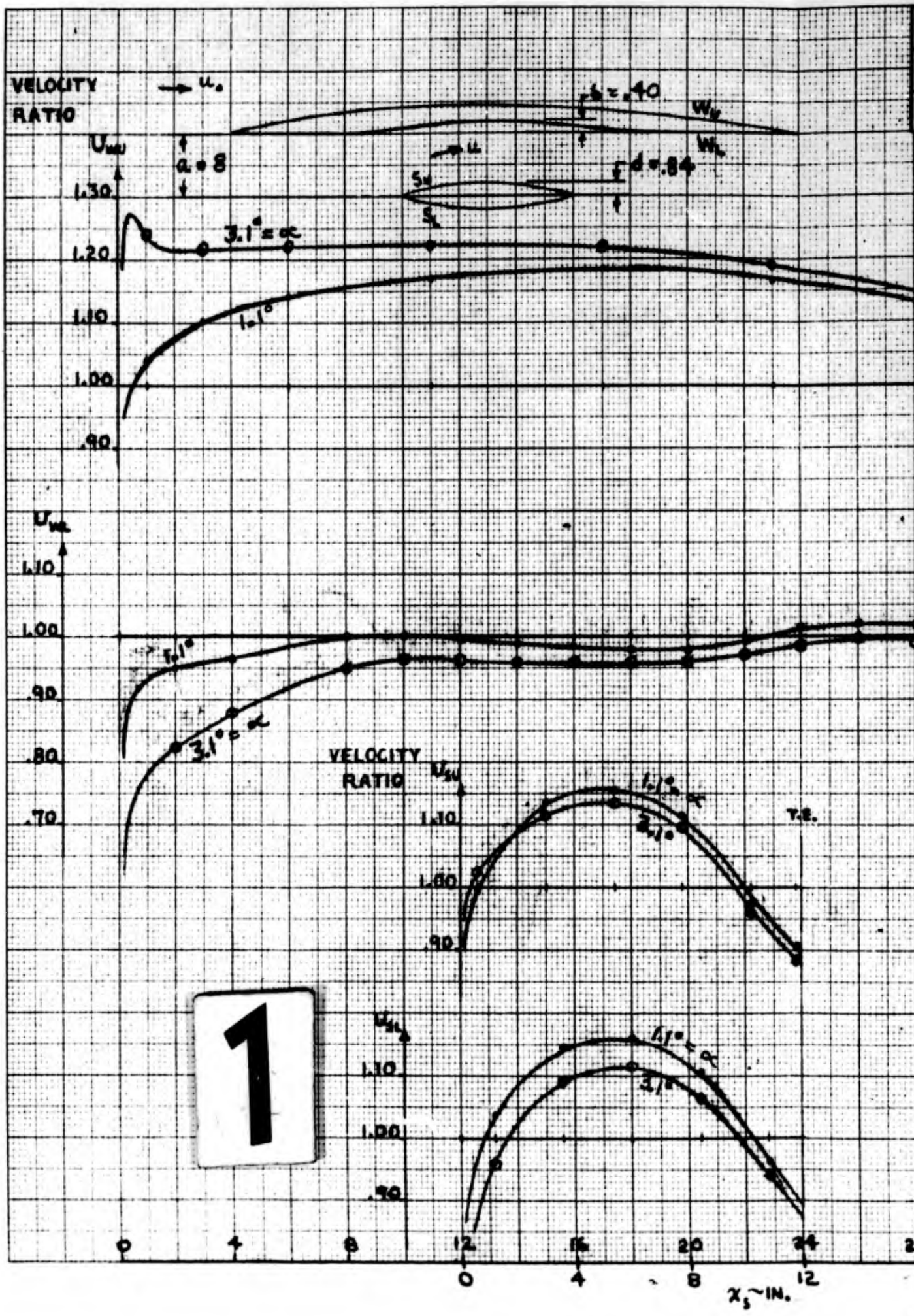
VELOCITY RATIO
u_o
$b = .40$
W_u
W_L
U_{wu}
$a = .8$
u
$d = .84$
S_u
S_L
1.30
1.20
1.10
1.00
.90
$3.1° = \alpha$
$1.1°$
U_{wL}
1.10
1.00
.90
.80
.70
$1.1° = \alpha$
$3.1°$
VELOCITY RATIO
U_{Su}
1.10
1.00
.90
$1.1° = \alpha$
$3.1°$
T.E.
U_{SL}
1.10
1.00
.90
$1.1° = \alpha$
$3.1°$
0
4
8
12
16
20
24
0
4
8
12
x_s ~ IN.

1

ENGINEER	Figure 8	PAGE
K. Rogers	NORTHROP AIRCRAFT INC.	24
CHECKER		REPORT NO. BLO-103
DATE July 1957	TEST RESULTS — TWO DIMENSIONAL WING WITH CUTOUT AND AUXILIARY AIRFOIL IN BLR WIND TUNNEL	MODEL

COMBINATION NO. 3

$a = 8$

W_U

W_L

T.E.

TURBULENCE ON W_L

- 1 BURST / SEC.
- 5 BURSTS / SEC.
- 10 BURSTS / SEC.

R_{CW} ~MILLIONS

q_o ~IN. H_2O

α

T.E.

α

X_W ~IN.

X_S ~IN.

$\left(\frac{x}{c}\right)_W$

2

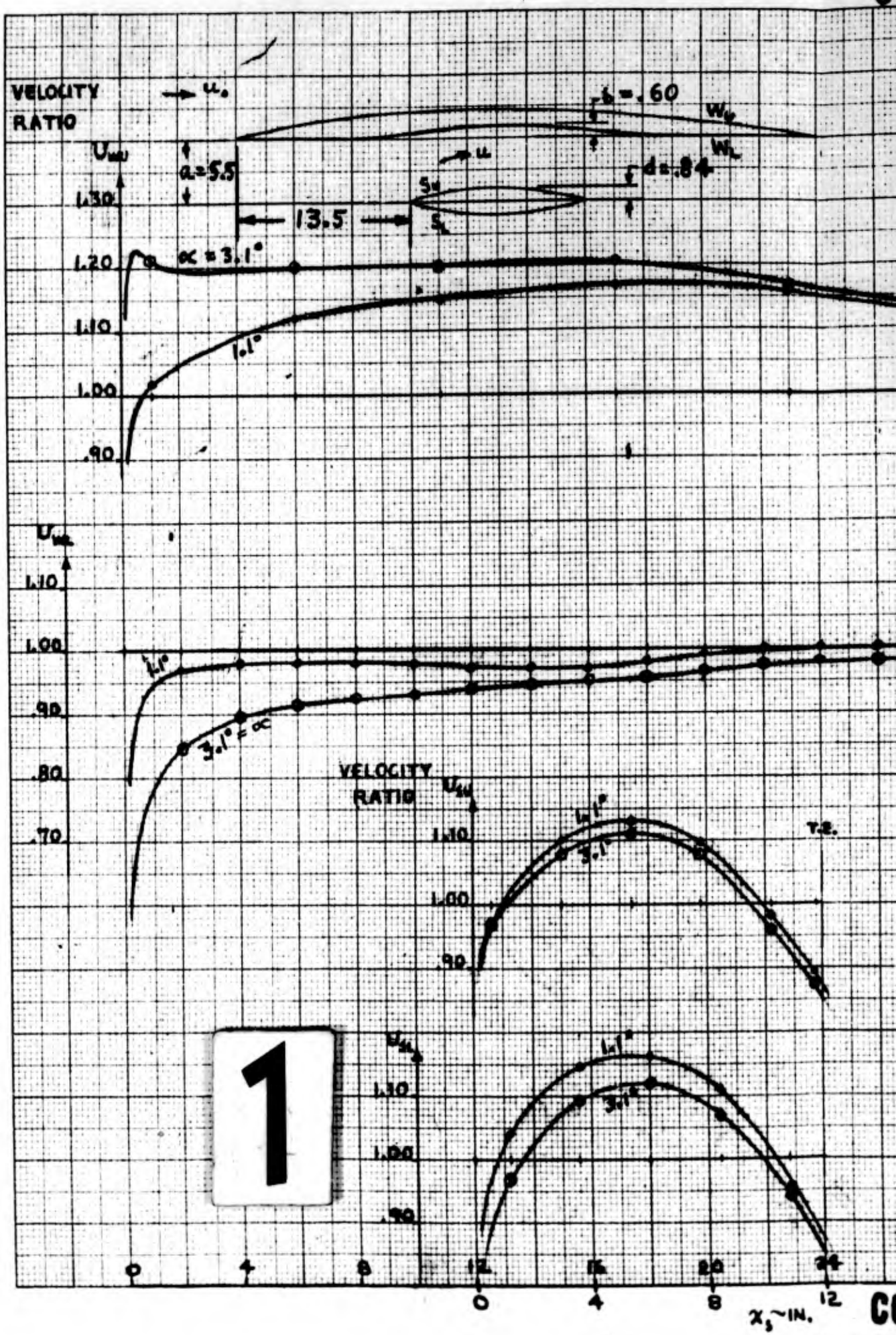
VELOCITY RATIO
u_∞
U_{uu}
a=5.5
13.5
b=.60
d=.84
W_u
W_L
S_u
S_L
α = 3.1°
1.30
1.20
1.10
1.00
.90
1.1°
3.1° = α
.80
.70
VELOCITY RATIO
T.E.
0
4
8
12
16
20
24
x_s ~IN.
1

FORM 20-118 (R. 6-51)

ENGINEER: K. Rogers	Figure 9	PAGE: 25
CHECKER:	NORTHROP AIRCRAFT INC.	REPORT NO.: NLO-103
DATE: July 1957	TEST RESULTS — TWO DIMENSIONAL WING WITH CUTOUT AND AUXILIARY AIRFOIL IN BLR WIND TUNNEL	MODEL:

COMBINATION NO. 4

$\alpha_s = 5.5$

STAGGER = 13.5

T.E.

TURBULENCE ON W_L

- 1 BURST / SEC.
- 5 BURSTS / SEC.
- 10 BURSTS / SEC.

R_{CW} ~MILLIONS

$\alpha = 3.1°$

ΔP ~IN. H_2O

T.E.

X_W ~IN.

X_S ~IN.

$\left(\frac{x}{c}\right)_W$

2

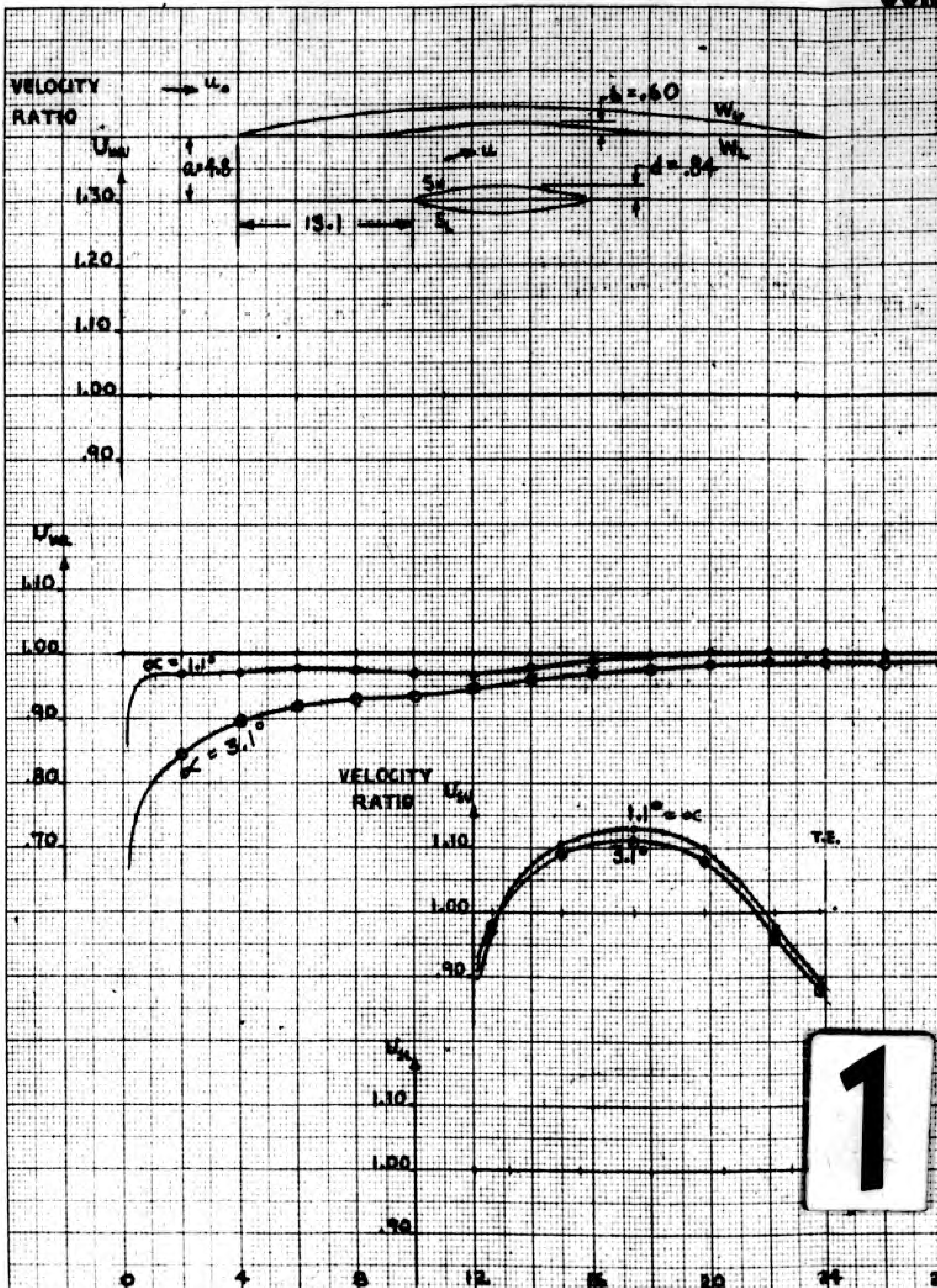
VELOCITY
RATIO
u_o
$b = .60$
W_U
W_L
U_{WU}
$a = 4.8$
u
$d = .84$
S_U
S_L
13.1
1.30
1.20
1.10
1.00
.90
U_{WL}
1.10
1.00
.90
.80
.70
$\alpha = 1.1°$
$\alpha = 3.1°$
VELOCITY
RATIO
U_{SU}
$1.1° = \alpha$
$3.1°$
T.E.
1.10
1.00
.90
U_{SL}
1.10
1.00
.90
0
4
8
12
16
20
24
0
4
8
12
x_s ~ IN.

1

CONFIDENTIAL

Form 20-118 (R. 6-51)

ENGINEER: K. Rogers	Figure 10 NORTHROP AIRCRAFT INC.	PAGE: 26
CHECKER		REPORT NO.: BLO-103
DATE: July 1957	TEST RESULTS — TWO DIMENSIONAL WING WITH CUTOUT AND AUXILIARY AIRFOIL IN BLR WIND TUNNEL	MODEL

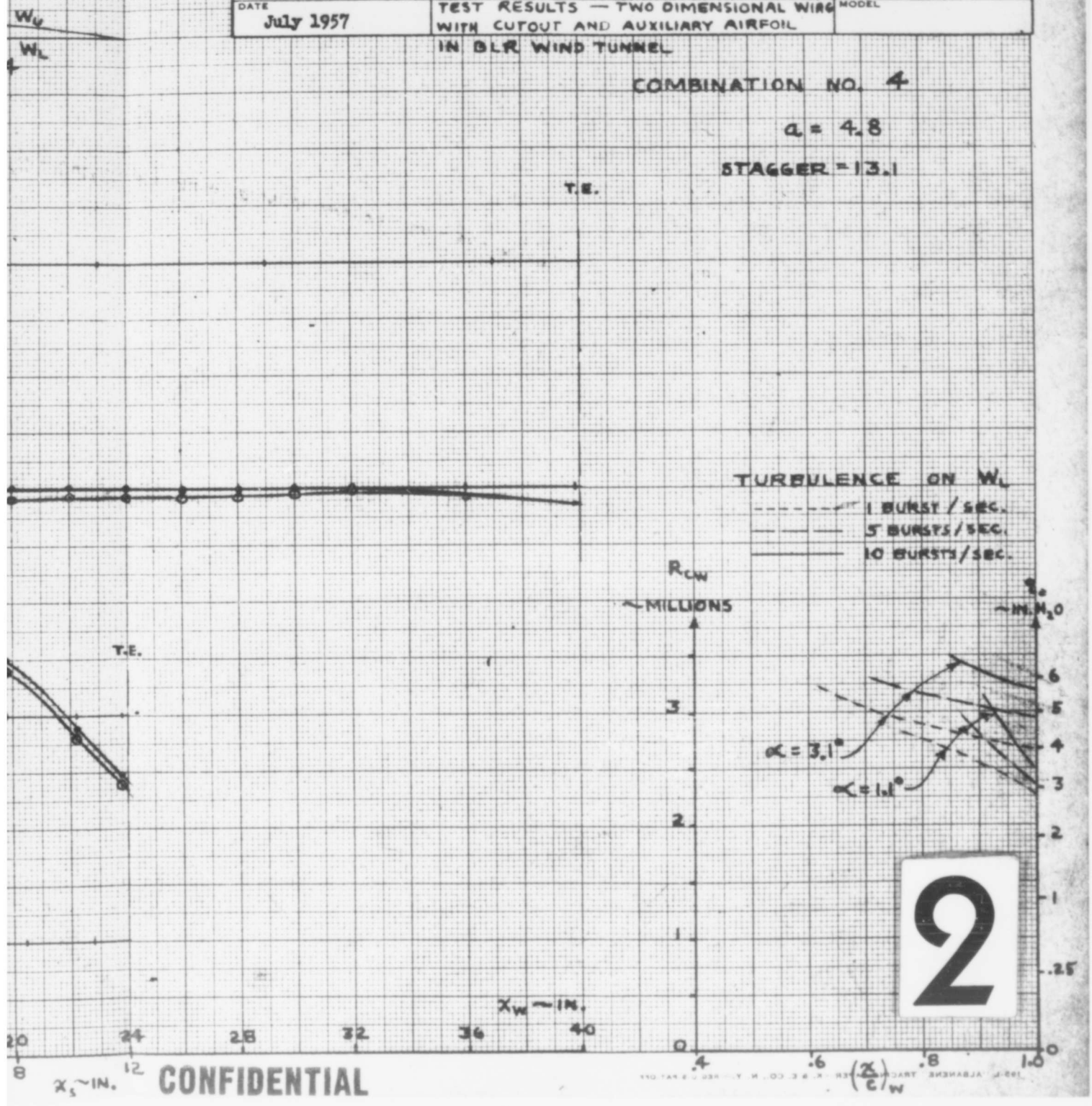

CONFIDENTIAL

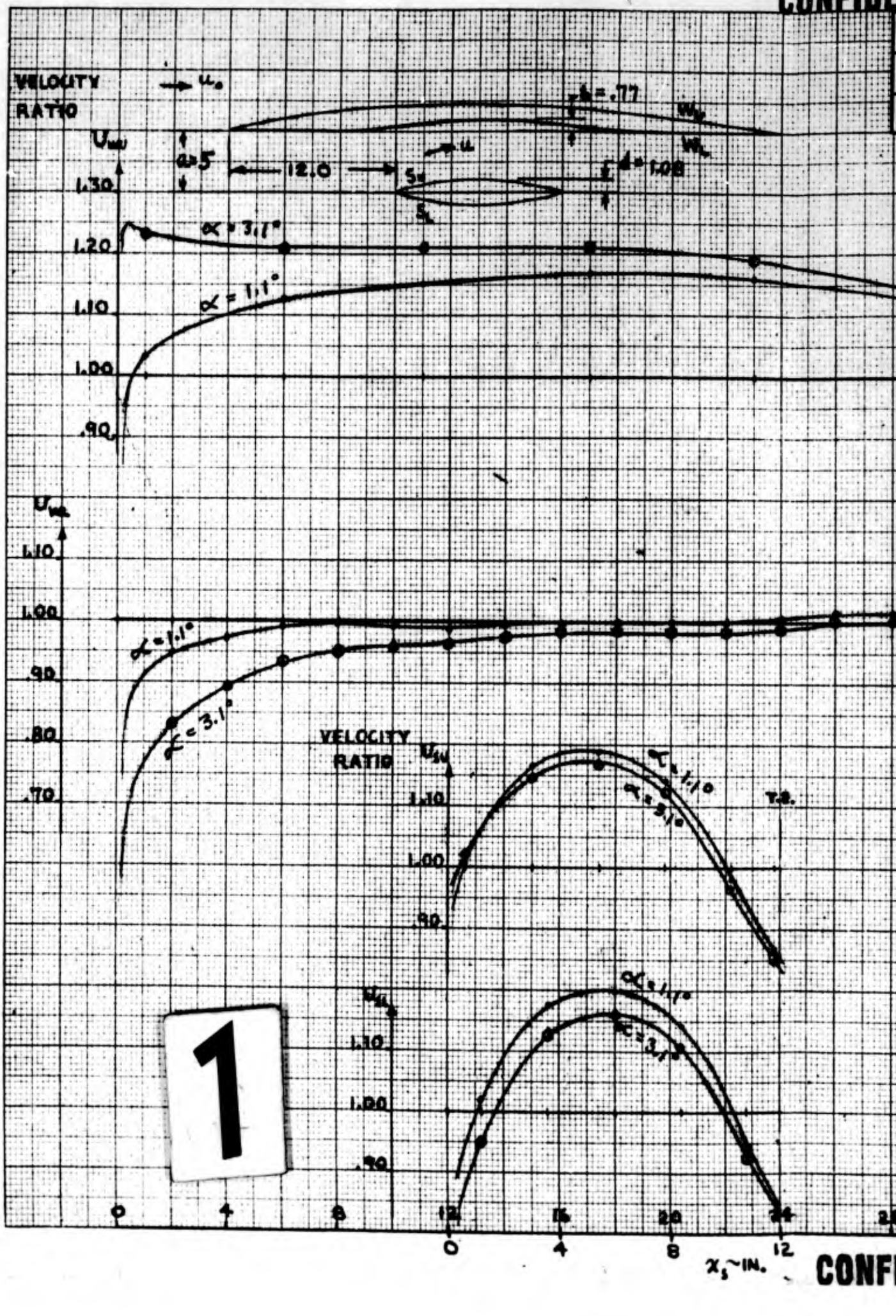

1

CONFIDENTIAL

Form 20-118 (R. 6-51)

ENGINEER K. Rogers	Figure 21	PAGE 27
CHECKER	NORTHROP AIRCRAFT INC.	REPORT NO. BLC-103
DATE July 1957	TEST RESULTS — TWO DIMENSIONAL WING WITH CUTOUT AND AUXILIARY AIRFOIL IN BLR WIND TUNNEL	MODEL

COMBINATION NO. 5

UNIFORM VELOCITY DISTRIBUTION

T.E.

T.E.

TURBULENCE ON W_∞

- 1 BURST / SEC.
- 5 BURSTS / SEC.
- 10 BURSTS / SEC.

R_{CW} ~MILLIONS

$\alpha_c = 5.1°$

~IN. H_2O

X_W ~IN.

X_S ~IN.

$\left(\frac{x}{c}\right)_W$

2

CONFIDENTIAL

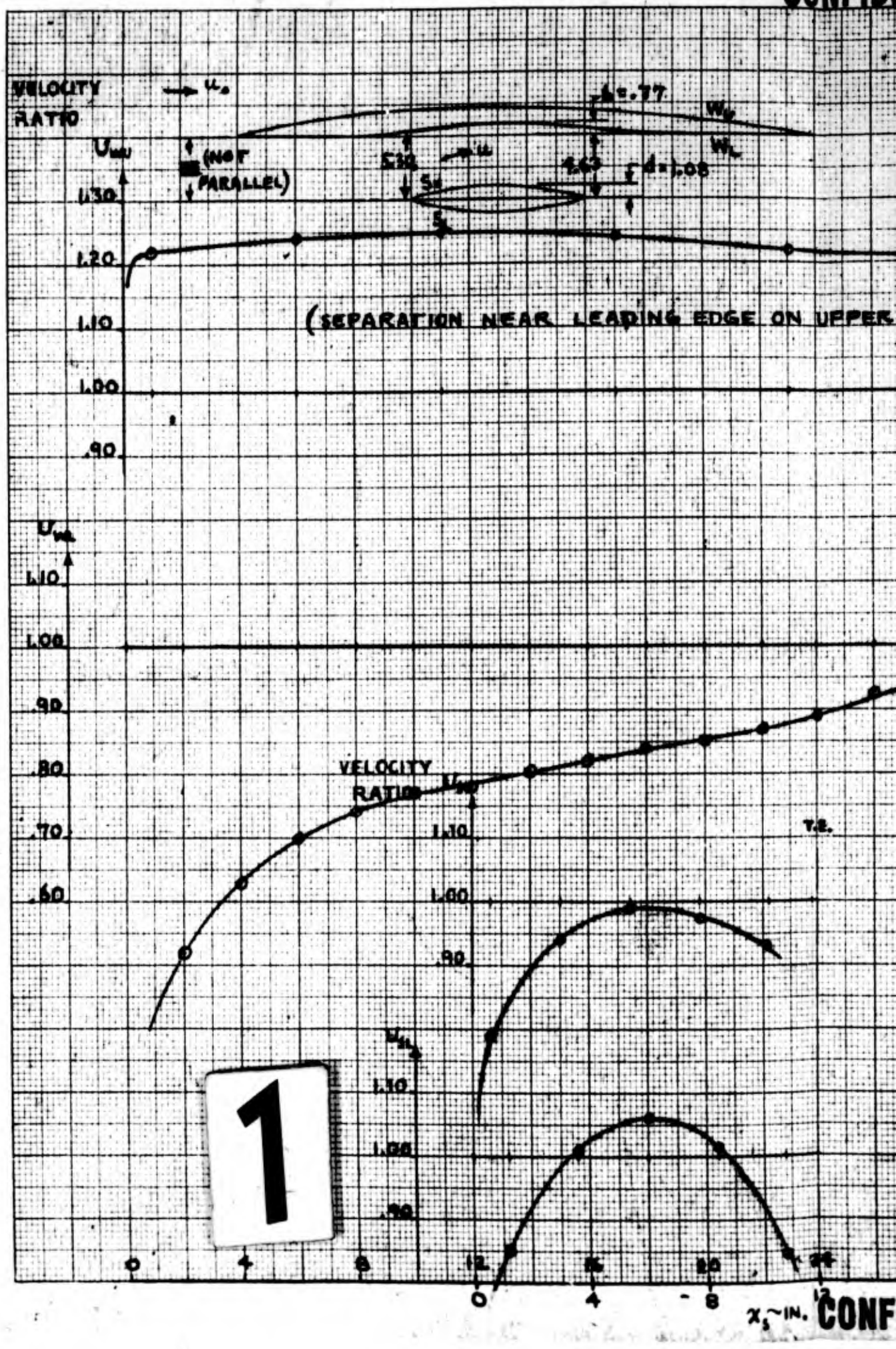

1

CONFIDENTIAL

FORM 20-11B (R. 6-51)

ENGINEER	Figure 12	PAGE
K. Rogers	NORTHROP AIRCRAFT INC.	28
CHECKER		REPORT NO. BLO-103
DATE July 1957	TEST RESULTS — TWO DIMENSIONAL WING WITH CUTOUT AND AUXILIARY AIRFOIL IN BLR WIND TUNNEL	MODEL

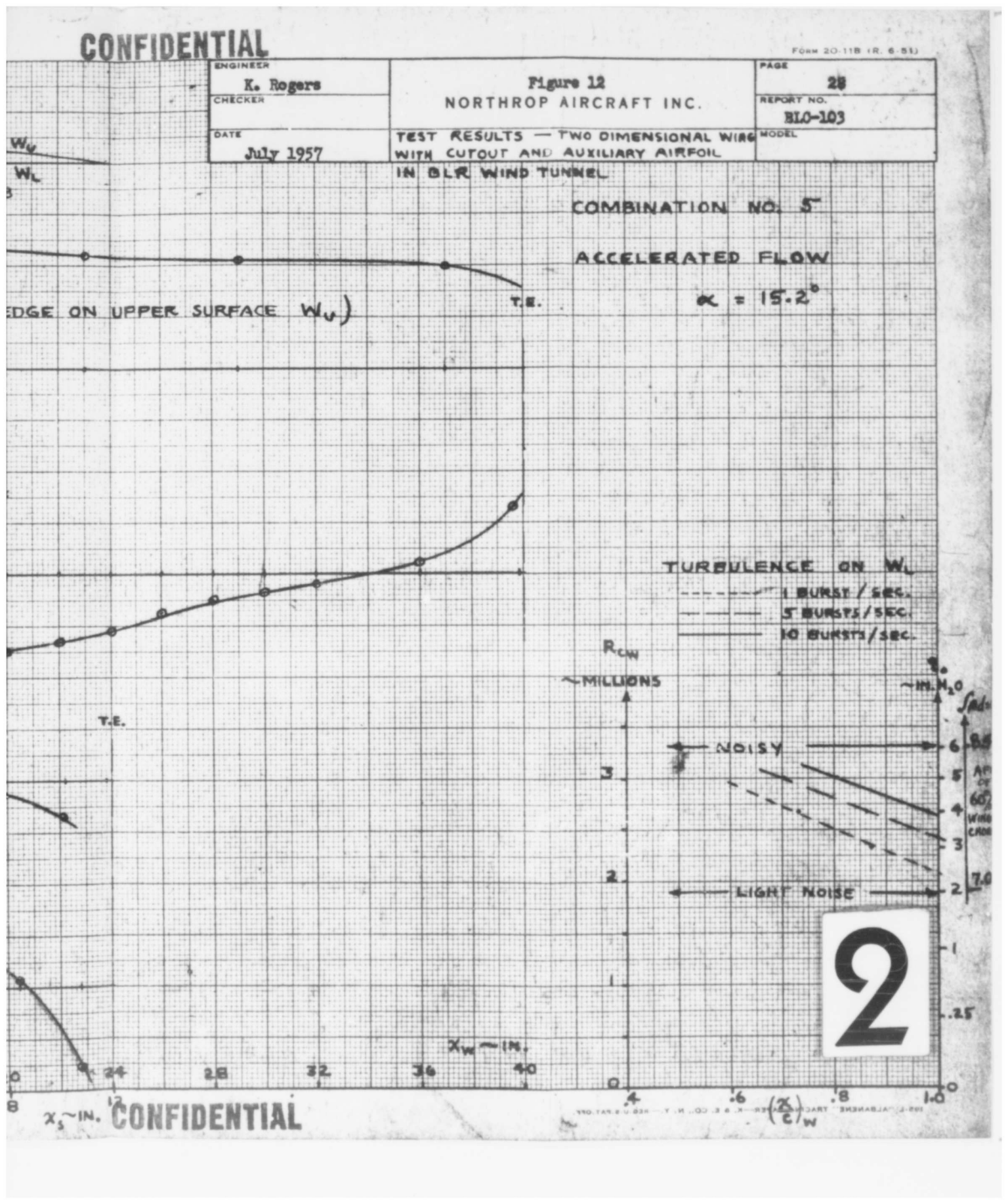

2

CONFIDENTIAL

SMITH PARAMETER

$\beta\theta \cdot R_\theta$

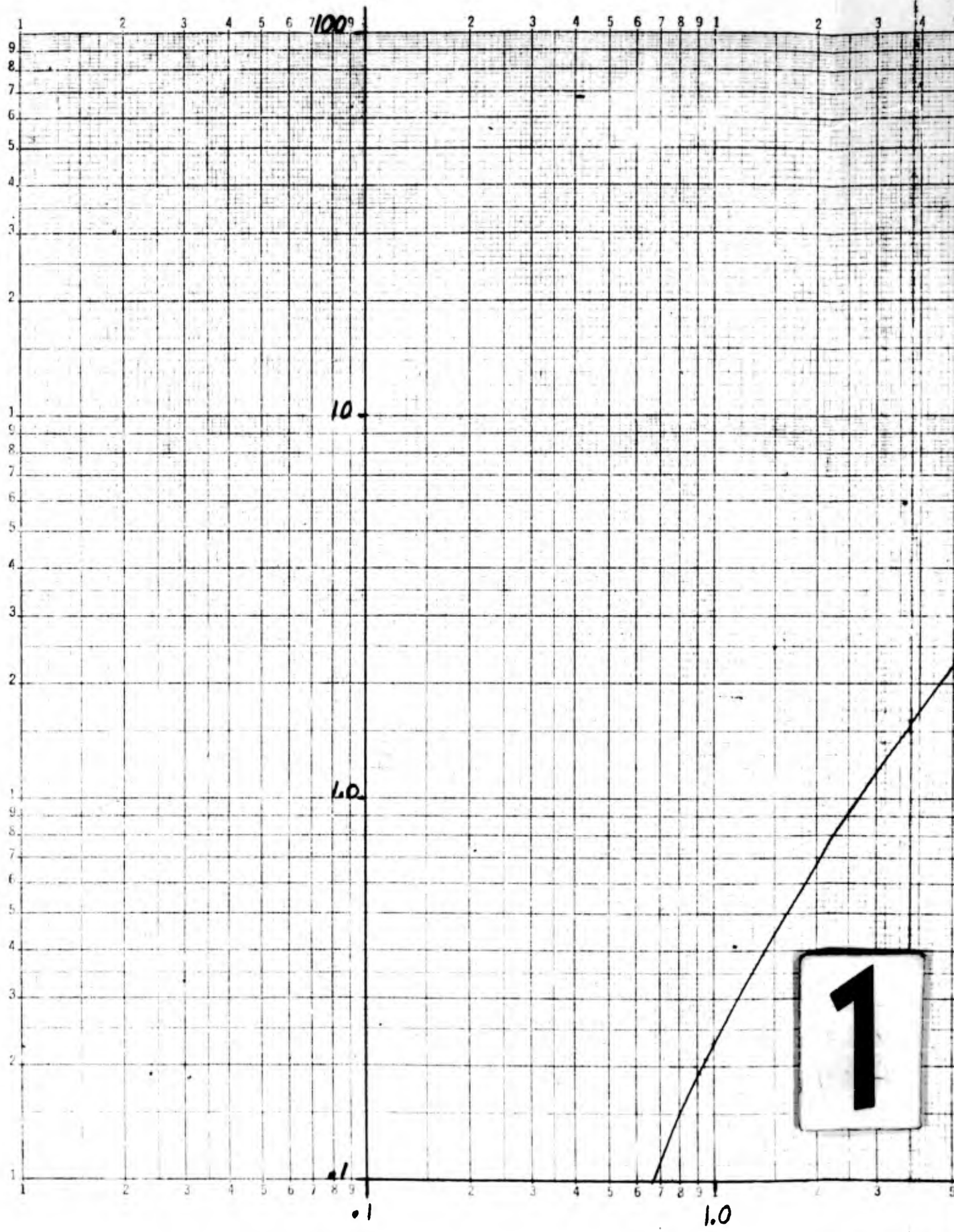

LOGARITHMIC 359-125LG

GÖRTLER

FIG 13. SMITH PARAMETER $\beta\theta R_\theta$ vs GORTLER PARAMETER $R_\theta\sqrt{\frac{\theta}{r}}$

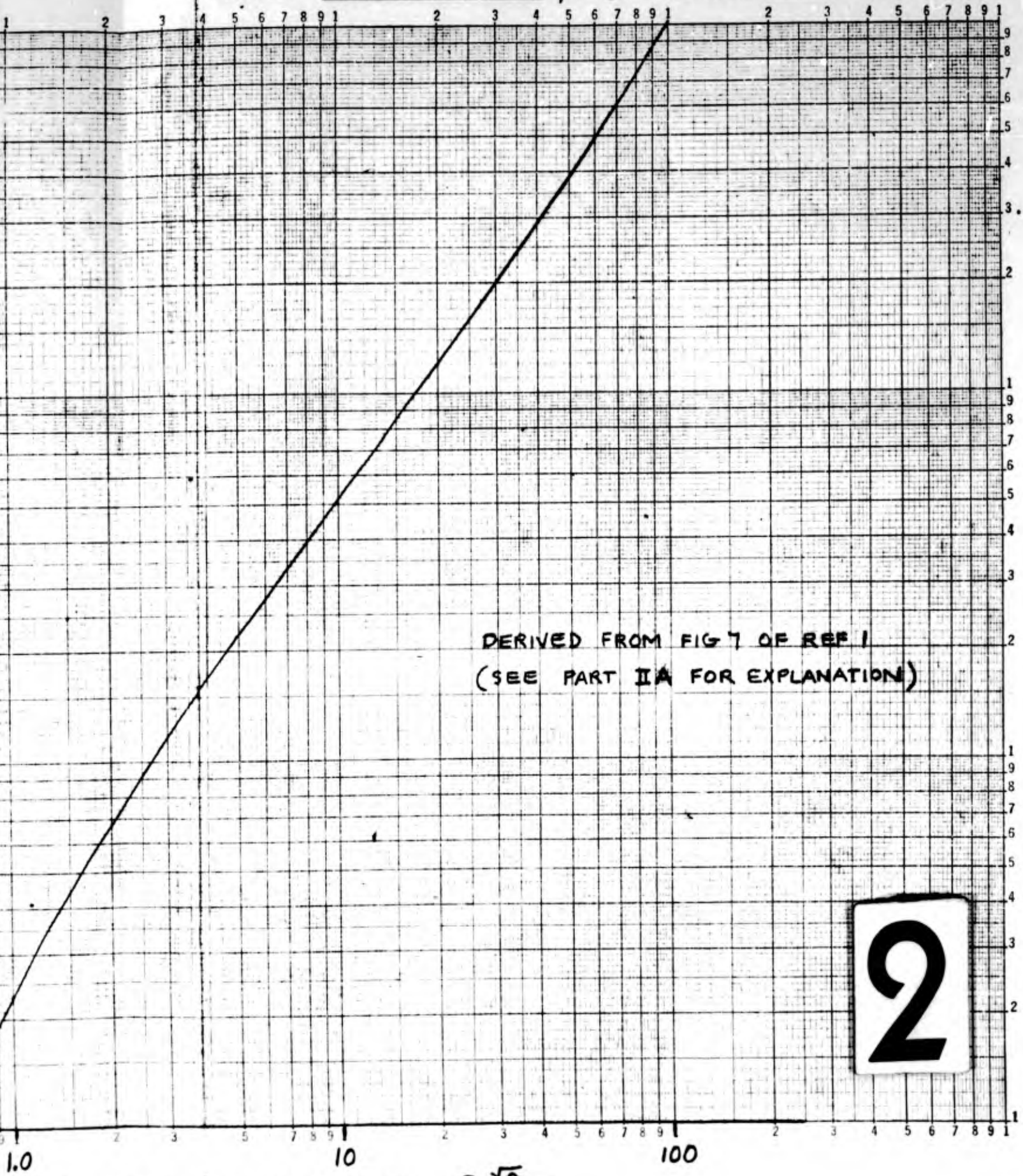

FIG 14. DESIGN CHART FOR WING-STRUT INTERFERENCE CUTOUTS

(CHART SHOWS DEPTH OF CUTOUT REQD TO PROVIDE NEARLY UNIFORM VELOCITY ON W_L)

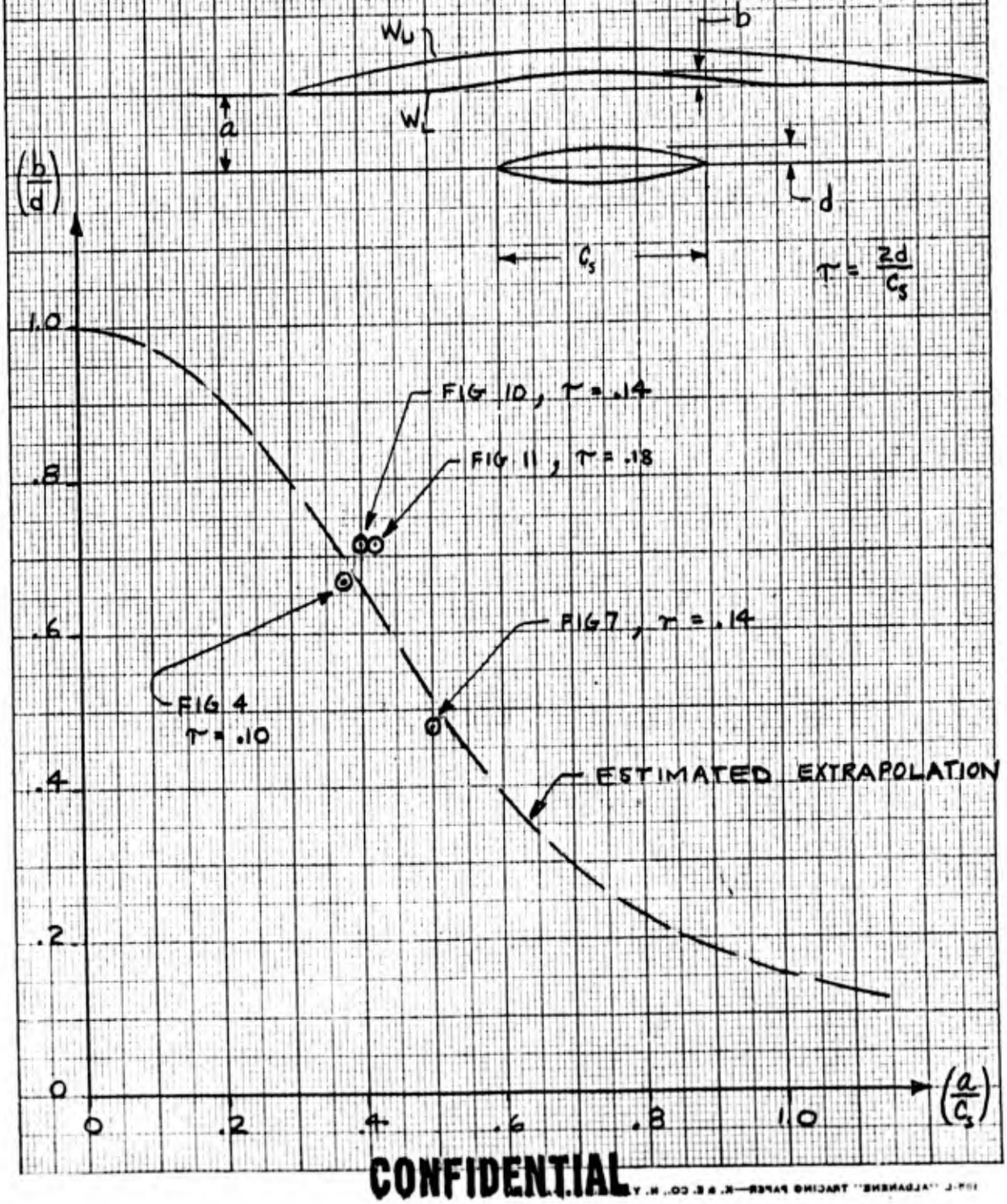

Northrop
Wind Tunnel Installation
Two-Dimensional Solid Wing Strut
Interference Model, Rear View N-97

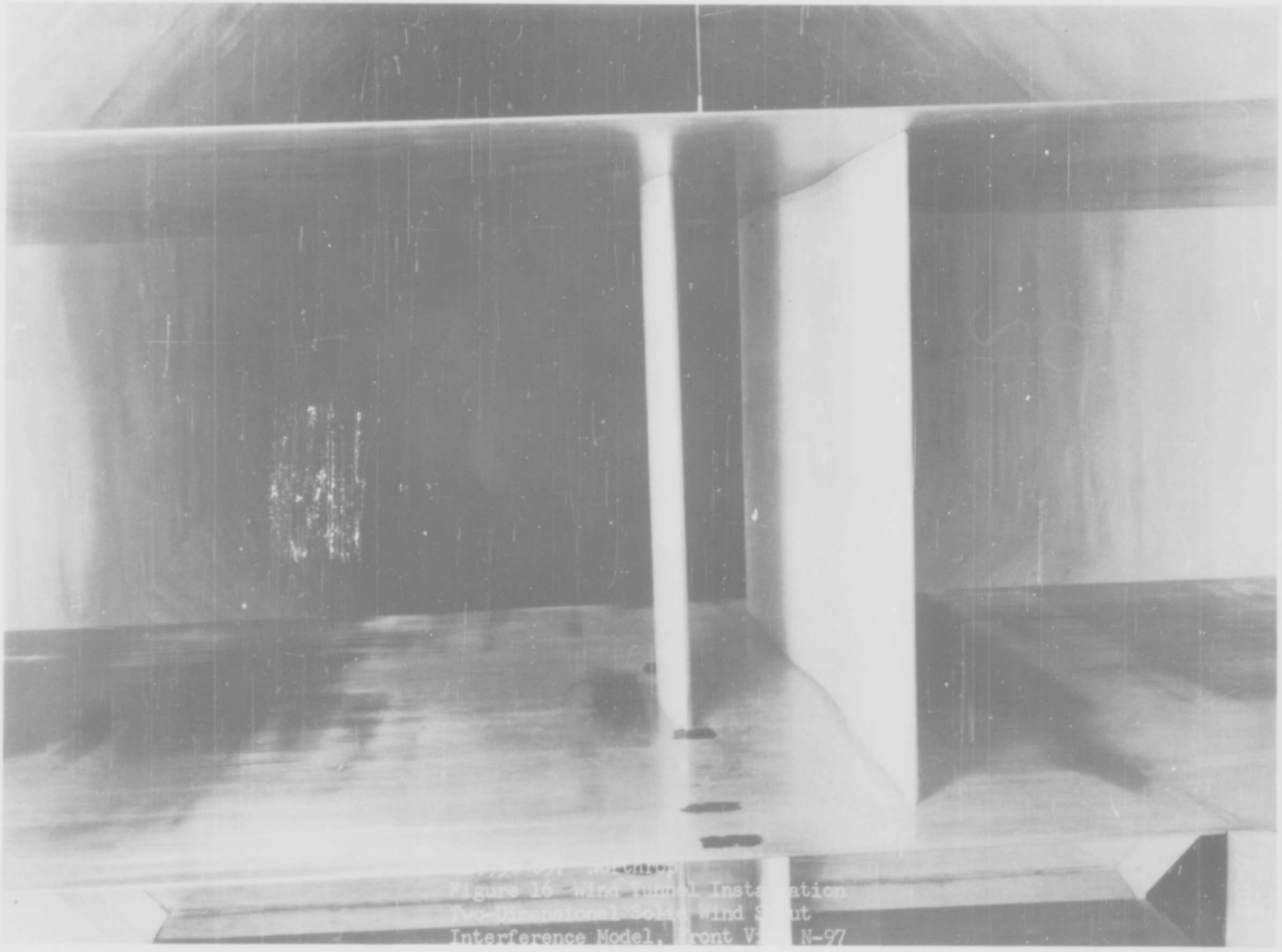

Figure 16 - [illegible] Installation
[illegible] Wind Tunnel
Interference Model, [illegible] Front View N-97

AD-150527(6)

CPO
AD-150 527 (b) (24 Feb 58 jb) CONFIDENTIAL

Northrop Aircraft, Inc., Hawthorne, Calif.
BOUNDARY LAYER TRANSITION ON BODIES OF REVOLUTION, by E. E. Groth. July 57 [34]p. incl. illus. (Rept. no. NAI 57-1162; BLC-100) (Appendice to Northrop Aircraft, Inc., Contract AF 33(616)3168, Progress rept. for 1-30 Sep 57, AD-150 527)
Confidential report

I. Auther
II Northrop Aircraft, Inc, Hawthorne, Calif.
III Contract AF33(616)3168

CONFIDENTIAL

NORTHROP AIRCRAFT, INC.

HAWTHORNE, CALIFORNIA

REPORT NO. NAI-57-1162

REPORT NO. BLC-100

BOUNDARY LAYER TRANSITION ON BODIES OF REVOLUTION

July 1957

PREPARED BY

E. E. Groth

E. E. Groth

APPROVED BY

W. Pfenninger

W. Pfenninger

REVISIONS

CHG. NO.	DATE	ENGR.	PAGES AFFECTED	REMARKS

CONFIDENTIAL

TABLE OF CONTENTS

SUMMARY

Boundary layer transition measurements on bodies of revolution at zero incidence have been made in two wind tunnels and in flight at subsonic speeds. The results of these experiments demonstrate the importance of the potential flow pressure distribution along the body on transition. A theoretical analysis comparing the experimental data with two-dimensional transition values indicates that the slope of the body contour has a major influence on transition of bodies of revolution. Increasing radius along the body axis moves transition forward, decreasing radius moves it aft of the station computed for two-dimensional flow. Since the ratio of the momentum thickness Reynolds numbers at transition for axially symmetrical and two-dimensional flow depends primarily on the local slope of the body, the results of this analysis might be used for an estimate of boundary layer transition on any body of revolution at zero degree angle of attack and incompressible flow.

I. INTRODUCTION

The development of the boundary layer along a body of revolution at zero incidence has been investigated only in a few cases so that the knowledge about boundary layer transition on bodies is very limited. Early British experiments at low speeds on an 80-inch long model of the airship R101 (Reference 1) consisted of the measurement of boundary layer velocity profiles and hot wire observations in laminar, transitional, and turbulent flow. Wind tunnel measurements up to high subsonic speeds were conducted by Goethert in Germany (Ref. 2) on bodies of different fineness ratio. Boundary layer transition was observed as a limiting line of a thin layer of dust accumulated on the model during a 15-minute tunnel run. The cross-section of the model corresponded to an NACA airfoil section with the maximum thickness at 45%L, the thickness ratio varied between 10 and 40%, the reference length was L = 1.94 ft. The location of transition is plotted as x_T/L and as transition Reynolds number

$$R_T = \frac{x_T}{L} R_L$$

vs length Reynolds number in Figure 1a and 1b. Maximum transition Reynolds numbers of the order of $R_T = 4 \cdot 10^6$ have been observed. The change in pressure distribution due to compressibility effects affected the results at high Mach numbers.

The results of transition observations on a modified ellipsoid of fineness ratio 4.7 and 2.8-ft length at the Swiss Federal Institute of Technology, Zurich (Ref. 3) and on a modified ellipsoid of fineness ratio 8.0 and 7-ft length at the Northrop Low Speed Wind Tunnel (Ref. 4) are also included in Figure 1.

During the years 1954 to early 1957, the Northrop Boundary Layer Research Group has conducted transition measurements on several bodies in wind tunnels and in flight as a preliminary step for a research program on the application of boundary layer suction to bodies of revolution. The test results have been reported briefly in the monthly progress reports and in the Summary Report (Ref. 5). A compilation of the experimental results and analysis of the data is presented herewith.

II. NOTATION

x coordinate along body axis

r body radius

L body length ($L = 96$ in. = reference length)

$f = \frac{L}{2\, r_{max}}$ = body fineness ratio

x_T location of transition

$R_L = \frac{L\, U_\infty}{\nu_\infty}$ = length Reynolds number

$R_T = \frac{x_T}{L} R_L$ = transition Reynolds number

θ = momentum thickness

δ^* = displacement thickness

$R_\theta = \frac{\theta U}{\nu}$ = momentum thickness Reynolds number

$\theta^* = \frac{\theta}{L} \sqrt{R_L}$ = nondimensional momentum thickness

U = local potential flow velocity along body

U_∞ = freestream velocity

$C_p = 1 - (U/U_\infty)^2$ = static pressure coefficient along body

III. DESCRIPTION OF THE MODELS

Three bodies of revolution of different contour have been used in the transition experiments. They are derived from the equations

$$\left(\frac{r}{r_{max}}\right)_{ell} = 2\left[\xi(1-\xi)\right]^{1/2} \quad \text{for the elliptic form}$$

$$\left(\frac{r}{r_{max}}\right)_{SH} = 2^{3/2}\left[\xi(1-\xi)\right]^{3/4} \quad \text{for the Sears Haack form}$$

$$\left(\frac{r}{r_{max}}\right)_{par} = 2^{2}\,\xi(1-\xi) \quad \text{for the parabolic form,}$$

where ξ is a nondimensional length coordinate. The bodies had a fineness ratio of 9, a maximum diameter of 10.5 in., and were faired into a cylindrical sting of 3.824 in. diameter at the station 96 in.

Since the Sears-Haack and parabolic body have a sharp nose, the contours were modified to allow for a finite nose radius. A list of the coordinates of the three bodies is presented in Table I. The values of the nose radii are .583 in. for the elliptic,.160 in. for the modified Sears-Haack, and .078 in. for the modified parabolic body.

It did not seem advisable to build bodies with a sharper nose section since British calculations (Ref. 6) indicated that the parabolic shape represents about the

most pointed body contour with a monotonic pressure distribution.

The elliptic body was built of aluminum, with static pressure orifices installed along the body length. Several of these orifices were connected to microphones to observe the status of the boundary layer acoustically. The modified Sears-Haack and parabolic bodies were built of wood, with no instrumentation built in the models. Typical pictures of the installation of the bodies on the F94 airplane are shown in Figures 2 and 3. Fig. 2 represents the elliptic body; the irregular spots at several places along the surface consist of paint which had been sprayed on to correct for low spots in the contour. The modified parabolic body is shown in Fig. 3; two total head rakes are visible for measuring the local boundary layer profile for detecting transition.

The three models were highly polished and of low waviness, waviness readings with a 2-inch dial gage never gave waves of an amplitude to length ratio exceeding .0005 in/in.

IV. PRESENTATION OF TEST RESULTS

Static pressure distribution measurements and boundary layer transition measurements were made on the elliptic body with the instrumentation installed inside the model. Transition was defined as the point along the contour with about one turbulent burst per second. The elliptic body was tested at the Northrop Low Speed Wind Tunnel, the NACA 12-ft Low Turbulence High Speed Tunnel at Ames Aeronautic Laboratory (published in Ref. 7) and in flight. Since transition at the high flight Reynolds number occurred ahead of the location of the first microphone, the surface was sprayed with a solution of fluorene in petrol ether; evaporation proceeds so slowly that its application to flight tests is possible. The results of the transition observations are

shown in Fig. 4a and 4b as x_T/L and R_T vs R_L. The flight data fair into the Ames data rather well. The difference in transition values between the Ames and Northrop tunnel must be due to the better tunnel turbulence level at Ames, since the same model and method for detecting transition was used in both tunnels. The steep reduction in transition length beyond $R_L = 7 \times 10^6$ at the Northrop tunnel is caused by an increase in tunnel turbulence, which is also noticeable as increasing noise. The curves R_T vs R_L show a local maximum at low Reynolds numbers ($R_L \sim 4 - 5 \times 10^6$), but R_T again increases with increasing R_L for $R_L > \sim 10 \times 10^6$.

Since it was expected that the static pressure distribution along the model surface has an influence on the boundary layer development, additional transition and pressure measurements were done at the Northrop tunnel with the same elliptic model moved forward into the contraction cone of the tunnel so that the changed velocity field of the tunnel was superposed on the flow field around the model. Two configurations of the model nose 16 in. and 40 in. ahead of the beginning of the test section were investigated. The results are shown in Figures 5 and 6 as pressure distribution and transition location. The effect of the more favorable pressure distribution in the front part of the body results in a considerable increase of the laminar flow regime.

For investigating the effect of different pressure distributions at higher Reynolds numbers, two bodies of revolution of modified Sears-Haack and parabolic contour were built and tested at the Northrop Wind Tunnel and in flight on the F94 airplane. Since no instrumentation was included in the model, it was necessary to probe the pressure distribution and transition from outside. In flight, a rake of total head probes was installed at several length-stations and the boundary layer profile measured. Typical laminar and turbulent profiles were measured so that the

transition location could be determined rather accurately. The measured pressure distributions for the bodies are shown in Fig. 7; the results of the transition measurements in Figures 8 and 9. The effect of the pressure distribution is the same as observed previously with the elliptic body at the different tunnel locations, a more favorable pressure gradient in the front part of the parabolic body results in higher transition Reynolds numbers than on the other bodies.

V. ANALYSIS OF THE TEST DATA

The measured pressure distributions and transition data for the different bodies in wind tunnels and in flight have been analyzed for the purpose of developing a method for predicting boundary layer transition on any body of revolution at zero incidence.

Stability investigations of the two-dimensional laminar boundary layer at various pressure gradients, expressed by the Hartree β parameter ($U = x^m$, $m = \frac{\beta}{2-\beta}$) by Pretsch (Ref. 8) resulted in a set of charts for the rate of amplification β_i of Tollmien-Schlichting type disturbances for various values of β. From these curves the Reynolds numbers $R_{\delta^*_{cr}}^{(2)}$ have been selected for which disturbances are amplified most (singular point of maximum amplification in the stability charts)*. The relation of $R_{\delta^*_{cr}}^{(2)}$ vs β can be changed to $R_{\theta_{cr}}^{(2)}$ vs β by dividing $R_{o}^{*(2)}$ by the boundary layer form parameter H which is known for each value of β. The curve of $R_{\theta_{cr}}^{(2)}$ vs m is shown in Fig. 10.

---

* As suggested by G. Raetz.

In order to apply these two-dimensional stability data to bodies of revolution, the following analysis was made: The boundary layer around a body of revolution can be transformed to a two-dimensional case by the Mangler transformation (Ref.9) resulting in a potential flow $U/U_o = f(x^{(2)})$. This velocity distribution can be approximated by Falkner polynomials $U/U_o = c(x^{(2)} - x_o^{(2)})^m$, so that the velocity gradient parameter m is known along $x^{(2)}$. The curve $R_{\theta_{cr}}^{(2)}$ vs m from Fig. 10 then provides a critical value $R_{\theta_{cr}}^{(2)}$ vs $x^{(2)}$ and - by means of the Mangler transformation - also along the body axis.

The Falkner calculation permits the computation of the nondimensional momentum thickness

$$\theta^* = \frac{\theta}{L}\sqrt{R_L}$$

which can be plotted vs x and is shown on Fig. 11. An experimental momentum thickness at transition is then defined by

$$R_{\theta_T} = \theta^*(x_T)\,\frac{U}{U_o}(x_T)\sqrt{R_L}$$

where x_T is the measured transition location at the given length Reynolds number R_L. The variation of R_{θ_T} and $R_{\theta_{cr}}^{(2)}$ along the body axis are shown in Figures 12, 13, 14 for the elliptic, modified Sears-Haack, and modified parabolic body. A few lines of constant length Reynolds number are included in each graph.

The difference between the experimental three-dimensional value R_{θ_T} and the theoretical two-dimensional value $R_{\theta_{cr}}^{(2)}$ is rather systematic. The two values are nearly equal at the point of maximum thickness, $R_{\theta_T} > R_{\theta_{cr}}^{(2)}$ in the rear part of the body, $R_{\theta_T} < R_{\theta_{cr}}^{(2)}$ in the front part. Since the rate of growth of the body radius

seems to be important, the slope $\frac{L}{r}\frac{dr}{dx}$ is plotted in Fig. 15 vs $\frac{x}{L}$ for the three bodies. The circumference of the body at the station x is equal to $2\pi\, r(x)$, at the station $(x + dx)$ equal to $2\pi\, r(x+dx) = 2\pi\, r(x)\left[1 + \frac{1}{r(x)}\frac{dr(x)}{dx}dx\right]$, so that the quantity $\frac{L}{r}\frac{dr}{dx}$ represents a measure for the percentage increase of the circumference of the body, or for the stretching or contracting, i.e., thinning or thickening of the boundary layer. The ratio $\tau = R\theta_T / R\theta_{cr}^{(2)}$ is plotted vs $\frac{L}{r}\frac{dr}{dx}$ in Fig. 16 for all the cases under consideration, including a second body of revolution of fineness ratio 7.5 investigated by the NACA in Ref. 7.

Figure 16 provides the following information. The ratio τ of the experimental and theoretical two-dimensional momentum thickness Reynolds numbers is near 1 at $\frac{dr}{dx} = 0$ for the data observed in flight and at the Ames low turbulence tunnel. The higher turbulence level at the Northrop tunnel reduces τ to .90 . The high Reynolds number flight data on the three bodies give $\tau = .78 \pm .08$ for $\frac{L}{r}\frac{dr}{dx} = 1$ to 3 . The values of τ below .65 have been obtained at rather high speeds in the Northrop tunnel, indicating the increase of the turbulence level with increasing speed (increasing tunnel noise).

The steep increase of τ for negative $\frac{dr}{dx}$ indicates that the thickening of the boundary layer in the rear part of the body seems to contribute considerably to its stability.

The differences in τ for the bodies under consideration might also be caused by the fact that the selected stability curve $R\theta_{cr}^{(2)}$ vs m has not yet been established sufficiently by experiments. The values seem to be rather correct around $m = 0$, but not much experimental evidence is available for $m \neq 0$.

For estimating the transition behavior at high Reynolds numbers, values of $\tau = .86$, $.80$, and $.74$ have been assumed for the elliptic, modified Sears-Haack, and modified parabolic body. The forward motion of $\frac{x_T}{L}$ and increase in R_T with increasing length Reynolds number is shown as "extrapolated" data in Figures 4, 8, 9 . A maximum transition Reynolds number of the order of 8×10^6 is expected for the modified Sears-Haack and parabolic body at length Reynolds numbers close to 100×10^6 at low subsonic speeds.

VI. CONCLUSIONS

Transition measurements on several bodies of revolution in wind tunnels and in flight produced the following results:

1. Transition moves forward from the point of laminar separation with increasing length Reynolds number at a rate which depends on the potential flow pressure distribution, and for the same model on the turbulence level of the air.

2. Wind tunnel tests showed that the transition Reynolds number R_T has a maximum value of the order of 3 to 4.5×10^6 at length Reynolds numbers of 4 to 6×10^6 . Beyond $R_L = 10 \times 10^6$, R_T increases again and reaches values of the order of $R_T = 6 \times 10^6$ for $R_L = 30 \times 10^6$, as observed in flight.

3. Comparison of the experimental transition Reynolds numbers R_{θ_T} with two-dimensional transition values $R_{\theta_{cr}}^{(2)}$ indicates that an increasing radius along the body axis reduces R_{θ_T} by 20 to 30% and that decreasing body radius increases R_{θ_T} considerably. Since the variation of $R_{\theta_T}/R_{\theta_{cr}}^{(2)}$ with $\frac{L}{r}\frac{dr}{dx}$ is not much different for the bodies investigated, the prediction of boundary layer transition for any body of revolution at zero incidence seems to be possible.

REFERENCES

1 Simmons and Brown: An Experimental Investigation of Boundary Layer Flow with Special Reference to Methods of Detecting the Transitional Region, British R & M 1547, November 1934.

2 Goethert, B.: High Speed Measurements on Bodies of Revolution, Nov/Dec 1944.

3 Pfenninger, W.: Diss. Zürich, Untersuchungen über Reibungsverminderungen an Tragflügeln insbesondere mit Hilfe von Grenzschichtabsaugung, JFA Mitt., Zürich No. 13, 1946. English Translation, Investigation on Reductions of Friction on Wings in Particular by Means of Boundary Layer Suction, NACA TM 1181, August 1947.

4 Groth, E.: Low Speed Wind Tunnel Measurements on a Body of Revolution of Fineness Ratio 8, Northrop Aircraft, Inc., Report No. BLC-6, August 1953.

5 Summary of Laminar Boundary Layer Control Research, Northrop Aircraft Inc., WADC TR 56-111, July 1956.

6 Neumark, S.: Velocity Distribution on Thin Bodies of Revolution at Zero Incidence in Incompressible Flow, British R & M 2814, 1954.

7 Bolz, F. W., Kenyon, G. C. and Allen, C. Q.: Measurements of Boundary Layer Transition at Low Speed on Two Bodies of Revolution in a Low Turbulence Wind Tunnel, NACA RM A56G17, August 1956.

8 Pretsch, J.: The Excitation of Unstable Perturbations in a Laminar Friction Layer, NACA TM 1343, September 1952.

9 Mangler, W.: Connection Between Two- and Three-Dimensional Boundary Layers in Compressible Flow, German ZAMM, v. 28, 1949.

FORM 60-136A (R.8-55)

LIST OF TABLES AND FIGURES

FORM 60-136A (R.8-55)

TABLE I

LIST OF COORDINATES OF BODIES OF REVOLUTION

x (in)	radius (in.) ell	Mod. Sears-Haack	Mod. Parabolic	
0	0	0	0	
.25	.539	.291	.204	
.50	.762	.423	.296	
1.00	1.074	.624	.439	
2	1.511	.944	.676	
4	2.114	1.456	1.088	
6	2.560	1.888	1.467	
8	2.922	2.267	1.824	
10	3.230	2.608	2.163	
12	3.496	2.918	2.484	
16	3.938	3.459	3.073	
20	4.289	3.912	3.593	
24	4.570	4.290	4.042	
28	4.794	4.599	4.422	
32	4.969	4.845	4.730	
36	5.099	5.031	4.967	
40	5.188	5.159	5.132	
44	5.250	5.250	5.250	
47.25	5.250	5.250	5.250	
50.5	5.237	5.232	5.227	
54.5	5.188	5.154	5.132	
58.5	5.099	5.031	4.967	
62.5	4.969	4.845	4.730	
66.5	4.794	4.599	4.422	
70.5	4.570	4.290	4.042	
74.5	4.289	3.912	3.593	
78.5	3.938	3.459	3.089	
82.5	3.496	2.937	2.640	
86.5	2.944	2.481	2.289	
90.5	2.389	2.148	2.050	
94.5	1.988	1.956	1.934	
96.0	1.912	1.912	1.912	(radius of supporting sting)
nose radius (in.)	.583	.160	.078	

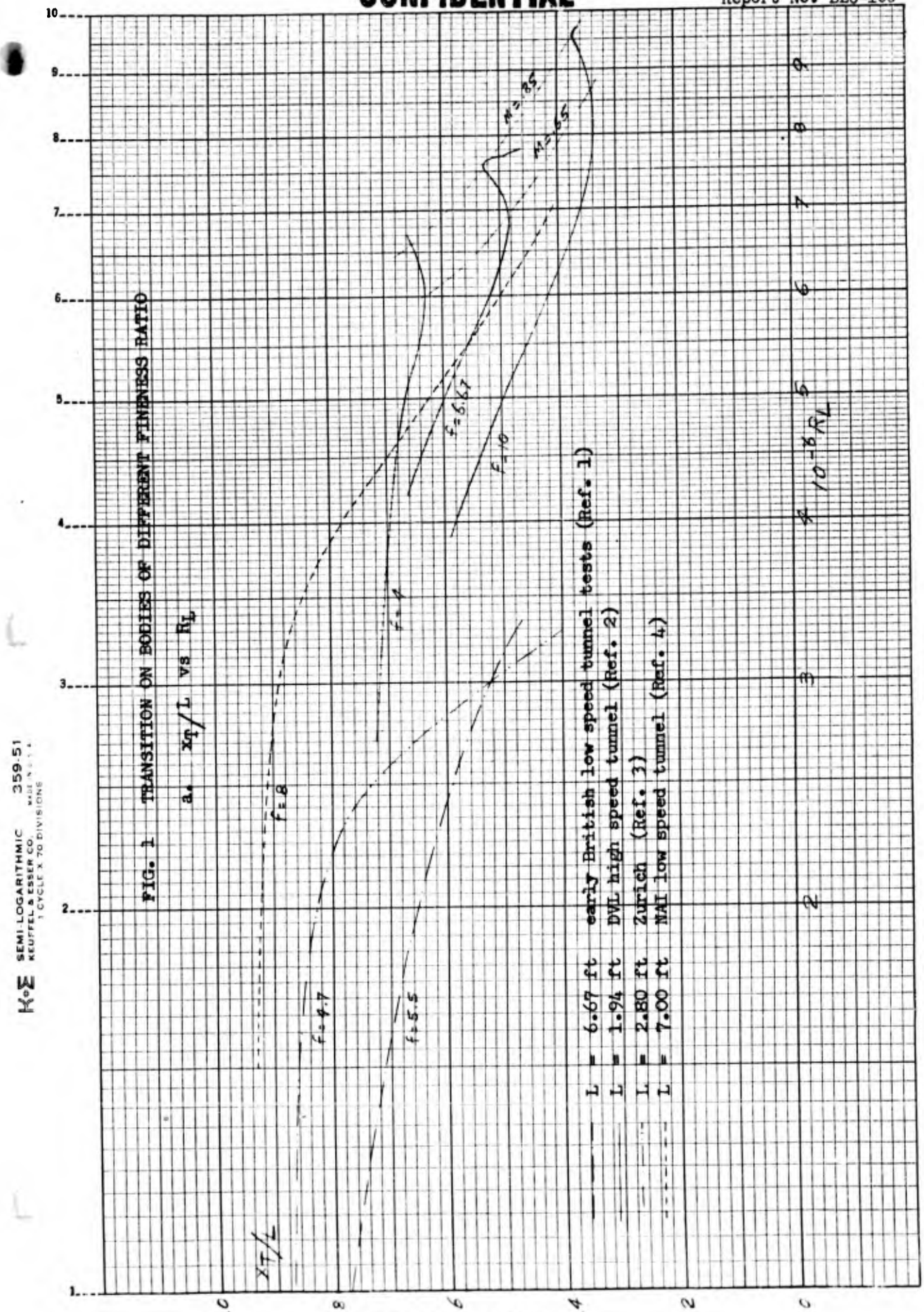
FIG. 1 TRANSITION ON BODIES OF DIFFERENT FINENESS RATIO
a. x_t/L vs R_L
x_t/L
$R_L = 10^{-6} RL$
f=8
f=6.67
f=5.5
f=4.7
f=4
f=3.85
f=3.55
f=10
L = 6.67 ft early British low speed tunnel tests (Ref. 1)
L = 1.94 ft DVL high speed tunnel (Ref. 2)
L = 2.80 ft Zurich (Ref. 3)
L = 7.00 ft NAI low speed tunnel (Ref. 4)
KE SEMI-LOGARITHMIC 359-51
KEUFFEL & ESSER CO.
1 CYCLE X 70 DIVISIONS

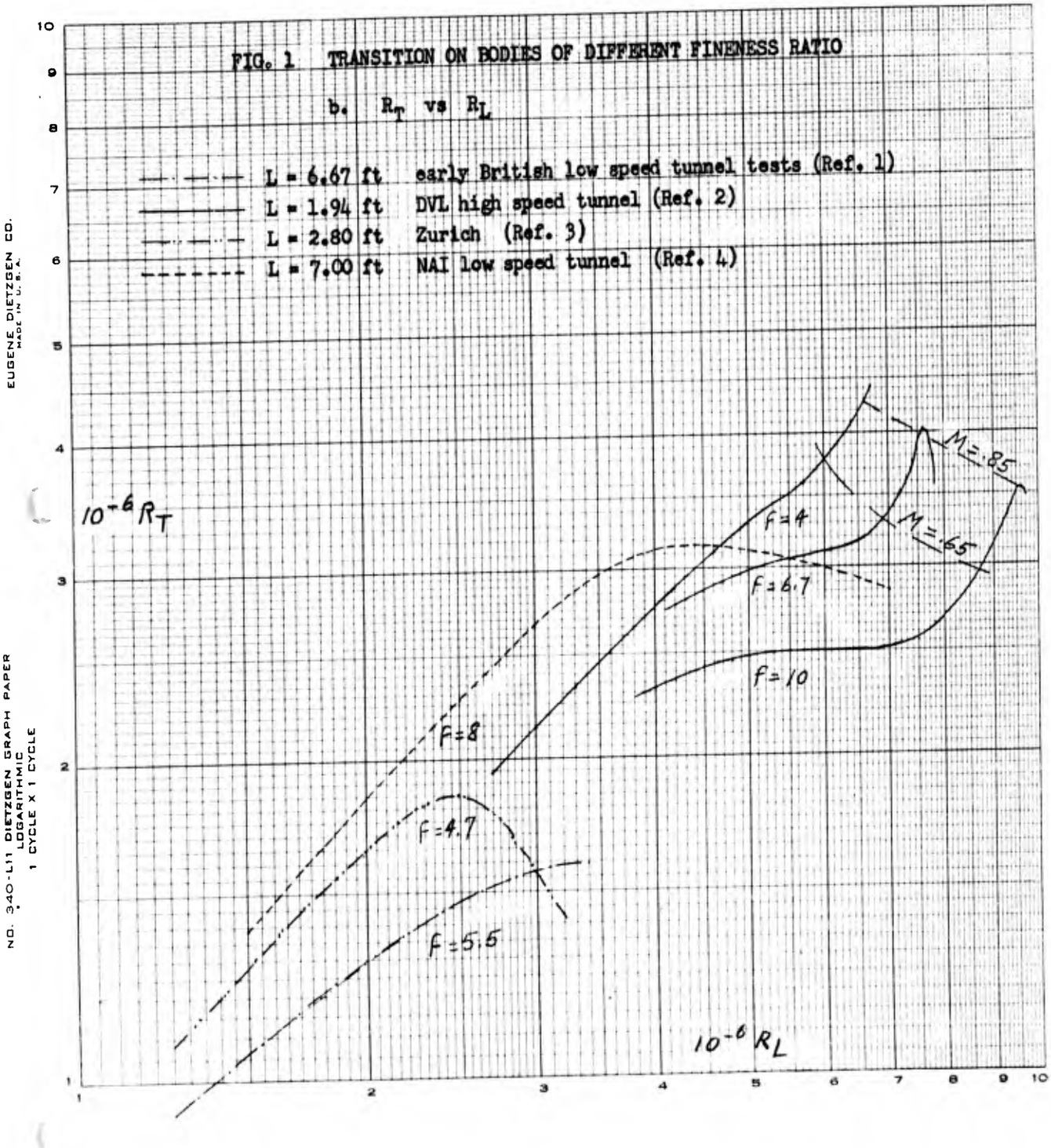
FIG. 1 TRANSITION ON BODIES OF DIFFERENT FINENESS RATIO
b. R_T vs R_L
L = 6.67 ft early British low speed tunnel tests (Ref. 1)
L = 1.94 ft DVL high speed tunnel (Ref. 2)
L = 2.80 ft Zurich (Ref. 3)
L = 7.00 ft NAI low speed tunnel (Ref. 4)
$10^{-6} R_T$
$10^{-6} R_L$
M=.85
M=.65
f=4
f=6.7
f=10
f=8
f=4.7
f=5.5
EUGENE DIETZGEN CO.
MADE IN U.S.A.
NO. 340-L11 DIETZGEN GRAPH PAPER
LOGARITHMIC
1 CYCLE X 1 CYCLE

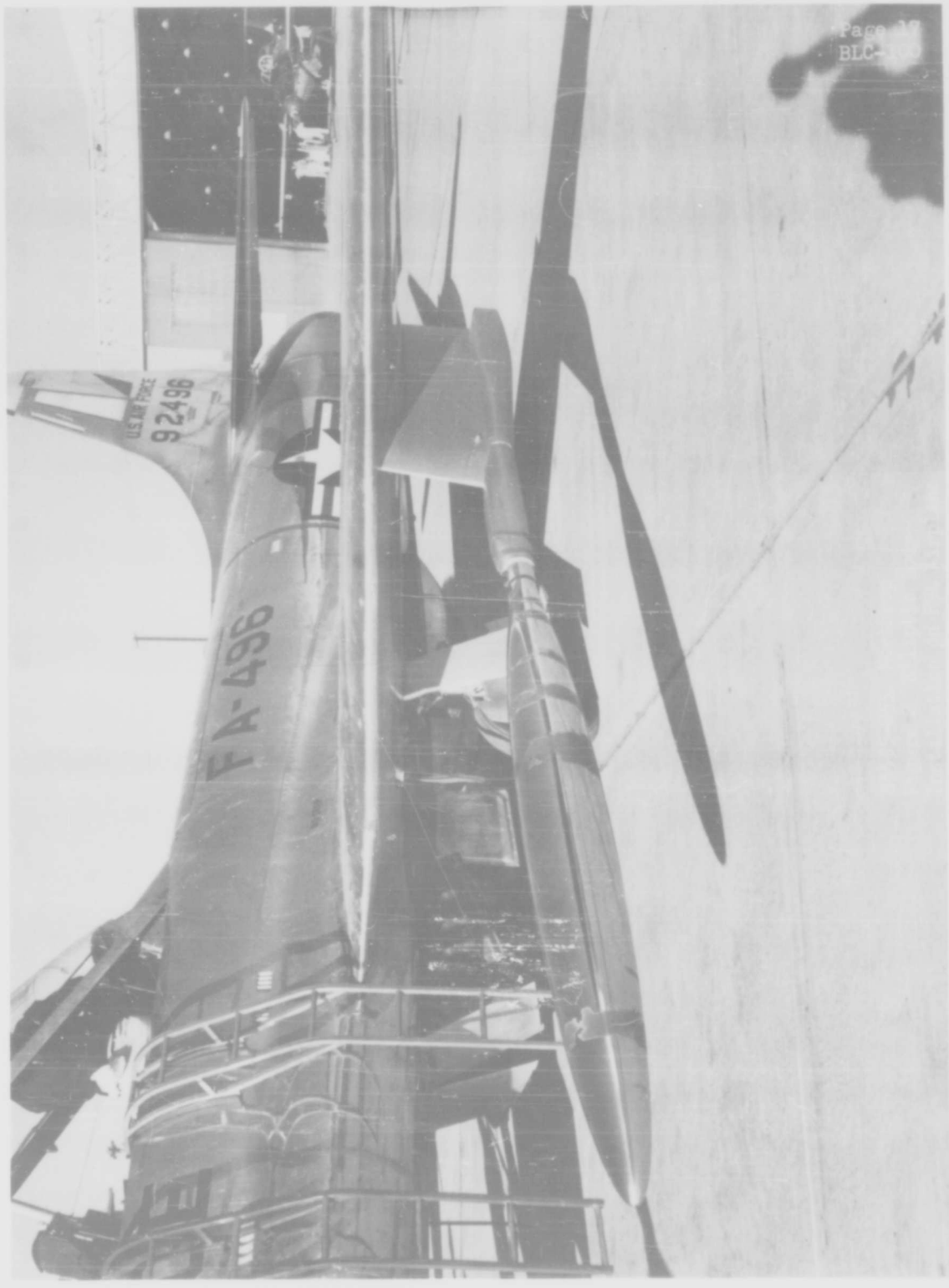
U.S. AIR FORCE
92496
FA-496

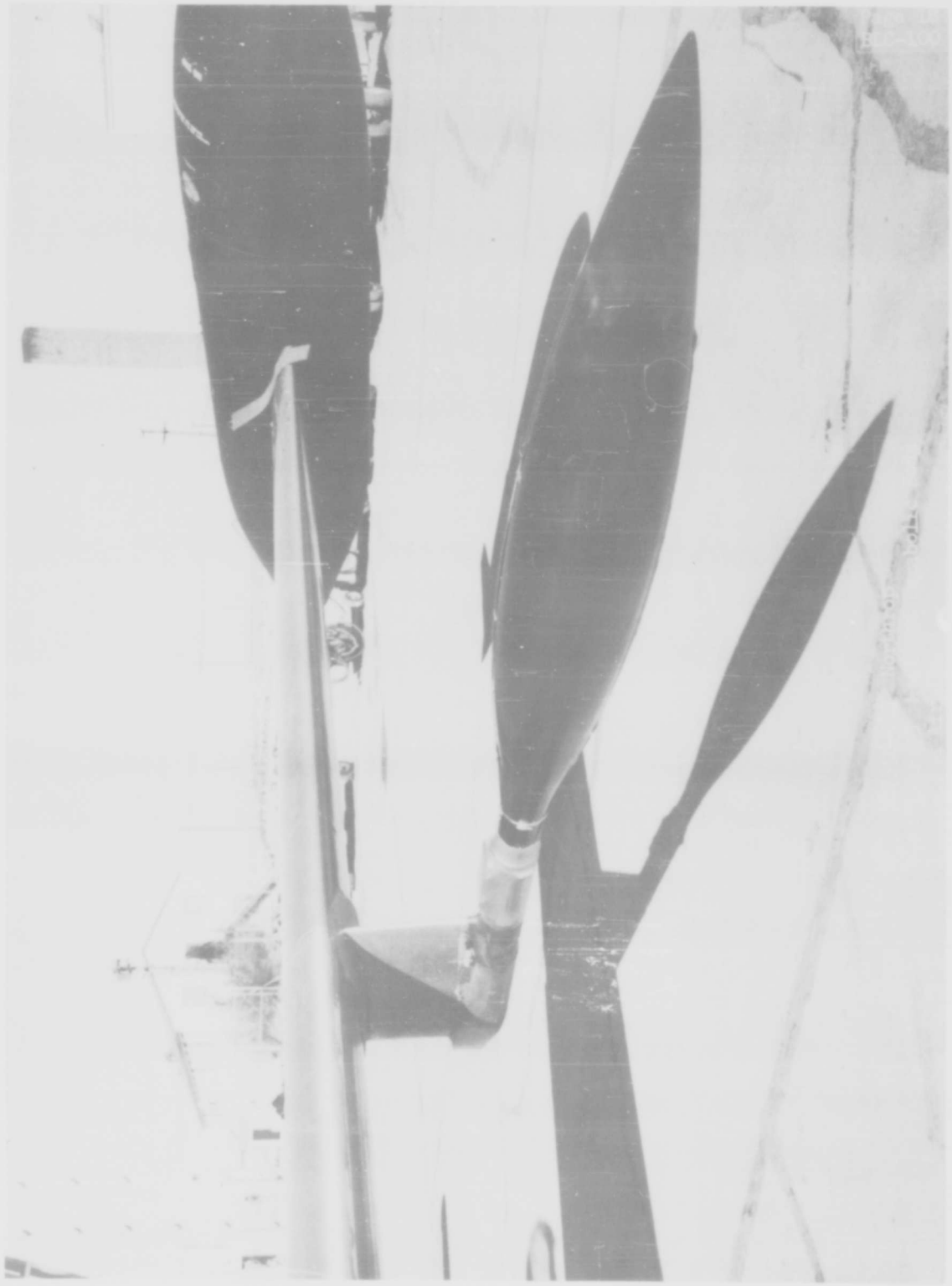

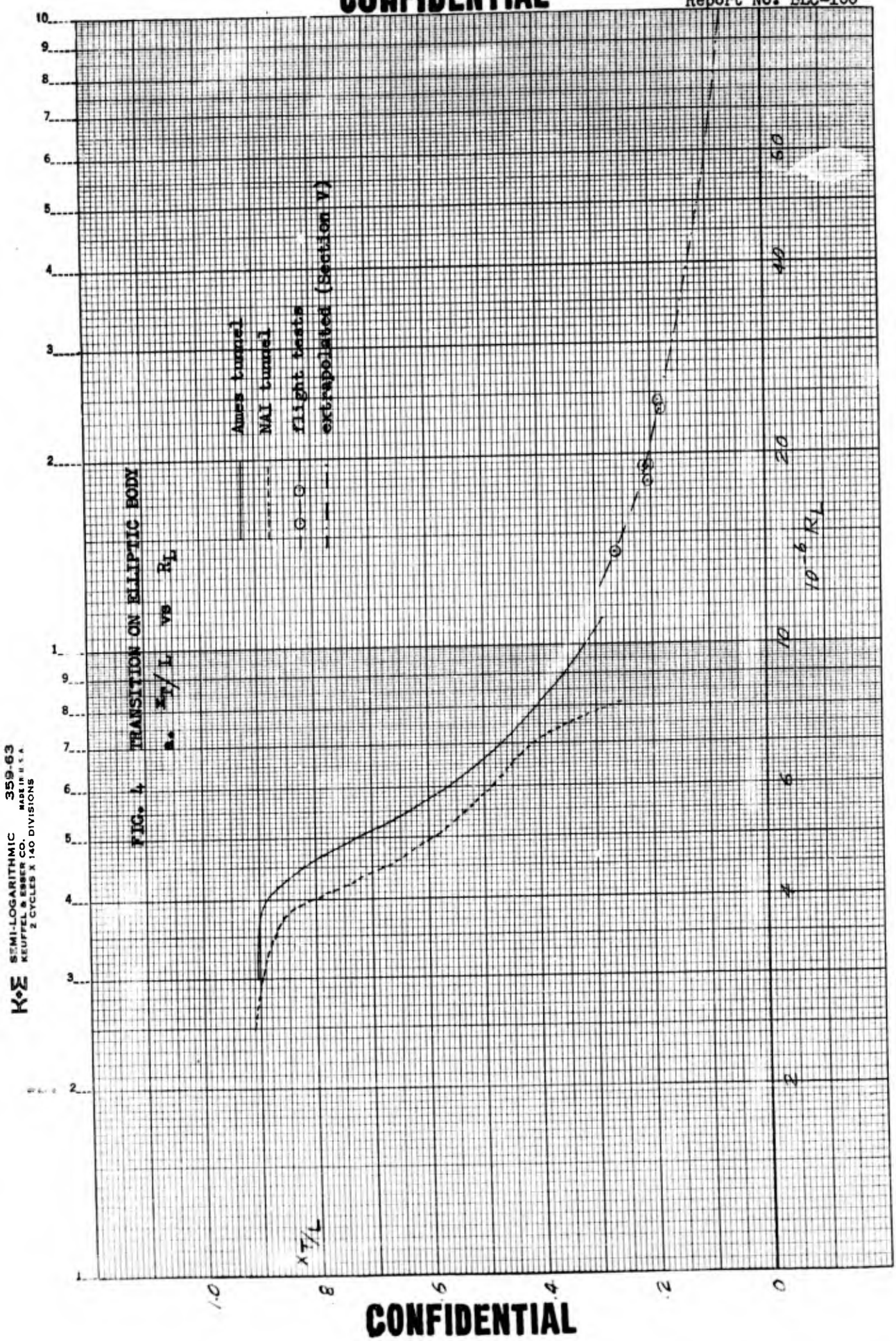

FIG. 4 TRANSITION ON ELLIPTIC BODY
a. x_T/L vs R_L

K+E SEMI-LOGARITHMIC 359-63
KEUFFEL & ESSER CO. MADE IN U.S.A.
2 CYCLES X 140 DIVISIONS

FIG. 4 TRANSITION ON ELLIPTIC BODY

b. R_T vs R_L

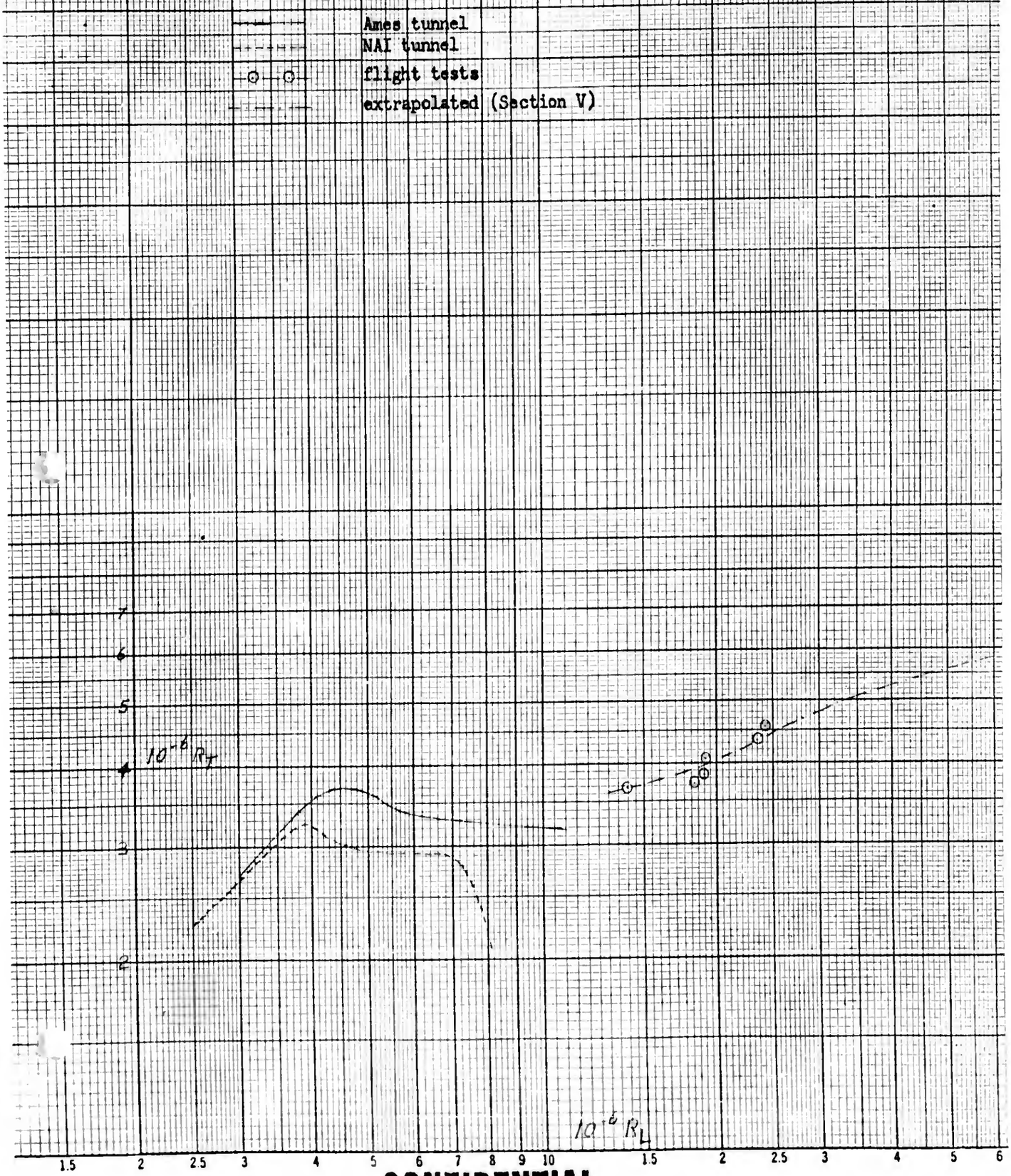

Form 20-10A
(R. 6-51)

ENGINEER: E. E. Groth	NORTHROP AIRCRAFT INC.	PAGE: 21
CHECKER:		REPORT NO.: BLC-100
DATE:		MODEL:

FIG. 5 PRESSURE DISTRIBUTION ALONG ELLIPTIC BODY AT DIFFERENT TUNNEL POSITIONS (NAI tunnel)

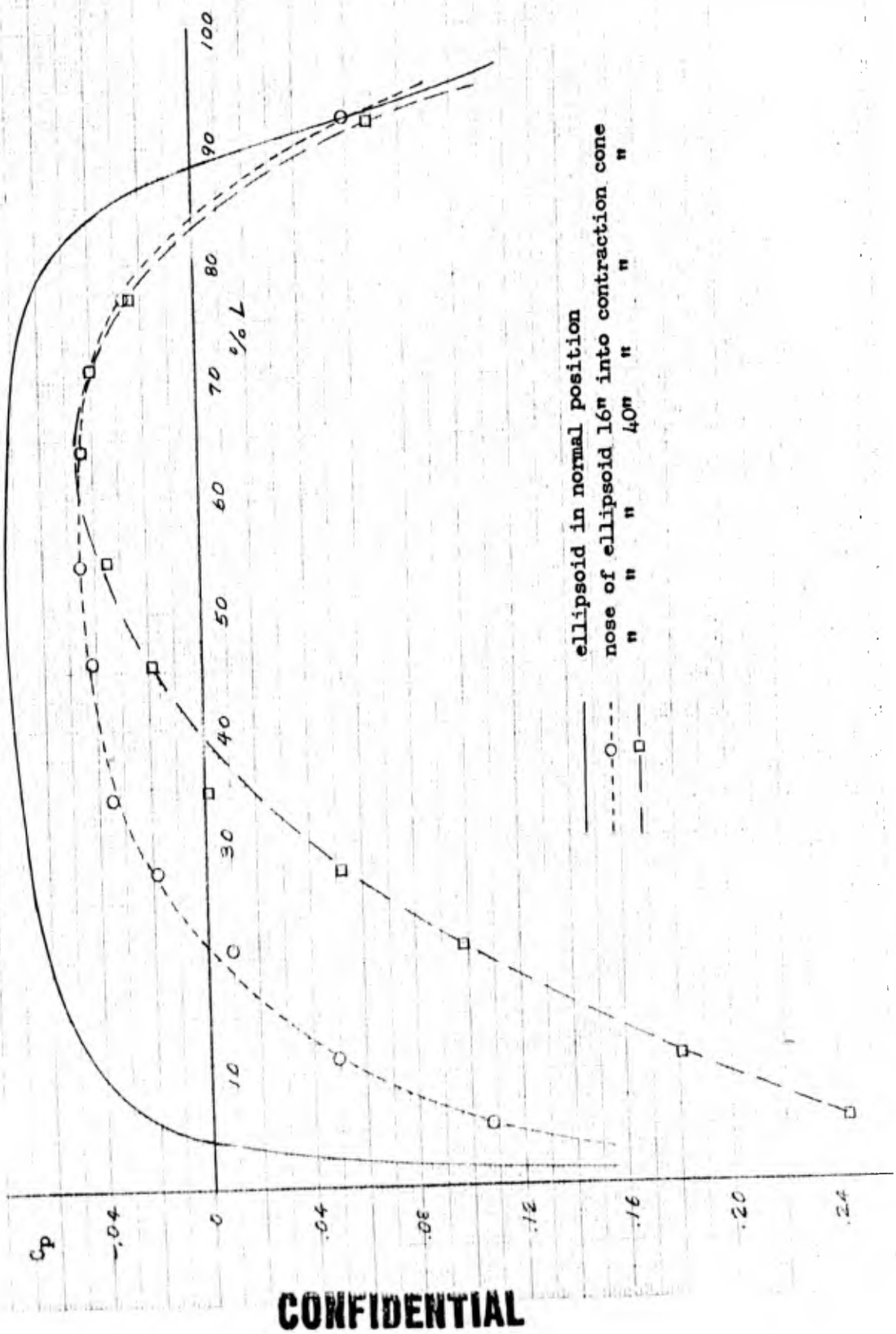

CONFIDENTIAL

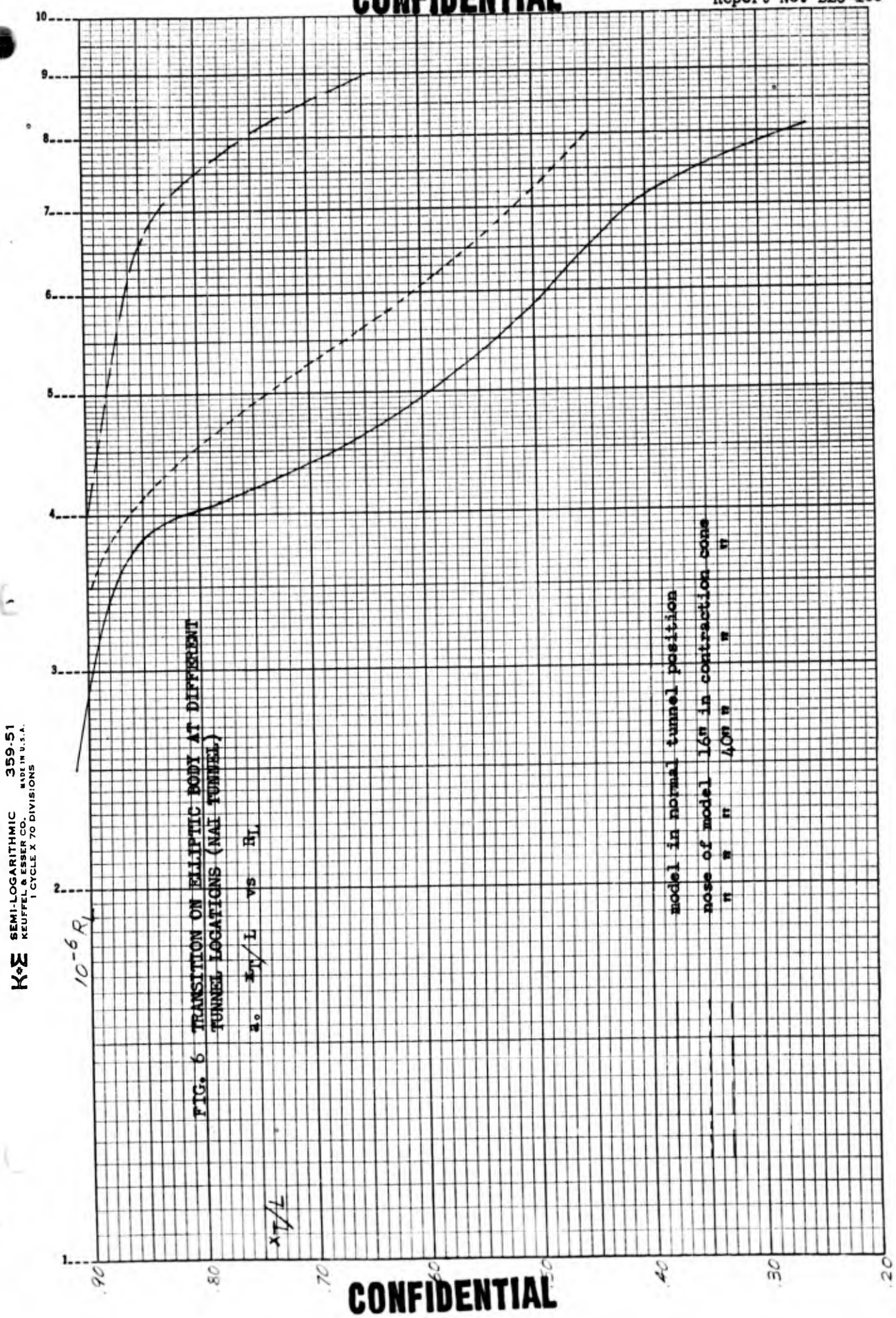

CONFIDENTIAL

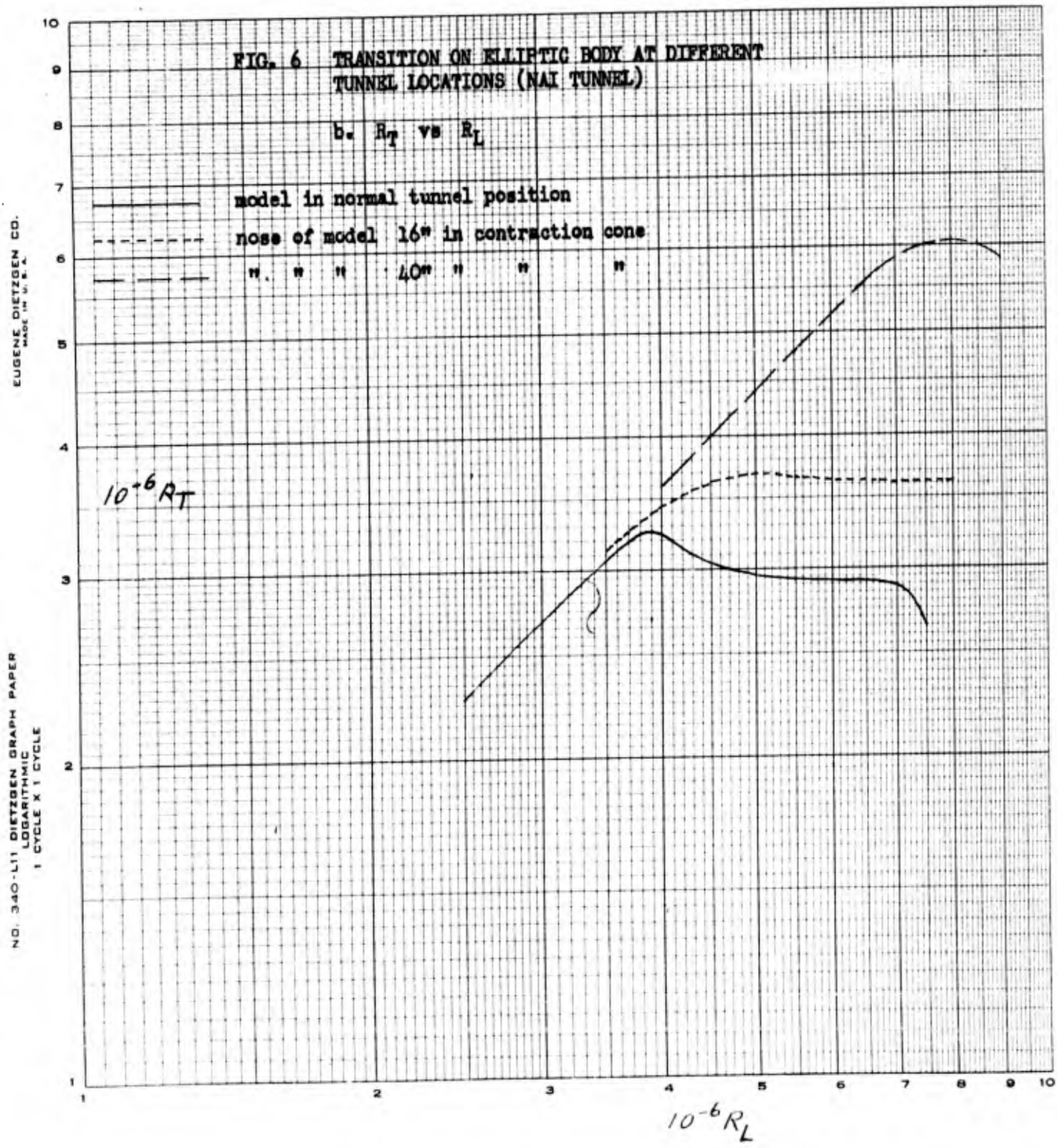
FIG. 6 TRANSITION ON ELLIPTIC BODY AT DIFFERENT TUNNEL LOCATIONS (NAI TUNNEL)
b. R_T vs R_L
model in normal tunnel position
nose of model 16" in contraction cone
" " " 40" " " "
$10^{-6} R_T$
$10^{-6} R_L$
EUGENE DIETZGEN CO.
NO. 340-L11 DIETZGEN GRAPH PAPER
LOGARITHMIC
1 CYCLE X 1 CYCLE

FORM 20-10A (R. 6-51)

ENGINEER: E. E. Groth	NORTHROP AIRCRAFT INC.	PAGE: 24
CHECKER:		REPORT NO.: BLC-100
DATE:		MODEL:

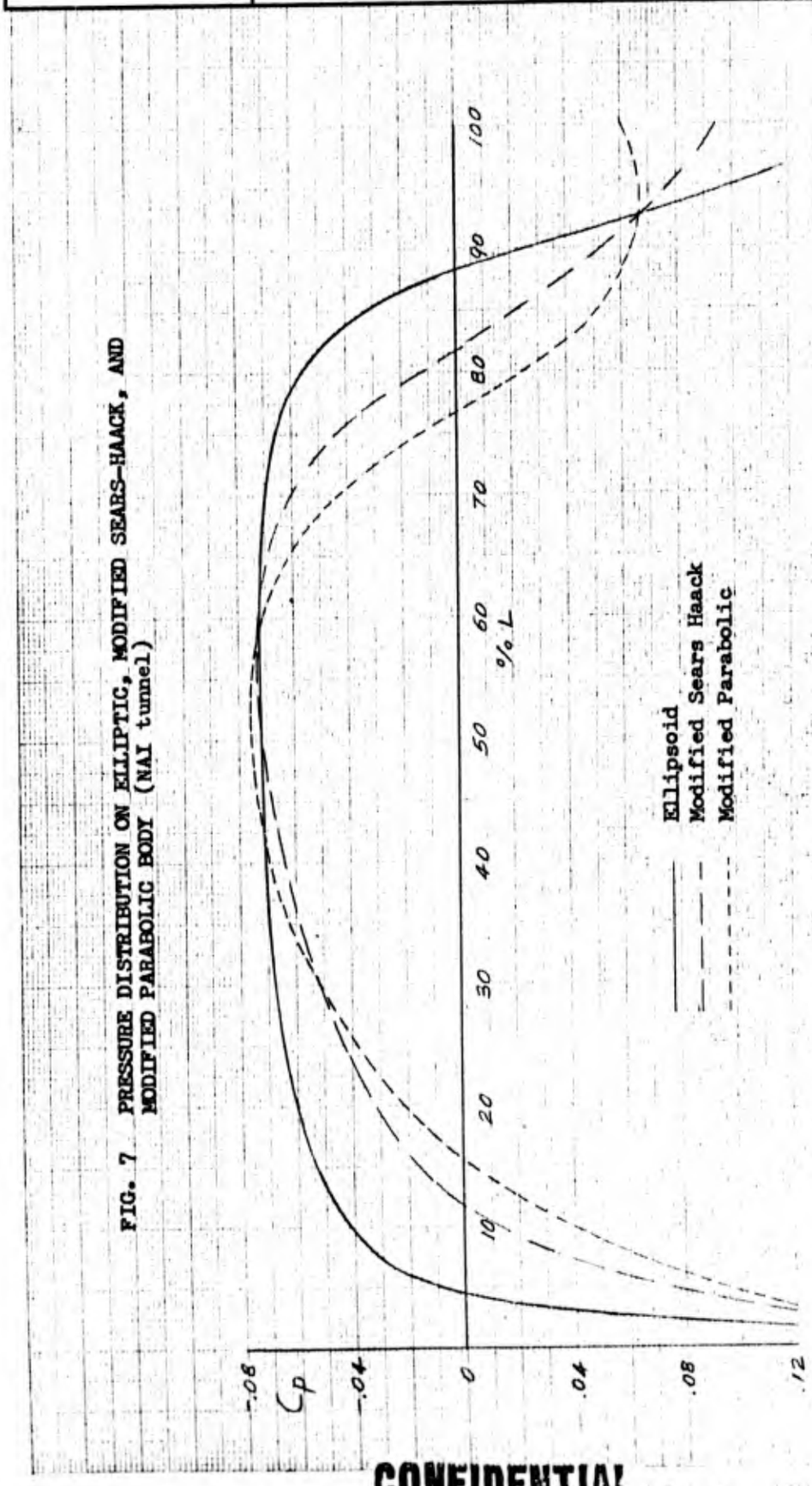

FIG. 7 PRESSURE DISTRIBUTION ON ELIPTIC, MODIFIED SEARS-HAACK, AND MODIFIED PARABOLIC BODY (NAI tunnel)

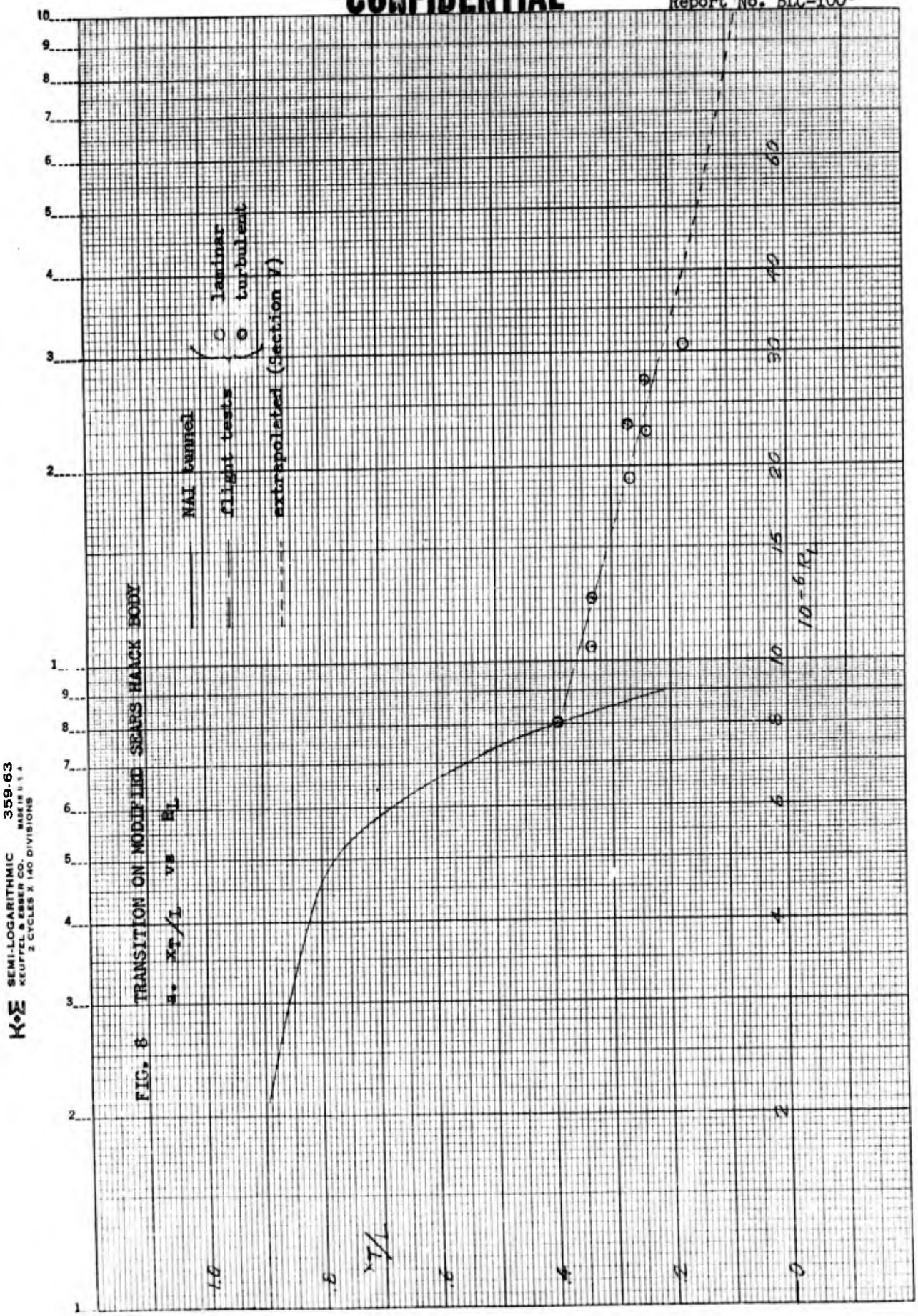

FIG. 8 TRANSITION ON MODIFIED SEARS HAACK BODY
a. x_T/L vs R_L

K&E 359-63 SEMI-LOGARITHMIC KEUFFEL & ESSER CO. MADE IN U.S.A. 2 CYCLES X 140 DIVISIONS

FIG. 8 TRANSITION ON MODIFIED SEARS HAACK BODY

b. R_T vs R_L

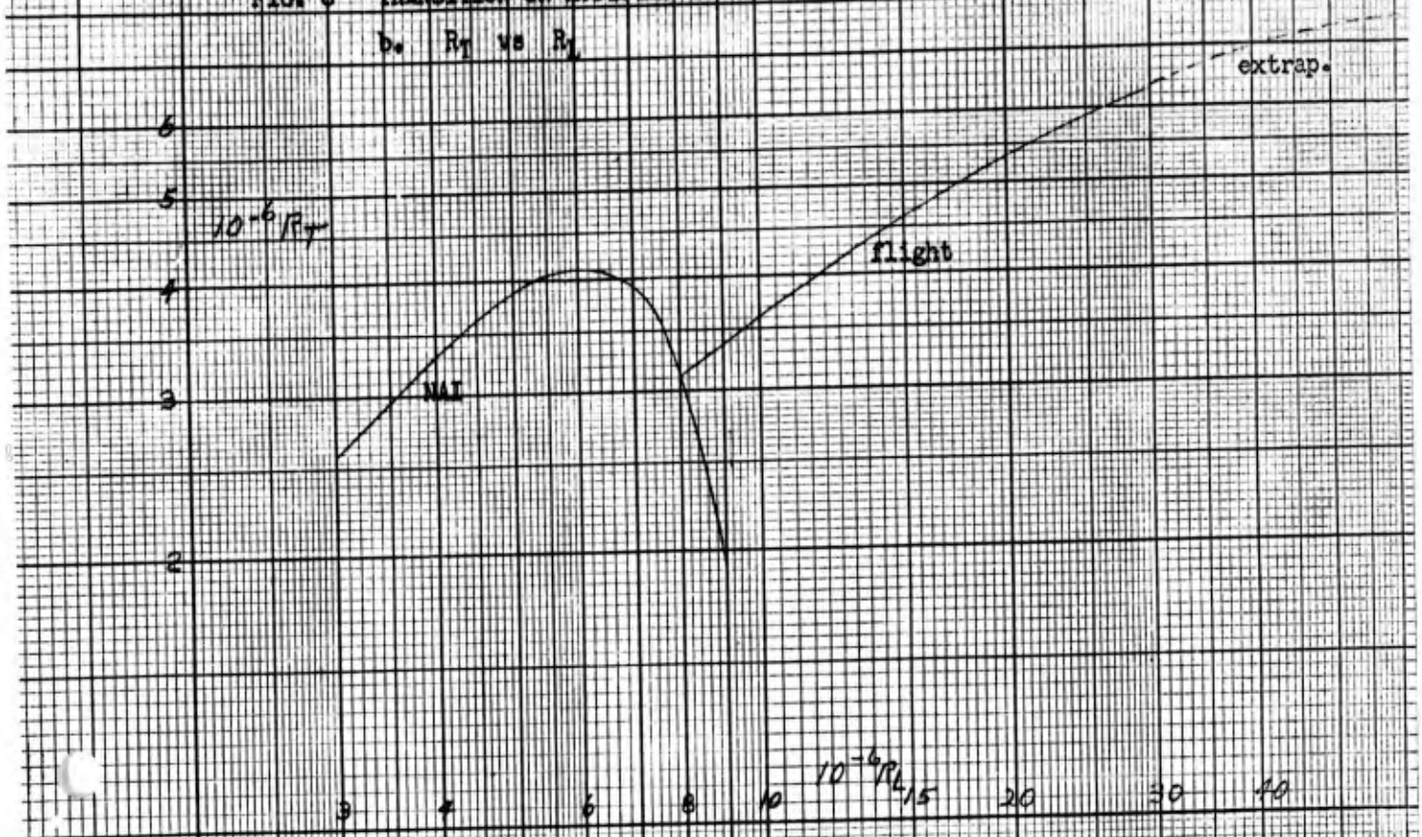

FIG. 9 TRANSITION ON MODIFIED PARABOLIC BODY

b. R_T vs R_L

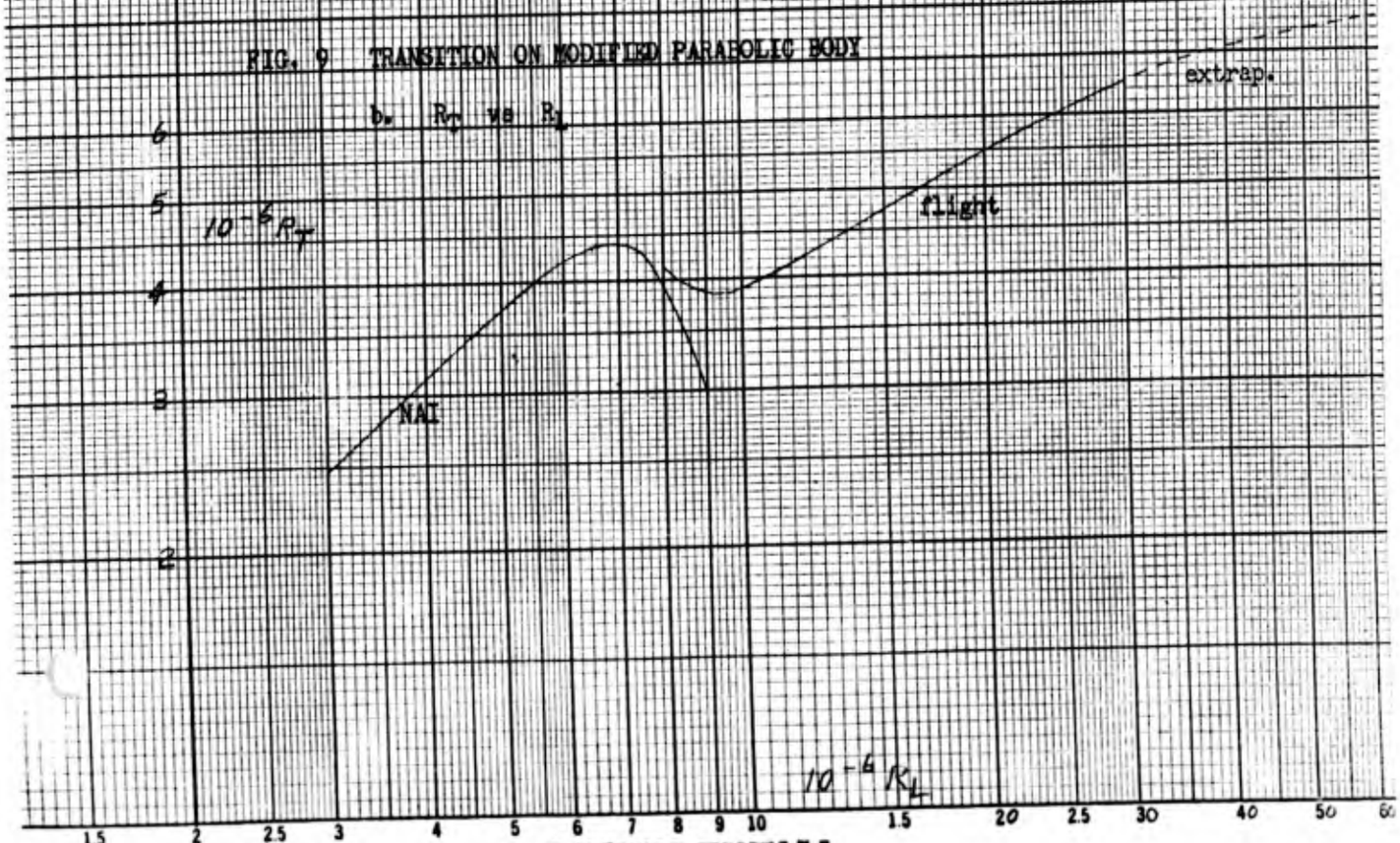

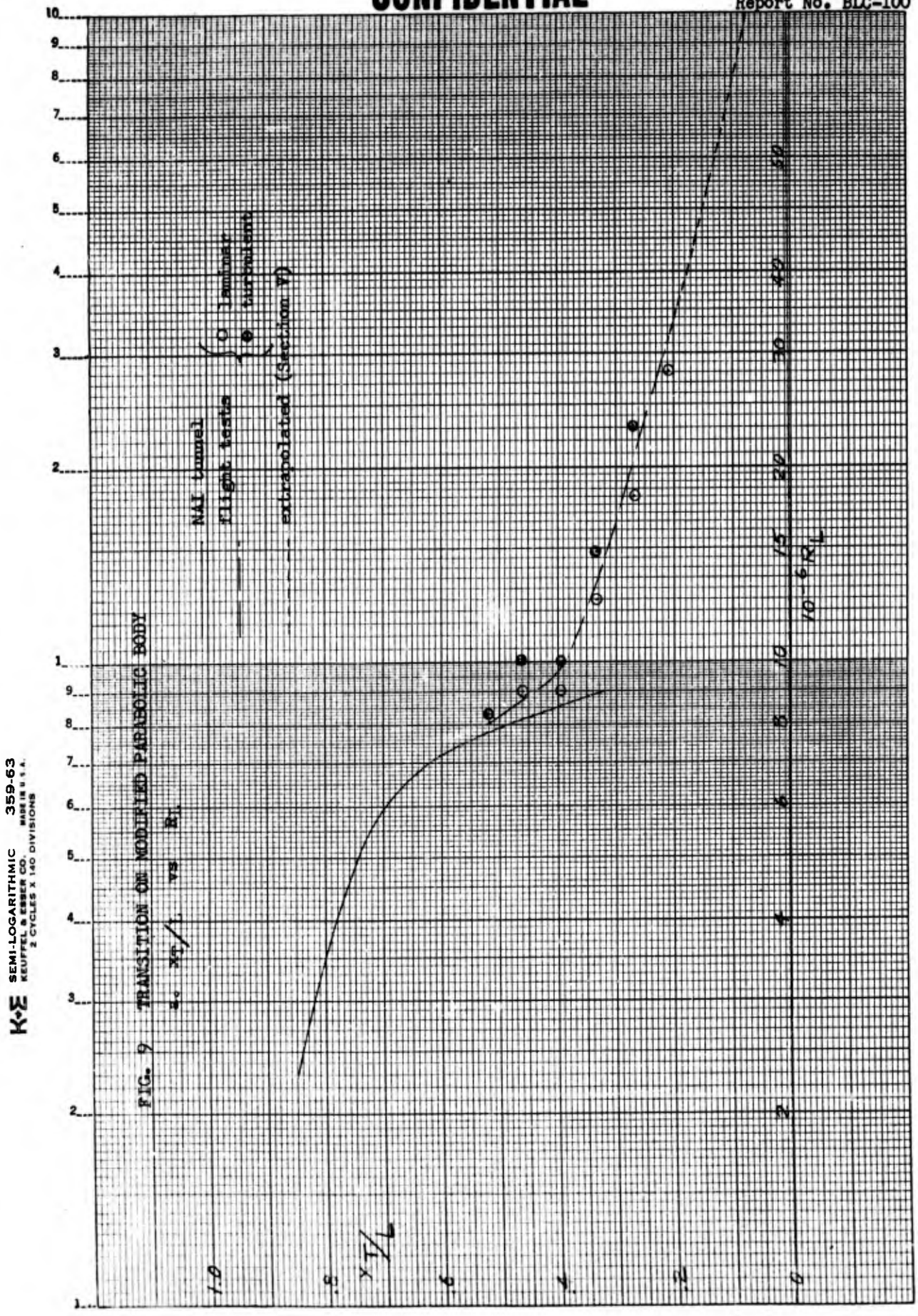

FIG. 9 TRANSITION ON MODIFIED PARABOLIC BODY

x_T/L vs R_L

KEUFFEL & ESSER CO. MADE IN U.S.A. 359-63 SEMI-LOGARITHMIC 2 CYCLES X 140 DIVISIONS

FORM 20-10A
(R. 6-51)

ENGINEER: E. E. Groth	NORTHROP AIRCRAFT INC.	PAGE: 28
CHECKER:		REPORT NO.: BLC-100
DATE:		MODEL:

FIG. 10 THEORETICAL TWO-DIMENSIONAL TRANSITION PARAMETER $R_{\theta_{cr}}^{(2)}$ vs m (Ref. 8)

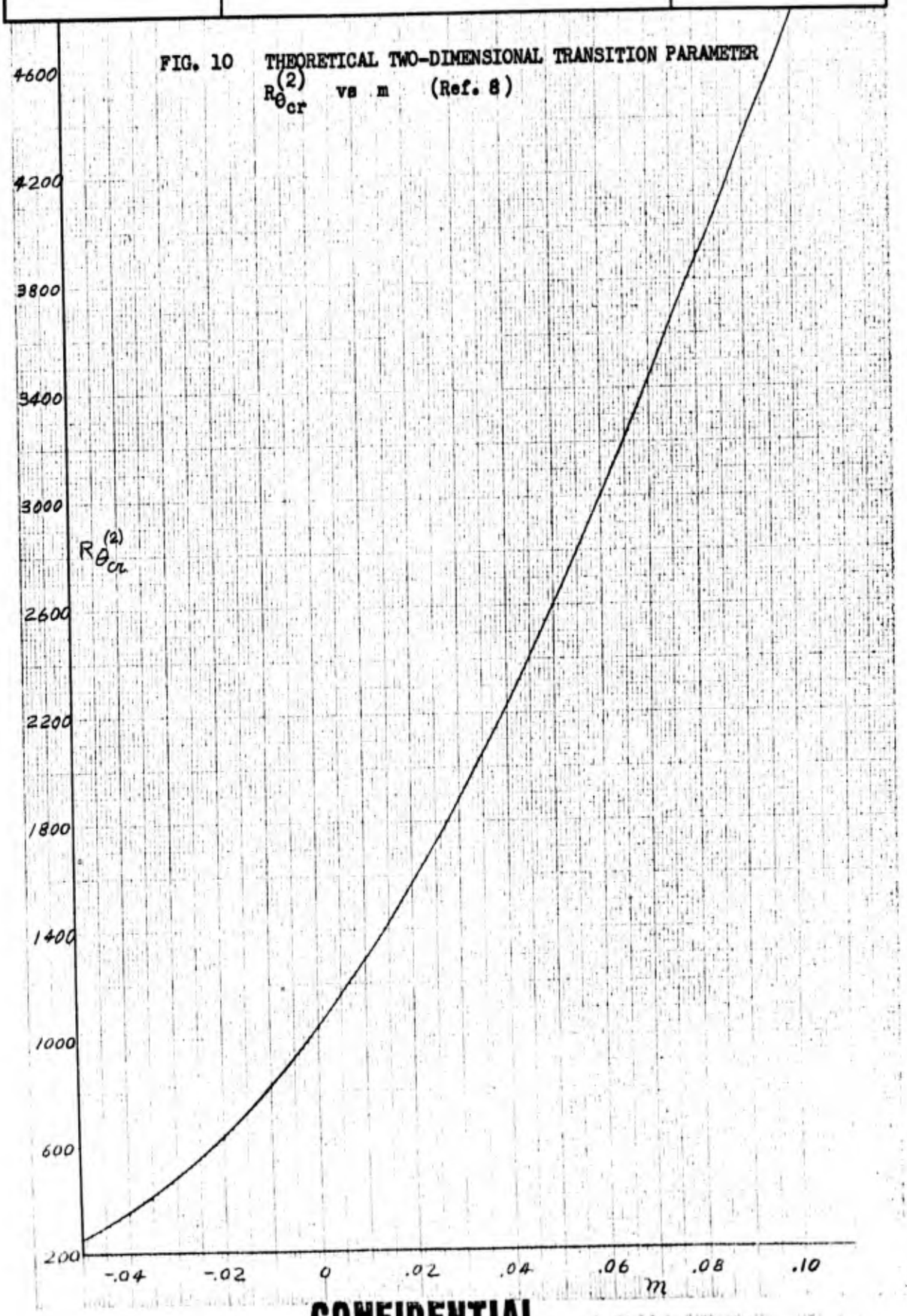

FORM 20-10A (R. 6-51)

ENGINEER	NORTHROP AIRCRAFT INC.	PAGE
E. E. Groth		29
CHECKER		REPORT NO.
		BLC-100
DATE		MODEL

FIGURE 11

θ^* vs x/L FOR THE ELLIPTIC, MODIFIED SEARS HAACK, AND MODIFIED PARABOLIC BODY

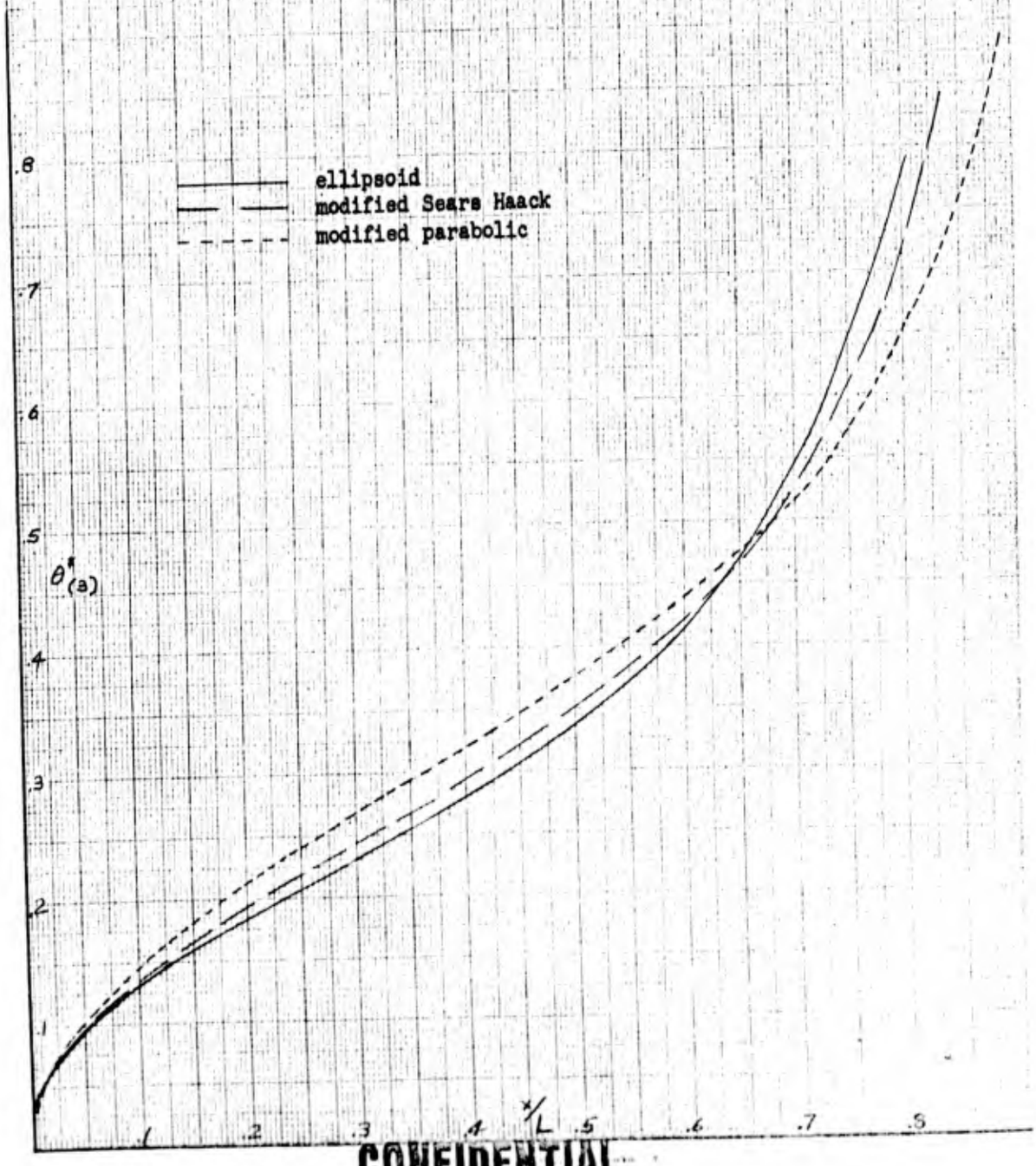

FORM 20-10A (R. 6-51)

ENGINEER: E. E. Groth	NORTHROP AIRCRAFT INC.	PAGE: 30
CHECKER:		REPORT NO.: BLC-100
DATE:		MODEL:

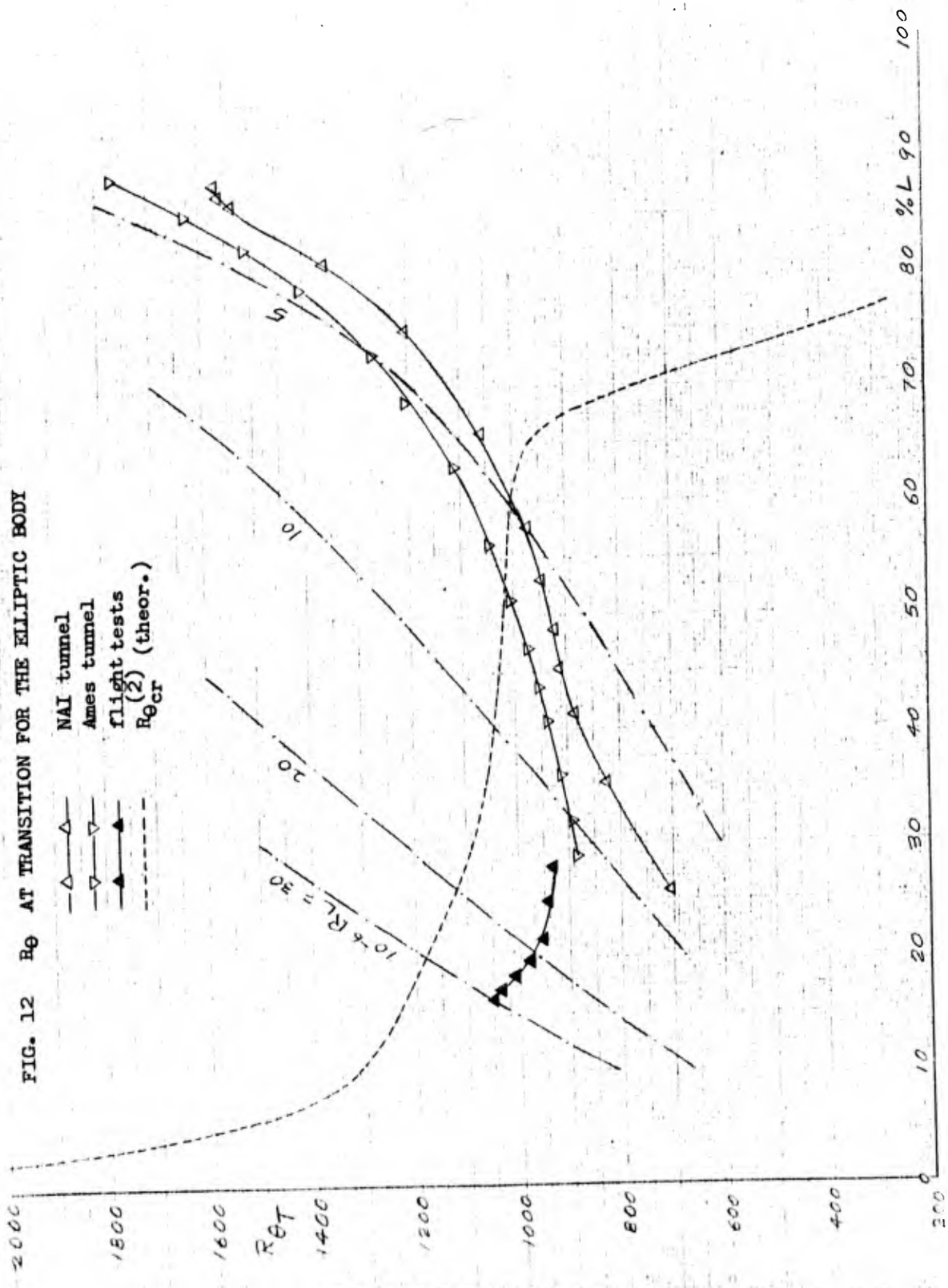

FORM 20-10A
(R. 6-51)

ENGINEER: E. E. Groth	NORTHROP AIRCRAFT INC.	PAGE: 31
CHECKER:		REPORT NO.: BLC-100
DATE:		MODEL:

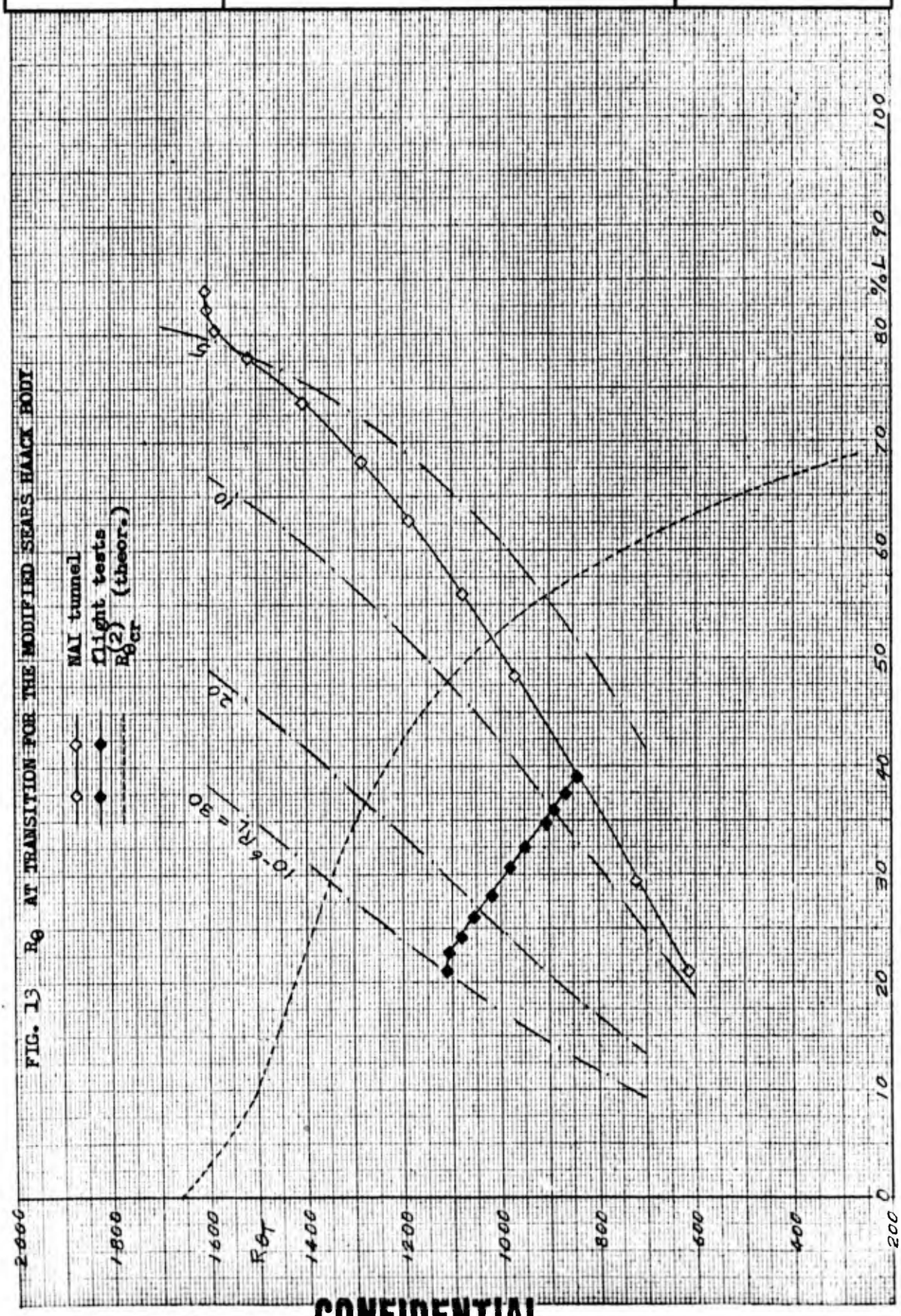

FIG. 13 R_θ AT TRANSITION FOR THE MODIFIED SEARS HAACK BODY

FORM 20-10A (R. 6-51)

ENGINEER: E. E. Groth	NORTHROP AIRCRAFT INC.	PAGE: 32
CHECKER:		REPORT NO.: BLC-100
DATE:		MODEL:

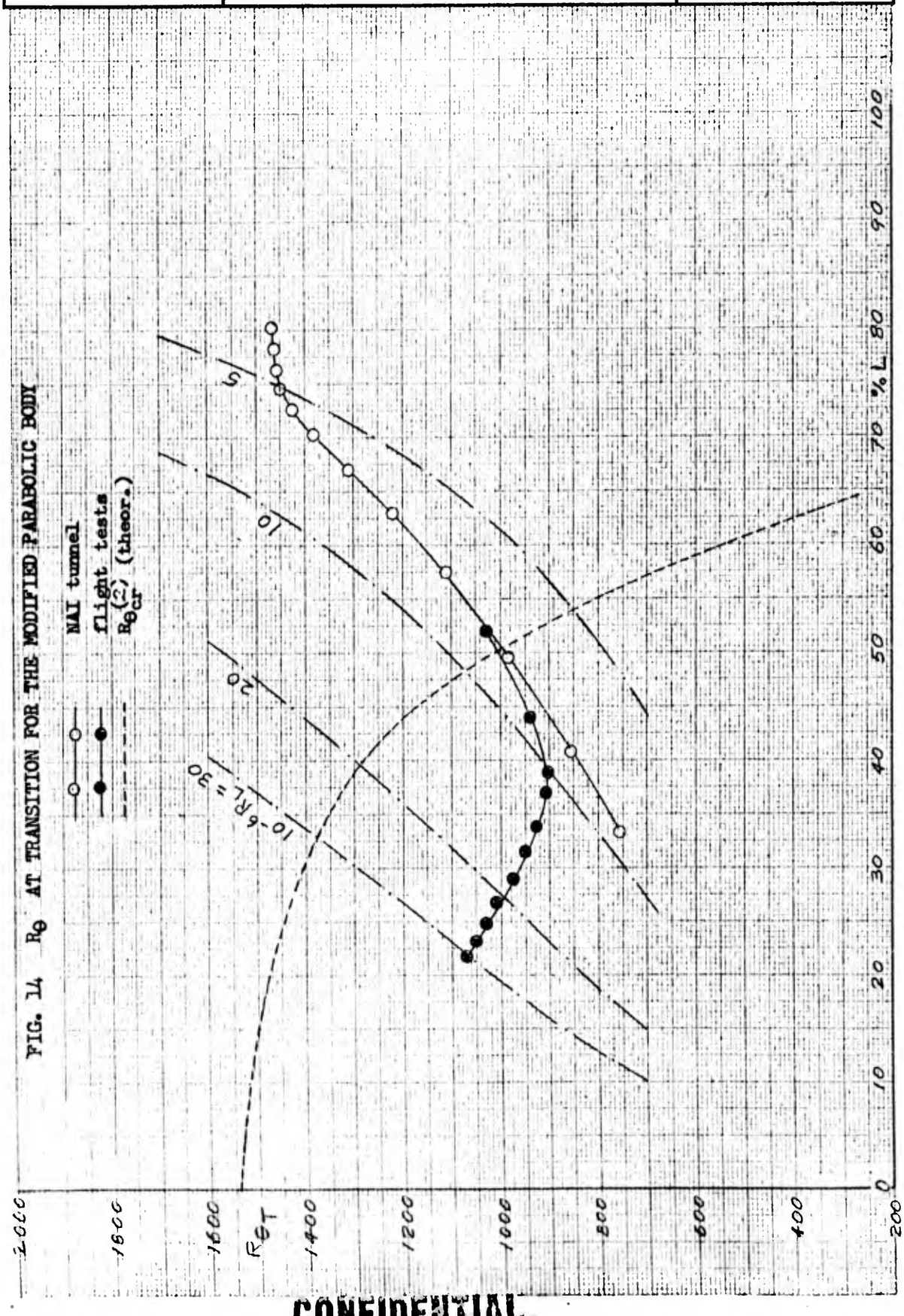

FIG. 14 R_θ AT TRANSITION FOR THE MODIFIED PARABOLIC BODY

FORM 20-10A
(R. 6-51)

ENGINEER E. E. Groth	NORTHROP AIRCRAFT INC.	PAGE 33
CHECKER		REPORT NO. BLC-100
DATE		MODEL

FIG. 15 SLOPES OF THE BODIES UNDER CONSIDERATION

$\frac{L}{r}\frac{dr}{dx}$ vs $\frac{x}{L}$

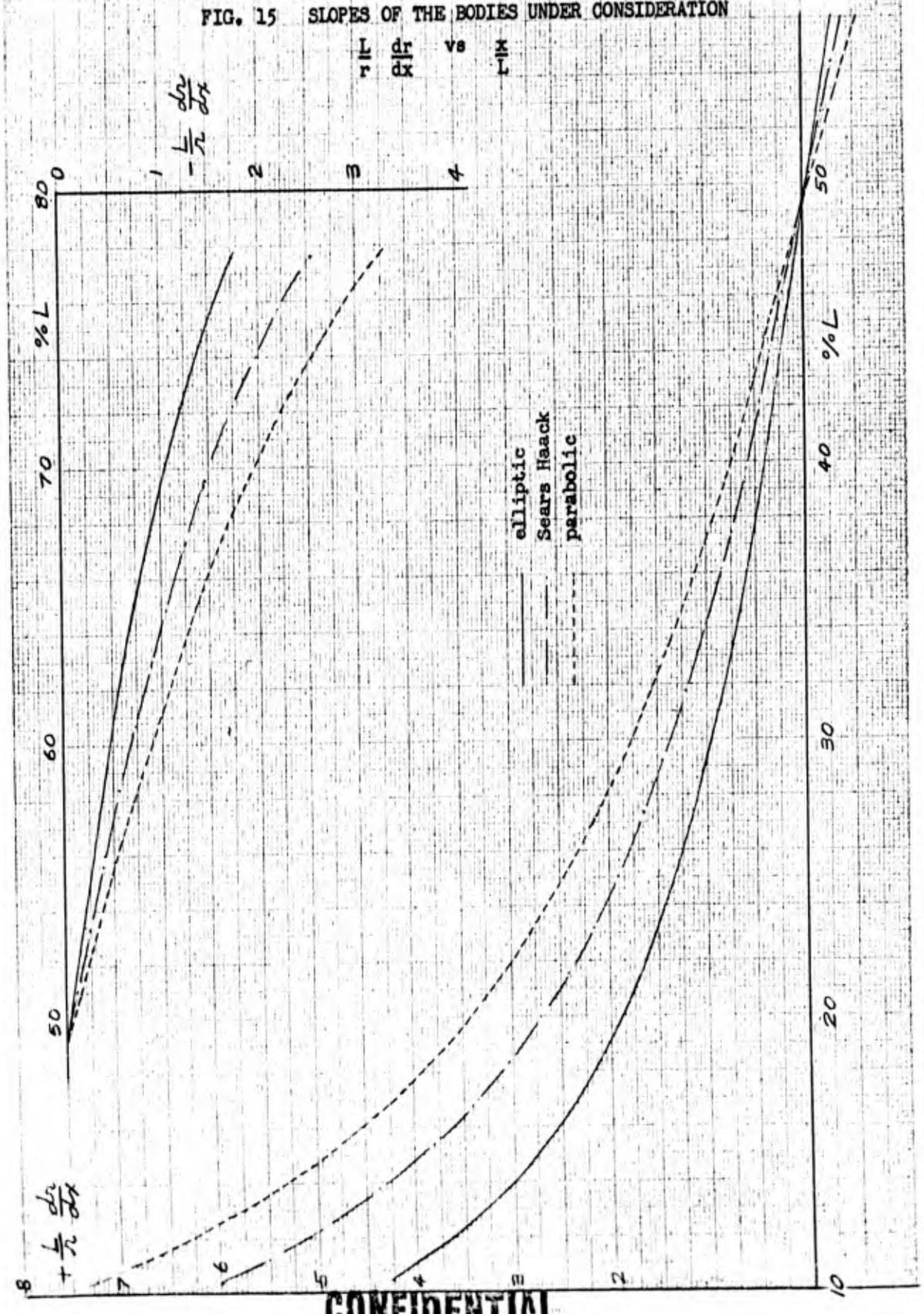

FORM 20-10A (R. 6-51)

ENGINEER: E. E. Groth	NORTHROP AIRCRAFT INC.	PAGE: 34
CHECKER:		REPORT NO.: BLC-100
DATE:	FIG. 16 $R_{\theta_T}/R_{\theta_{cr}^{(2)}}$ vs $\frac{L}{r}\frac{dr}{dx}$	MODEL:

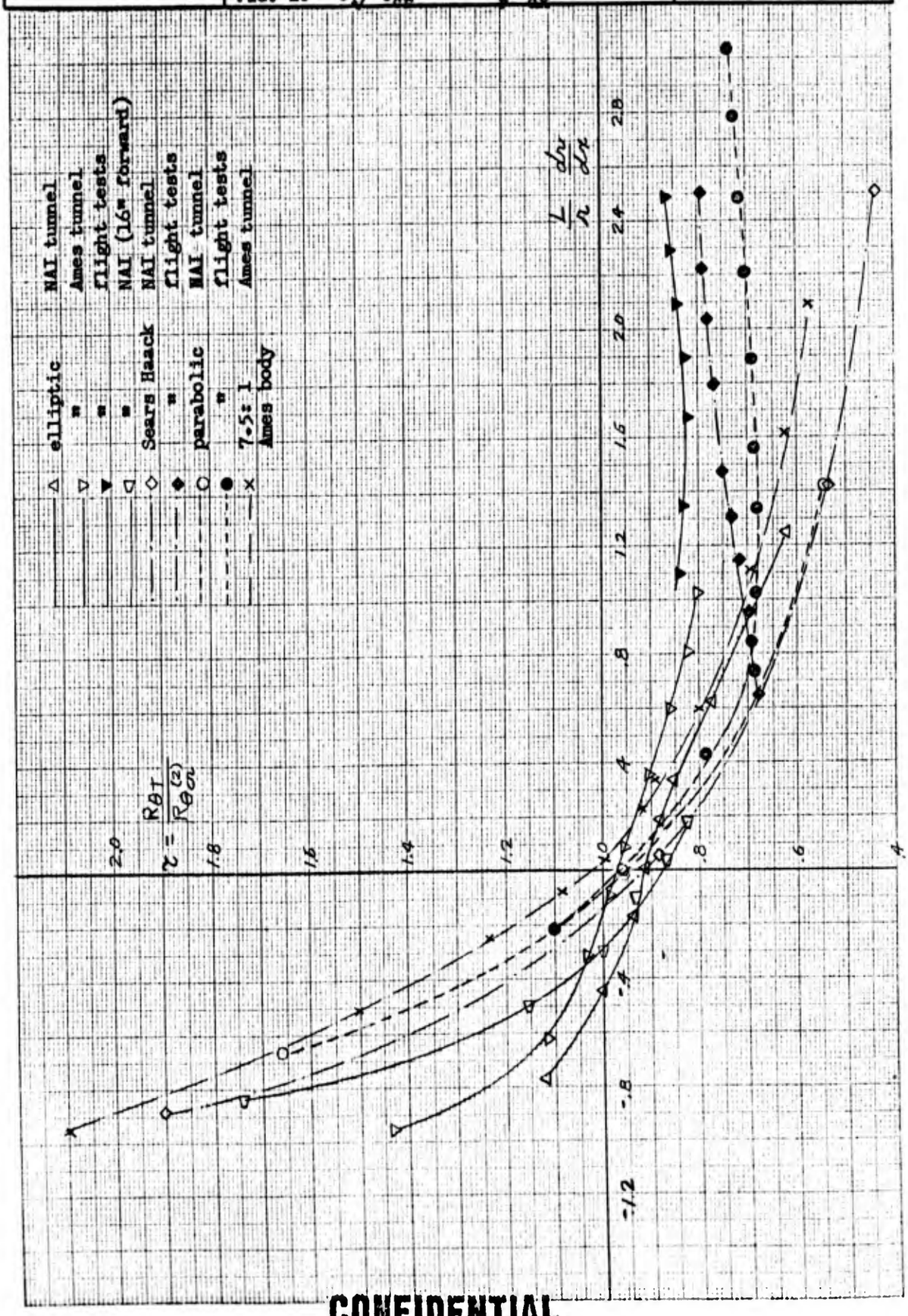

AD-150527(c)

GPO
AD-150 527 (c) (24 Feb 58 jb) CONFIDENTIAL

Northrop Aircraft, Inc., Hawthorne, Calif.
LOW DRAG BOUNDARY LAYER SUCTION EXPERIMENTS IN FLIGHT ON THE WING GLOVE OF AN F94A AIRPLANE. PHASE III. LAMINAR SUCTION AIRFOIL TOLERANCES, by B. H. Carmichael and R. C. Whites. Aug 57 [47]p. incl. illus. tables (Rept. no. NAI 57-1163; NLC-101) (Appendice to Northrop Aircraft, Inc., Contract AF 33(616)3168, Progress rept. for 1-30 Sep 57, AD-150 527)

Confidential report

I. II. Authors
III. Northrop Aircraft, Inc., Hawthorne, Calif.
IV. Contract AF 33(616)3168

CONFIDENTIAL

NORTHROP AIRCRAFT, INC.

HAWTHORNE, CALIFORNIA

REPORT NO. NAI-57-1163
REPORT NO. BLC-101

LOW DRAG BOUNDARY LAYER SUCTION EXPERIMENTS IN FLIGHT ON THE WING GLOVE OF AN F94A AIRPLANE

PHASE III - LAMINAR SUCTION AIRFOIL TOLERANCES

August 1957

PREPARED BY

B. H. Carmichael
B. H. Carmichael

Roy C. W Rites
R. C. Whites

W. Pfenninger

APPROVED BY

W. Pfenninger

REVISIONS

CHG. NO.	DATE	ENGR.	PAGES AFFECTED	REMARKS

CONFIDENTIAL

FORM 20-5 (R.9-54)

TABLE OF CONTENTS

TABLE OF CONTENTS (cont'd.)

I. SUMMARY

Four types of deviation from the high quality condition of the 69-slot suction airfoil as mounted on the F94A are summarized below. The first three conclusions are approximately true over the entire flight condition range described by Fig. 3.

(1) The suction level as an even distribution could be increased 75 per cent, any individual chamber suction could be increased 170 per cent, and very uneven suction distributions could be tolerated before the flow at the trailing edge became turbulent.

(2) Local blockages of suction slots which are flush with the surface, limit the maximum permissible inflow. For blockage spans between 1 and 10 times the local boundary layer momentum thickness, the maximum permissible inflow is lower than that normally employed for this model. Laminar flow for these cases was retained by slight suction increases at other chordwise positions.

(3) At 28%-chord, the permissible surface wave height for a 2.00 inch wave length decreased from 0.009 inch for a single crest wave to 0.0046 inch for four waves in series. A 0.015-inch by 2-inch wave was permissible at 64%-chord in the suction region provided the local suction was increased. In non-suction regions, the stabilizing influence of the chordwise pressure gradient history was predominant in determining the permissible wave size. The permissible wave height varied as the square root of the wave length.

(4) Permissible three-dimensional surface roughness element sizes were found to be of practical working size at a flight Reynolds number per foot of 2.0×10^6 ,

(h = 27,000 ft. M = 0.65). Single element values varied from 0.004-inch for a disc at 2.5%-chord (R_ϵ = 580), to 0.011-inch for a sphere at 22% chord (R_ϵ = 680). Multiple grain roughness 0.005-inch high was permissible at 22%-chord (R_ϵ = 168).

II. INTRODUCTION, PURPOSE

As reported in Reference 2, laminar flow was consistently established to the trailing edge of the 69-slot suction airfoil over a range of chord Reynolds numbers of 13×10^6 to 36×10^6 and with attendant low total drag values. The surface quality with respect to waviness and roughness was excellent. It was now desirable to investigate the allowable deviations from this initial high quality condition. This report deals with investigations of: allowable suction variation, effect of slot blockage, allowable surface waviness and allowable surface roughness. An attempt was made to determine the suction and drag penalty for small disturbances as well as the minimum size of disturbance which would result in turbulent flow at the trailing edge for all conditions.

References 5 through 12 present useful information on the subject of waviness and roughness from previous studies. The purpose of the experiments reported here and carried out during the period November 1955 through November 1956 was to check the validity of prediction methods from the above references when applied to a wing with suction over the rear 60% chord and operating at high Reynolds numbers.

III. NOTATION

Atmospheric Properties

p_o	ambient pressure	lb/ft^2
ρ_o	ambient density	$lb.sec^2/ft^4$
T_o	ambient temperature	^oR
μ_o	ambient viscosity	$lb.sec/ft^2$
ν_o	ambient kinematic viscosity	ft^2/sec

Flight Conditions

h'	altitude	ft.
U_o	true speed	ft/sec
a_o	speed of sound	ft/sec
$M_o = \frac{U_o}{a_o}$	Mach number	-
W	aircraft weight	lb.
W/S	wing loading	lb/ft^2
$q_o = \frac{\rho_o}{2} U_o^2$	dynamic pressure	lb/ft^2
n	normal load factor = $\frac{\text{lift}}{\text{weight}}$	-

Flight Conditions (cont'd.)

$C_{L_A} = \frac{n(W/S)}{q_o}$	airplane lift coefficient	-
$R_1 = U_o/\nu_o$	Reynolds number per foot	$(ft.)^{-1}$
$R_c = U_o c/\nu_o$	chord Reynolds number	-

Geometric Characteristics

X	length in flight direction	ft
Y	length perpendicular to flight direction	ft
h	wave height	inches
λ	wave length	inches
ϵ	roughness height	inches
d	roughness diameter (for discs)	inches
SP	span of slot blockage	inches
C	test wing chord = 7.5	feet
S	airplane wing area = 238	$(ft)^2$

Boundary Layer Characteristics

u	velocity at height Y in B.L.	ft/sec
u_ϵ	velocity at height ϵ in B.L.	ft/sec

Boundary Layer Characteristics (cont'd.)

δ	total boundary layer thickness	inches
μ_s	viscosity close to the wing surface	$lb.sec^2/ft^4$
ν_s	local kinematic viscosity at surface	ft^2/sec
$\theta = \int_0^\delta \frac{u}{U}(1 - \frac{u}{U})dy$	momentum thickness	inches
$\delta^* = \int_0^\delta (1 - \frac{u}{U})dy$	displacement thickness	inches
$R_\epsilon = \epsilon u_\epsilon / \nu_s$	roughness Reynolds number, based on ϵ and u_ϵ	-
$R_F = \epsilon U / \nu_s$	roughness Reynolds number, based on ϵ and U	-

Potential Flow Characteristics

U	local velocity at outer edge of B.L.	ft/sec
p	local surface static pressure	lb/ft^2
$C_p = \frac{p-p_o}{q_o}$	local static pressure coefficient	-
$\frac{\Delta C_p}{\Delta x/c}$	average chordwise pressure gradient between 22 and 42% c	-

Suction Characteristics

v_o	inflow velocity for equivalent area suction	ft/sec
$v_o^* \equiv \frac{v_o}{U_o}\sqrt{R_c}$		-

IV. INDEX OF ILLUSTRATIONS

FORM 60-136A (R.8.55)

IV. INDEX OF ILLUSTRATIONS (cont'd.)

V. EXPERIMENTAL SETUP

A. Aircraft

The F94-A, serial number 496, was used as the test vehicle to establish the flow environment. All flights originated from Edwards Air Force Base and occurred over the adjacent region in Southern California. A photograph of the aircraft is presented as Figure 1.

B. Sixty-Nine Slot Suction Airfoil

The modified 65_2-213 airfoil of 7.5-ft chord with suction applied through 69 slots on the upper glove surface in the region between 41 and 95 per cent chord was employed for all tolerance tests covered in this report. A photograph of the suction glove is presented as Fig. 2. A more complete description of the airfoil and suction system may be found in References 1 and 2.

C. Flight Condition Range

The flight condition range was restricted to those combinations of Mach number, Reynolds number, and lift coefficient for which laminar flow for the clean suction airfoil extended to the trailing edge. Figure 3 indicates the working range imposed by delay of start of suction until 41% chord, and by shock formation on the 13%-thick airfoil, in terms of lift coefficient and Mach number. Although the airplane lift coefficient ranges from about 0.1 to 0.3 with increasing altitude, the C_{L_A} range with full laminar flow at constant altitude averages 0.055 . The


T-A-496

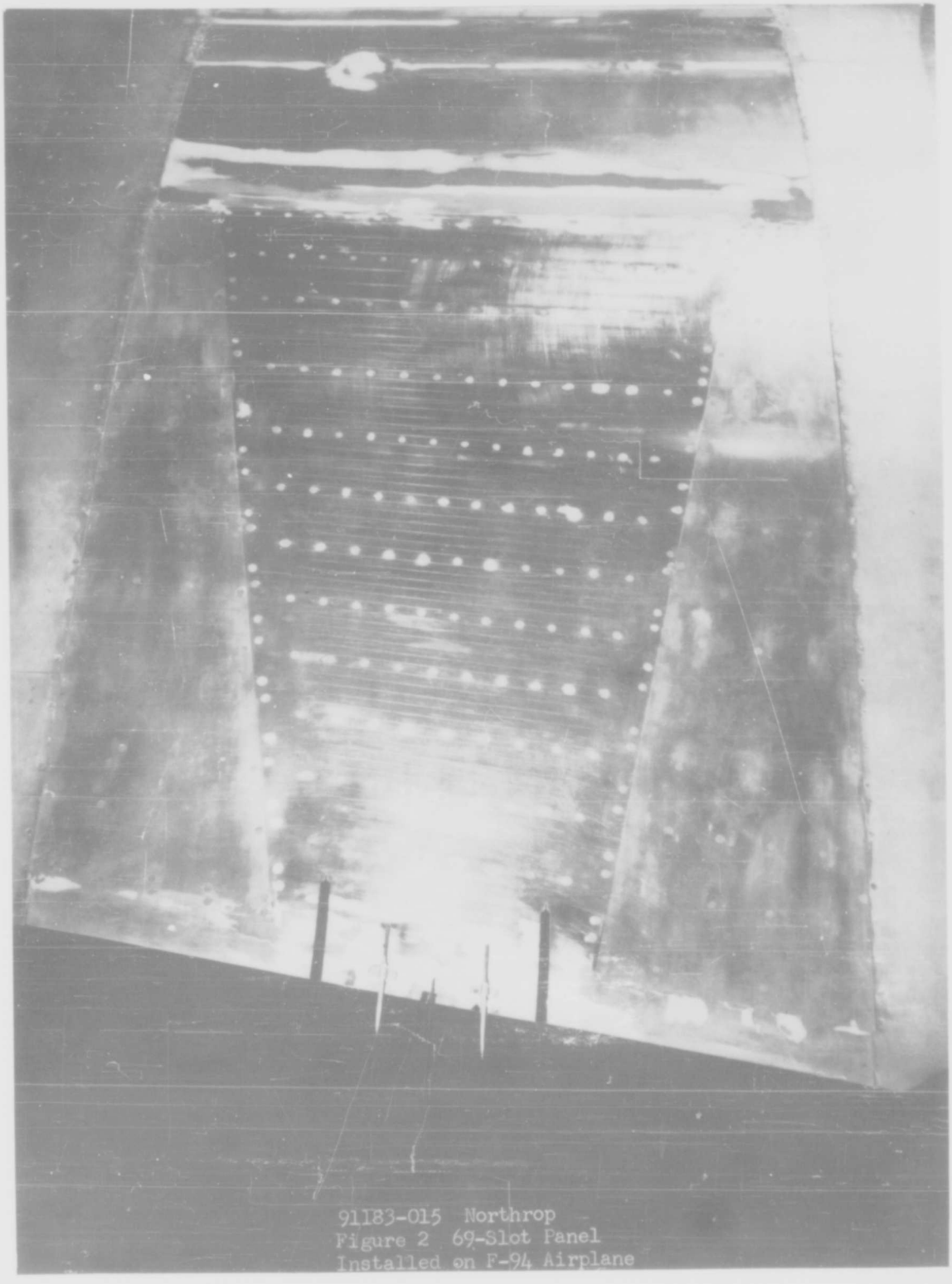

91183-015 Northrop
Figure 2 69-Slot Panel
Installed on F-94 Airplane

FORM 20-10A (R. 6-51)

ENGINEER	NORTHROP AIRCRAFT INC.	PAGE
B. Carmichael		12
CHECKER		REPORT NO.
		BLC-101
DATE		MODEL
August 1957		

FIG. 3 - FLIGHT CONDITION RANGE

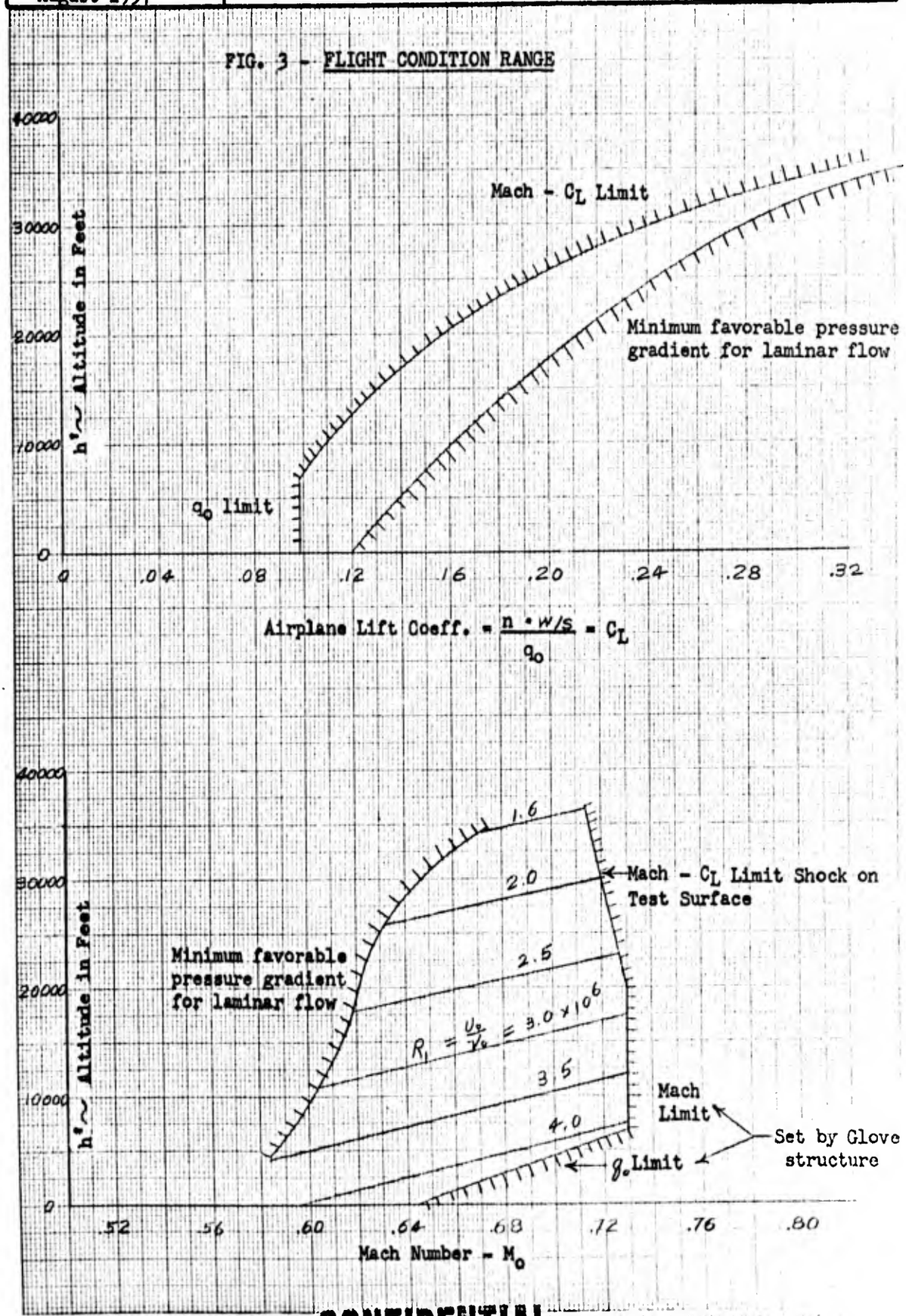

Mach number range varies from about 0.58 to 0.73 . The Reynolds number per foot increases from 1.6×10^6 at 35,000 to over 4.0×10^6 near sea level.

VI. MEASUREMENTS AND EVALUATION

The static pressure distribution along the test surface, the pressure in the suction chambers, the flow from the suction chambers, and the total head values through the boundary layer at the trailing edge were measured with differential pressure gauges and recorded with a movie camera. In addition, the flight conditions (indicated airspeed, pressure altitude, and temperature) were recorded in similar manner. The suction quantities and boundary layer velocity profiles were displayed on the observer's panel so that the experiment could be monitored in flight. The total boundary layer thickness at the trailing edge when laminar, was about one tenth of an inch. The condition of the boundary layer at the trailing edge could easily be determined by observing how many of the upper rake tubes were indicating undisturbed total head.

The compressible flow type of evaluation described in detail in Ref. 1, was again used to arrive at wake drag, equivalent drag due to suction and total profile drag.

VII. EXPERIMENTS AND EXPERIMENTAL RESULTS

A. Tolerance to Suction Distribution Variations

The first phase of the 69-slot flight program was devoted to determination of the optimum suction distribution for minimum total profile drag coefficient. The practical problem of allowable deviations from this optimum distribution was next investigated. The airfoil was found to be insensitive to suction variation to a much greater degree than required for most practical design considerations. Any individual chamber suction could be increased to the maximum obtainable (about 2.7 times normal) without disturbing the laminar boundary layer at the trailing edge, providing the remaining eleven chambers were near normal values.* A moderate increase in the overall suction level above the minimum, permitted reduction of individual chamber suction to about half the normal value with the exception of those chambers immediately following the onset of the adverse pressure gradient.* All chambers could be increased as an even distribution to 1.6 times the normal quantity without disturbing the laminar boundary layer at the trailing edge. When the even distribution was increased to 1.9 times the normal values, the flow at the trailing edge became turbulent as shown in Fig. 4.** The uneven suction distribution shown in Fig. 5** permitted laminar flow to the trailing edge. The corresponding inflow distribution for the individual slots within chambers 5, 6, and 7 are presented in Figure 6.**

---

* At $h = 30{,}200$ ft, $M_o = .697$, $R_c = 14.7 \times 10^6$, $C_{L_A} = 0.28$
Normal inflow values vary linearly from $V_o^* = -1.5$ for chamber 1 to $V_o^* = -6.3$ for chamber 12.

** At $h = 18{,}000$ ft, $M_o = 0.65$, $R_c = 20 \times 10^6$, $C_{L_A} = 0.19$
Normal inflow values noted for each chamber in Figures 4, 5, and 6.

B. Tolerance to Slot Blockage

1. Experimental Arrangement

The next investigation of a practical nature with the 69-slot suction airfoil was determination of the effect of slot contamination upon the allowable suction variation while maintaining complete laminar flow. The specific test conditions (which also apply to the previous section) are given below:

Altitude	Mach Number	Chord Reynolds No.	Local Momentum Thickness*
Ft.	-	-	$\theta \sim$ inches
6000	0.625	28×10^6	.007
12000	0.645	23×10^6	.008
18000	0.660	19.5×10^6	.009
24000	0.675	16.5×10^6	.010
30000	0.695	14×10^6	.012

*under normal suction distribution

All of the tests were confined to the second slot of chamber 5 (63.4% chord). The slot was blocked at the glove centerline with paint plugs which were flush with the surface and extended completely across the 0.0045 in. width of the slot. Plugs of 0.007 inch, 0.0115 inch, 0.015 inch, 0.030 inch, 0.20 inch, 0.50 inch and 1.0 inch span were individually tested. In an additional test, the slot was blocked from the glove centerline to its outboard end (a length of 10 inches). With a normal suction distribution in all other chambers, the suction level in chamber 5 was raised in small increments until the flow became turbulent at the trailing edge.

2. Results

Figure 7 presents graphically the results expressed below.

(1) The 0.007-inch plug (less than θ in span) did not produce turbulence up to the maximum suction obtainable.

(2) The 0.0115-inch plug (slightly greater than θ in span) did not produce turbulence until the suction quantity in chamber 5 had been increased to 2.4 times the normal value.

(3) The 0.015-inch plug (1.5 θ) and the 0.030-inch plug (3 θ) produced turbulence with normal suction in chamber 5. Reduction to 80% of normal suction quantity re-established laminar flow. Normal V_o^* for chamber 5 was-3.6.

(4) The 0.20-inch plug (20 θ), the 0.50-inch plug (50 θ), and the 1.0-inch plug (100 θ) exhibited suction limits greater than normal suction values with an increasing tendency with increasing plug span.

(5) The 10-inch half-span block (1000 θ) gave somewhat lower limits than the 1-inch plug but nevertheless greater than normal values.

(6) With the exception of the half-span block, decreasing Reynolds number increased the upper suction limit.

It was not found possible to re-establish laminar flow at the trailing edge by altering suction upstream or downstream of the chamber containing the contaminated slot. Laminar flow could only be re-established by reduction of suction in the contaminated chamber. The fact that there was a critical range of slot spans was not unexpected. The flow investigations in a tube with rows of suction holes (see Refs. 3, 4 and 12) clearly illustrated the interaction of trailing vortices in an interrupted suction line. The vortex pattern from a slot end or single hole does not form horseshoes and has a critical suction quantity well above the values used on this airfoil. However, with a slot block of critical span or a

pair of holes of critical spacing, two adjacent vortices combine and form a horse-shoe which grows out through the boundary layer leading to turbulent flow at a suction level which is lower than the previous mentioned case.

The results of these blockage tests should not be indiscriminately applied to other cases. All the tests were conducted at a single chordwise location, with a single slot width and a single slot spacing. It might be expected that with wider slot spacing (thus higher inflow into any given slot) transition to turbulent flow might occur at a lower percentage of necessary suction than reported here. Likewise, for closer slot spacing, the critical suction level may be higher than reported here. The case of many blockages (particularly when spread out in the streamwise direction) may also produce different results than the case reported here.

FORM 20-10A (R. 6-51)

ENGINEER: B. Carmichael	NORTHROP AIRCRAFT INC.	PAGE: 18
CHECKER:		REPORT NO.: BLC-101
DATE: August 1957		MODEL:

FIG. 4

MAXIMUM PERMISSIBLE SUCTION WHEN INCREASED AS AN EVEN DISTRIBUTION

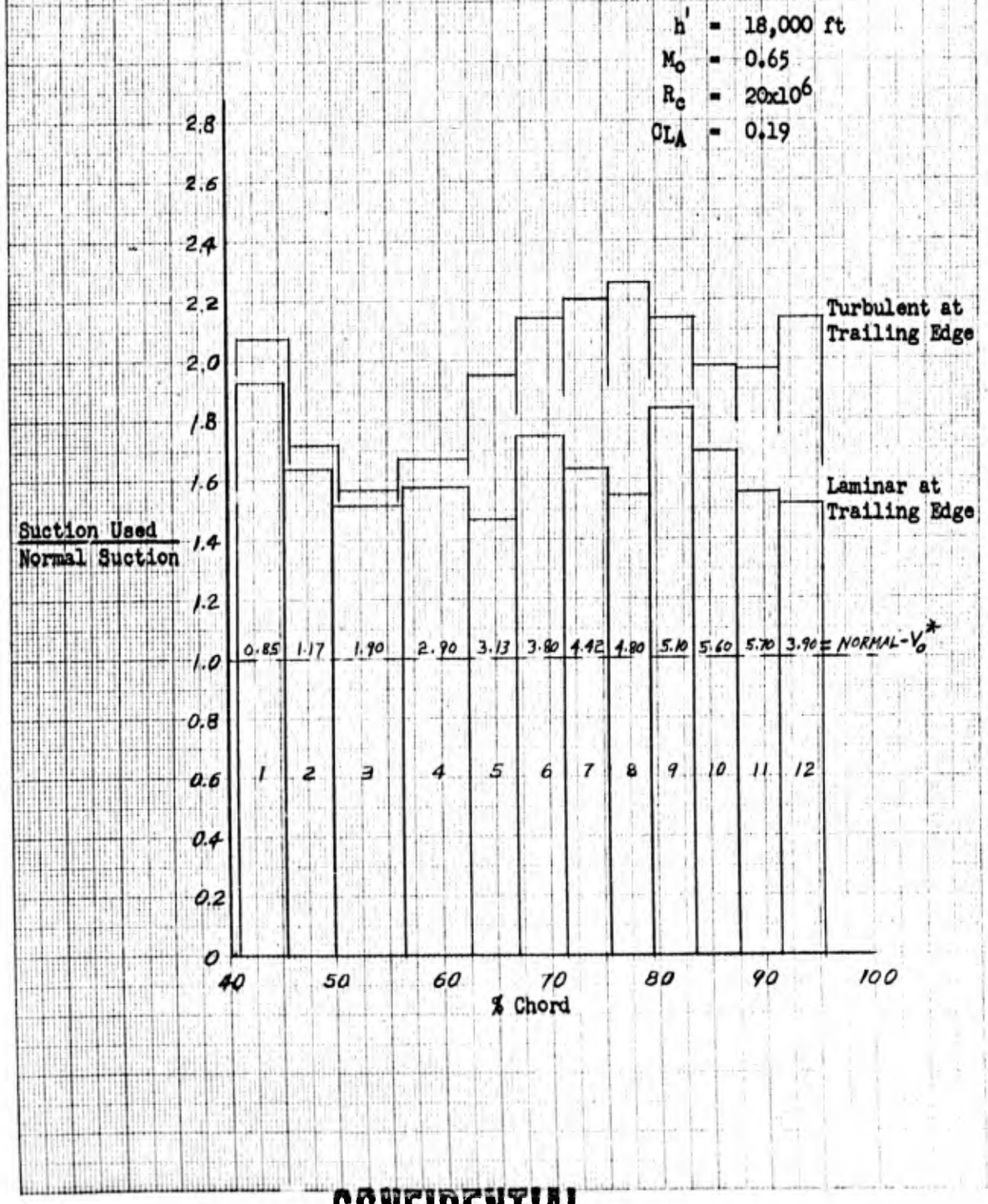

FORM 20-10A (R. 6-51)

ENGINEER: B. Carmichael	NORTHROP AIRCRAFT INC.	PAGE: 19
CHECKER:		REPORT NO.: BLC-101
DATE: August 1957		MODEL:

FIG. 5

PERMISSIBLE SUCTION DISTRIBUTION IRREGULARITY WITH COMPLETE LAMINAR FLOW

$h' = 18{,}000$ ft $\quad M_o = 0.65$ $\quad R_c = 20 \times 10^6$ $\quad C_{L_A} = 0.19$

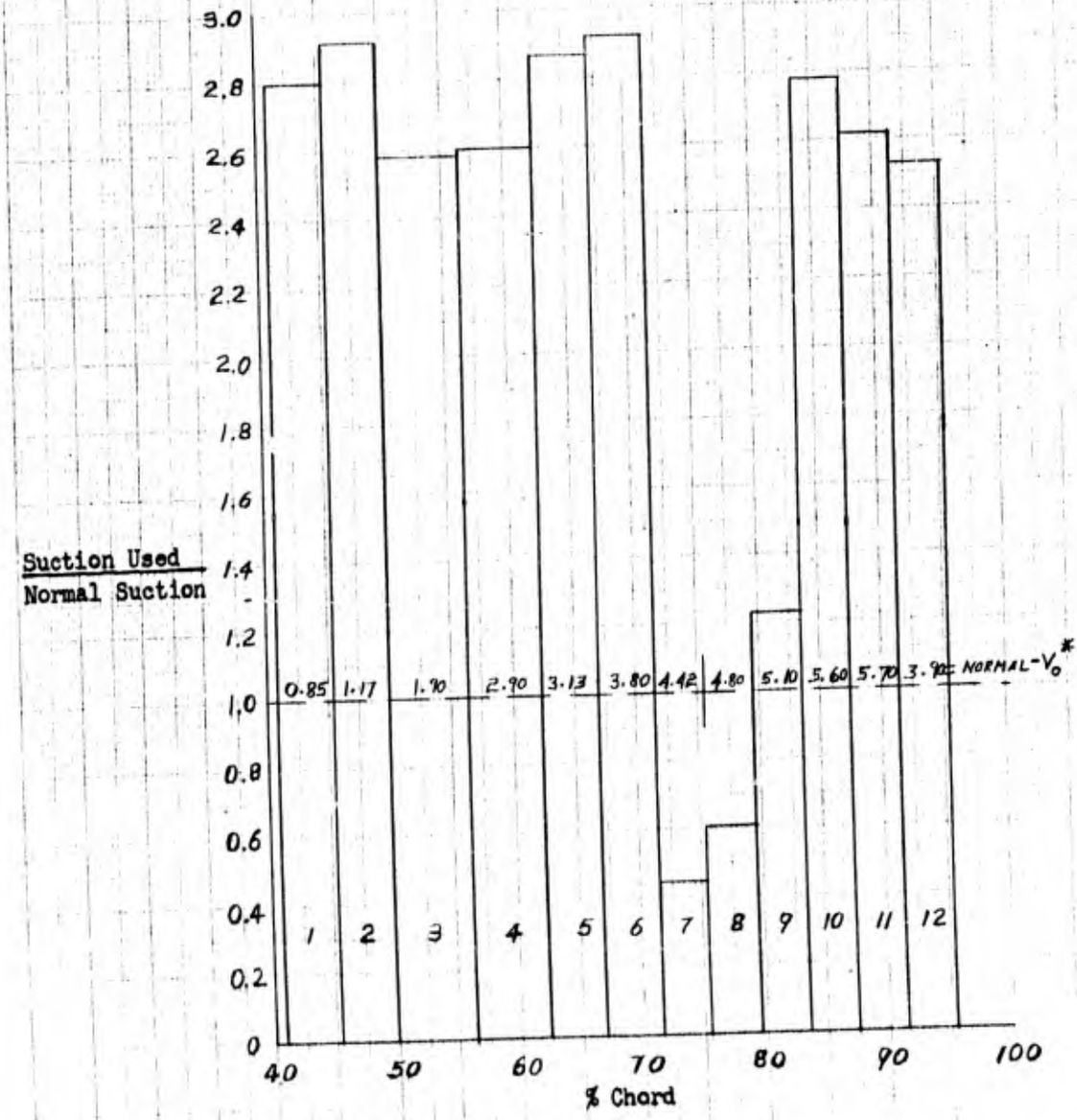

Form 20-10A (R. 6-51)

ENGINEER	NORTHROP AIRCRAFT INC.	PAGE
B. Carmichael		20
CHECKER		REPORT NO.
		BLC-101
DATE		MODEL

FIG. 6

COMPARISON OF SLOT TO SLOT INFLOW (COMPUTED FROM PRESSURE DROP) WITH CHAMBER INFLOW (MEASURED BY NOZZLE) ILLUSTRATING PERMISSIBLE SUCTION IRREGULARITY

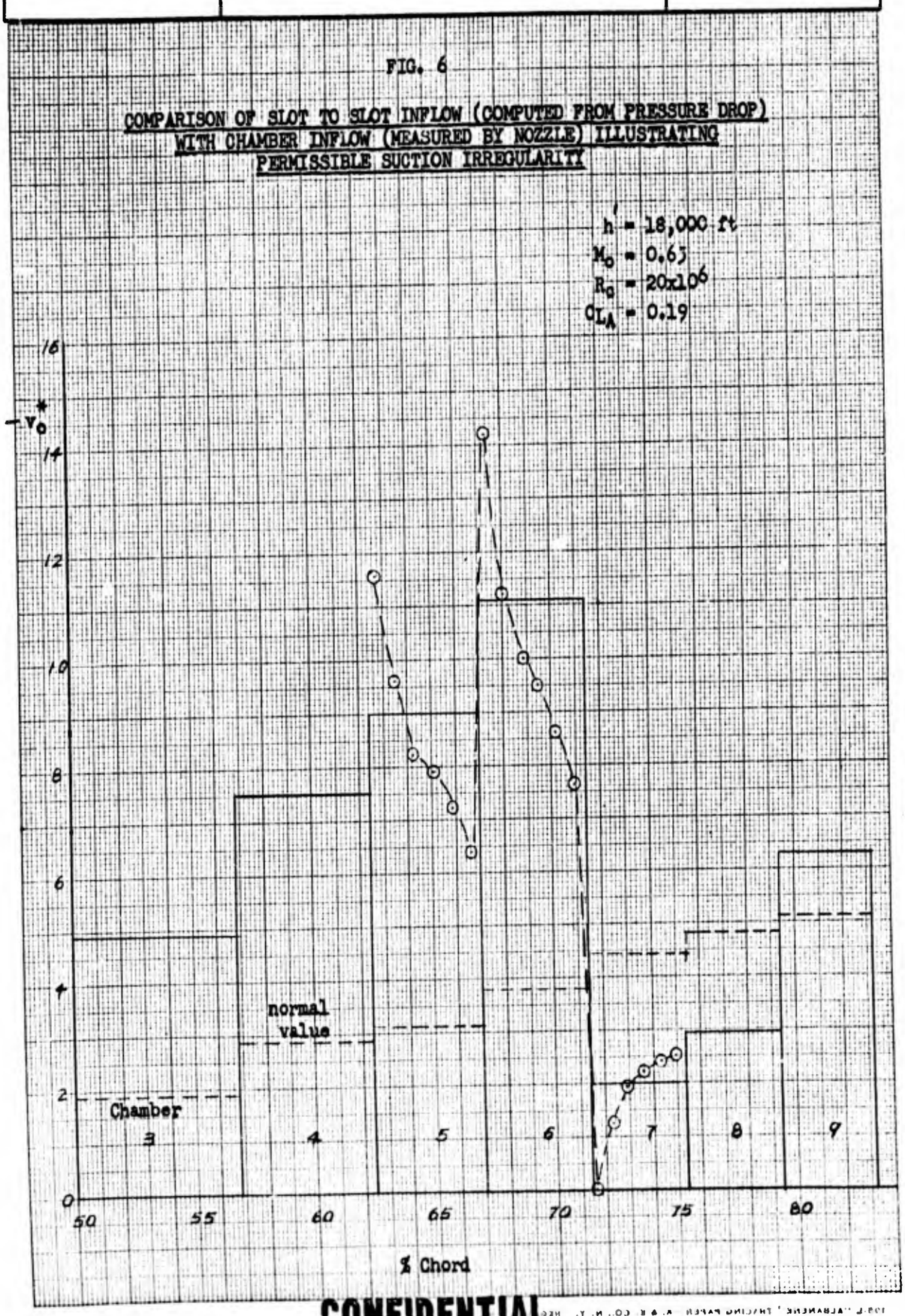

K&E SEMI-LOGARITHMIC 359-91
KEUFFEL & ESSER CO. MADE IN U.S.A.
5 CYCLES X 70 DIVISIONS

FIG. 7. UPPER SUCTION LIMIT WITH SLOT BLOCKAGE

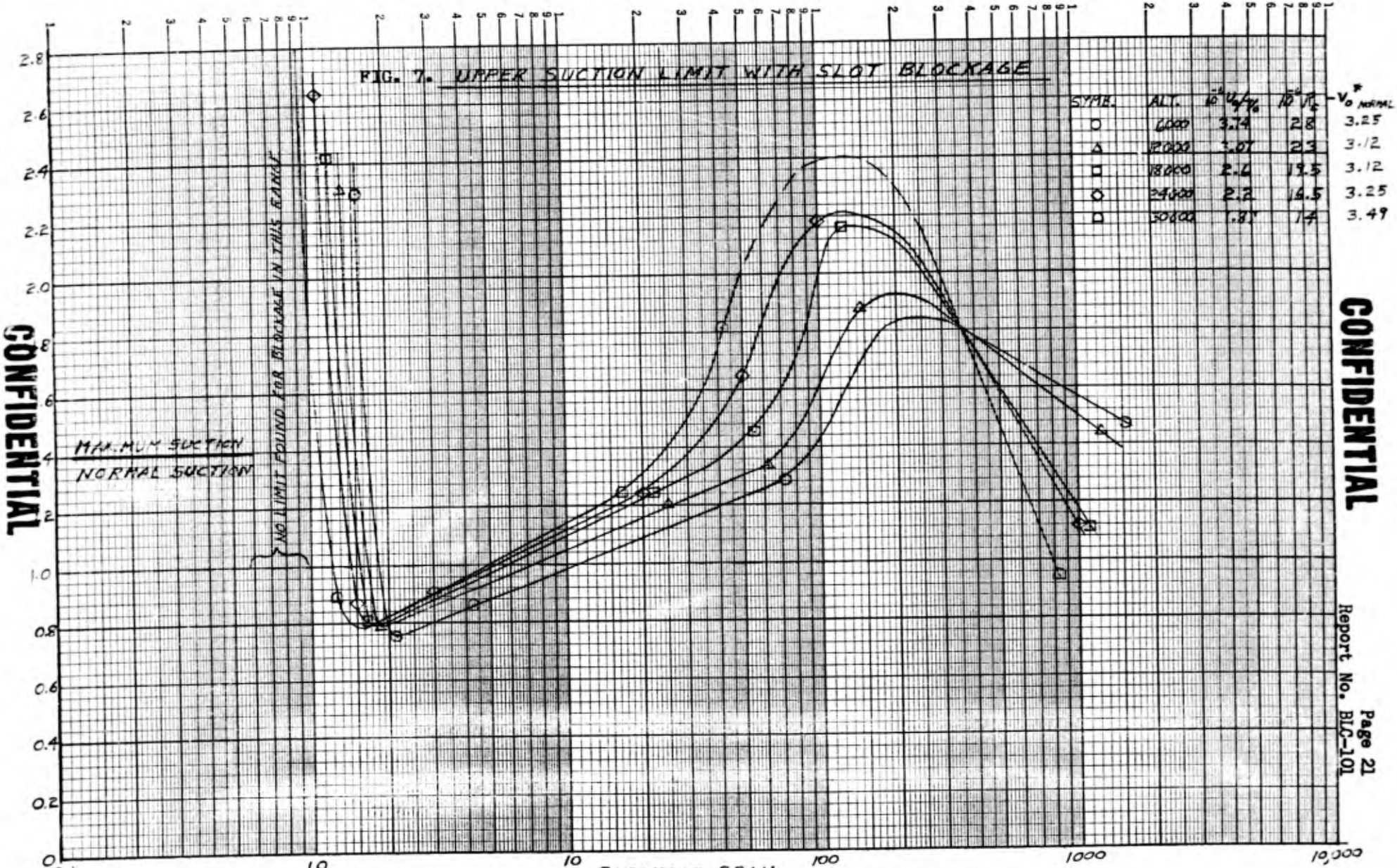

C. Tolerance to Surface Waviness

1. Experimental Arrangement

Single and multiple crest waves of sinusoidal form were employed in this series of experiments. Single hollow waves would have necessitated mutilation of the model and so were not investigated at this time. The multiple waves may, however, be considered as a series of crests and hollows.

The surface waves were built up of surfacing paint by J. Roberts of the BLC Shop. The waves extended completely across the width of the test section. The local surface was first surveyed in the clean condition to obtain the base values of curvature using an Ames Dial. Masking tape at leading and trailing edge set the wave length. After spraying, the edges were feathered out and the maximum wave height was set all along the span with the aid of an Ames Dial. The combination of edge feathering and proper rounding of the crest produced a close approximation to sinusoidal form. A plot of curvature against chordwise position was then made and compared with the desired sinusoidal wave shape at two-inch intervals along the span. The final corrective sanding required was approximately 0.0003-inch. Roberts rapidly developed such skill that the required number of ten-thousandths-inch of paint was invariably removed in a single operation. The success of the wave program owes a great deal to the skill, patience, and energy of this outstanding technician.

2. Experimental Results

a. Single Sinusoidal Crest Waves Located at 28% Chord

A systematic variation of wave height and length was first undertaken. The choice of the 28% chord location for these experiments was made on the basis of boundary layer stability considerations.

Whether a boundary layer will remain laminar or become turbulent has been predicted theoretically and found experimentally to be dependent upon the streamwise history of the combinations of boundary layer Reynolds number and boundary layer shape. For the case without suction, the boundary layer Reynolds number is primarily a function of the flight conditions and length of surface while the boundary layer shape is primarily a function of the pressure distribution. Suction can be used to limit the increase in boundary layer Reynolds number but has an even stronger and more immediate effect on the local boundary layer shape. Prevention of transition to turbulent flow then becomes a matter of providing everywhere a boundary layer profile of sufficiently stable shape to be compatible with the attending boundary layer Reynolds number.

The boundary layer Reynolds number and shape combination at 28% chord was more critical than the regions further forward, while a foot of run behind the wave permitted the disturbance from the wave to amplify before the stabilizing influence of suction was applied.

It very rapidly became apparent that the effect of the available variation in the chordwise pressure distribution on boundary layer shape (as determined by lift coefficient and Mach number) far overshadowed the effect of the available variation of Reynolds number in determining the state of the boundary layer at

the trailing edge for flow over a critical wave. Experiments with the airfoil in the clean condition have been reported in Ref. 2. At each Reynolds number, the pressure distribution was noted where any further reduction in Mach number would lead to turbulent flow at the trailing edge. For this critical condition, no waviness could be tolerated. To maintain laminar flow with a wave, required an increase in the favorable chordwise pressure gradient. The results of this series of tests took the form of allowable waviness versus required increase in pressure gradient over the minimum laminar value for the no wave case. A wave which caused turbulent flow at a normal clean airfoil laminar flight condition could become subcritical with an increase in Mach number and Reynolds number due to the more favorable chordwise pressure distribution. The relationship between critical wave height and wave length $(h^2/\lambda)_{cr}$ = constant was found to hold true for these experiments. The conventional procedure of expressing surface waviness as a simple wave ratio h/λ is not valid when considering different wave lengths. An improved relationship appears to be h^2/λ or, to make the expression non-dimensional, $h^2/\lambda C$, or to bring in the boundary layer thickness, one might write $h^2/\lambda\theta$. It should be emphasized that the wave parameter $h^2/\lambda\theta$ is empirical in nature. The same relationship ($h \propto \sqrt{\lambda}$) was found previously by Fage (Ref. 5) for the case of very small pressure gradients (flat plate). The use of θ appears to correlate the data from the different flight Reynolds numbers employed in these experiments.

Table I-A-I presents the qualitative results for single waves at 28% chord. The two-inch waves were investigated first. Relatively small wave heights were chosen for the first trials until the beneficial effect of favorable pressure gradient was realized. The six-inch waves which were tested next, were chosen a bit oversize until the h^2/λ relationship was validated by the flight tests. The short 0.67-inch length waves were then easily chosen so

that the complete range of interest was covered with three wave heights. Fig. 8 shows the required increase in chordwise pressure gradient to be a linear function of $h^2/\lambda C$ (at constant Reynolds number). Fig. 9 shows the required increase in pressure gradient with points from the entire Reynolds number range as a function of $h^2/\lambda\theta$. Fig. 10 presents complete information (including pressure distributions) for a few examples of the last laminar condition preceeding transition.

b. Single Sinusoidal Crest Wave Located at 15% Chord

The wave location was next shifted to 15% chord. The local pressure gradient was 2.5 times greater than at 28% chord and the boundary layer was about three-fourths as thick as at 28% c . The qualitative results of Table I-A-2 indicate small increases in allowable waviness as compared to the 28% chord location. When the values of $\Delta C_p/\Delta(x/C)$ were plotted versus $h^2/\lambda\theta$ for the 0.010, 0.015, and 0.020-inch waves, the average line fell very close to the 28% chord data. The failure of the greater favorable pressure gradient in the vicinity of the wave to permit an increase in allowable waviness may perhaps be explained by the following considerations. A given size wave will protrude further into the boundary layer at 15% chord than at 28% chord. The pressure fluctuation and therefore disturbance over the wave may be greater for this reason. Even though the strong favorable pressure gradient just aft of the wave provides improved damping initially, the disturbance must still traverse the low stability region (as previously defined) just forward of the start of suction. The length of run between the 15% chord waves and start of suction was also greater than for the 28% chord waves.

c. Single Sinusoidal Crest Wave in a Region of Distributed Suction

Single 2-inch wide waves were next investigated on the surface at 64% chord (over the fifth suction chamber) in a region of a strong adverse pressure gradient. The local slots were cut through the wave. The results are summarized in Table I-A-3.

The 0.015-inch high wave permitted laminar flow over a large range of flight conditions. Use of deflected wing flaps to augment the favorable pressure gradient was not required in this experiment as was the case for the 0.015-inch high wave in non suction area at 15% chord. An increase of 18% in the minimum suction quantity in chamber 5 was required to maintain laminar flow to the trailing edge. This was obtained by reducing the suction compartment pressure by 8% of flight dynamic pressure. In future studies, the maximum size wave which will permit laminar flow to the trailing edge with no change in compartment pressure, should be determined.*

The 0.030-inch high wave was too large to be considered allowable for this location. Although sufficient suction pump power was available to prevent outflow due to the wave pressure peak, laminar flow was only obtained at the lowest Reynolds number possible and with maximum help from the wing flaps.

---

* Although this investigation has not been carried out to date in the adverse pressure gradient region, a single wave of length 2.00 inches, and height 0.010 inch, has been tested at 25% chord. Suction had been extended forward to 8% chord (BLC 102) previous to this test. No influence of this wave could be detected in the required suction quantities and chamber pressures over the entire range of Reynolds numbers and lift coefficients available.

d. Multiple Waves at 28% Chord

Multiple waves are of interest from the practical standpoint since they may appear in the surface of a multi-web wing due to fabrication or under applied flight loads. The flow phenomenon in the regions between a continuous series of crest waves may be similar to the flow phenomenon over a hollow wave, in that the boundary layer may approach the aft side (adverse pressure gradient region) of a crest on one of the rear waves with less energy than it approaches the aft side of a single wave. There is also the possibility that if the wave length of a multiple system has a value predicted by the Tollmien-Schlichting theory* as most critical, disturbance amplification may occur, leading to early transition.

Table I-B summarizes the results of the multi-wave tests. To maintain laminar flow to the trailing edge with a given value of average pressure gradient necessitated reduction of the wave parameter h^2/λ ~~θ~~ as the number of waves was increased. It should be remembered that these experiments covered only the case of waves in close series (producing a continuous sinusoidal surface).

e. Comparison and Discussion

The clearest manner in which to indicate the relative effect of the various wave experiments is believed to be the one employed in Table I-C. All waves and wave groups chosen require the same average pressure gradient for laminar flow. Figure 11 presents the surface static pressure distributions for these "equivalent" waves. Figure 12 indicates an average increase in minimum laminar Mach

* Laminar flow was maintained with six 0.0035-inch high waves of 0.67-inch wave length. The Tollmien-Schlichting theory predicts 0.67 in. to be the most critical wave length at the average flight condition of these tests.

number of 0.05. These waves also required an 8% increase in suction over the clean airfoil case. Laminar operation was possible in all cases through a Reynolds number per foot of 3.5×10^6 (chord = 7.5 ft).

Figure 13 indicates the effect of Mach number on the pressure peak associated with a wave 0.009-in. in height and 2.00 inches in length. The effect of increasingly high local Mach number on the pressure peak associated with a small surface wave is very pronounced. Laminar aircraft which are to be operated very close to critical Mach number will require excellent surface waviness control in minimum pressure regions.

The relationship between critical wave height and wave length $h \propto \sqrt{\lambda}$ observed in these experiments also appears in the final equations of Ref. 5. The allowable waviness, however, was much greater than predicted by the method of Ref. 5. This is in no way a contradiction since the advantages of strong favorable pressure gradients forward and distributed suction aft in the present work were not present in the experiments of Ref. 5. For those cases where length Reynolds numbers to natural transition are low enough to permit laminar flow without suction in regions of small pressure gradients ($R_{x_T} \leq 4 \times 10^6$), Reference 5 should still be of value. The present report should be of aid for relatively thick airfoils with suction over the aft portion of the chord.

FORM 20-10A (R. 6-51)

ENGINEER: B. Carmichael	NORTHROP AIRCRAFT INC.	PAGE: 29
CHECKER:		REPORT NO.: BLC-101
DATE: August 1957		MODEL:

FIG. 8

SINGLE CREST WAVES AT 28% CHORD AND $R_c = 20 \times 10^6$

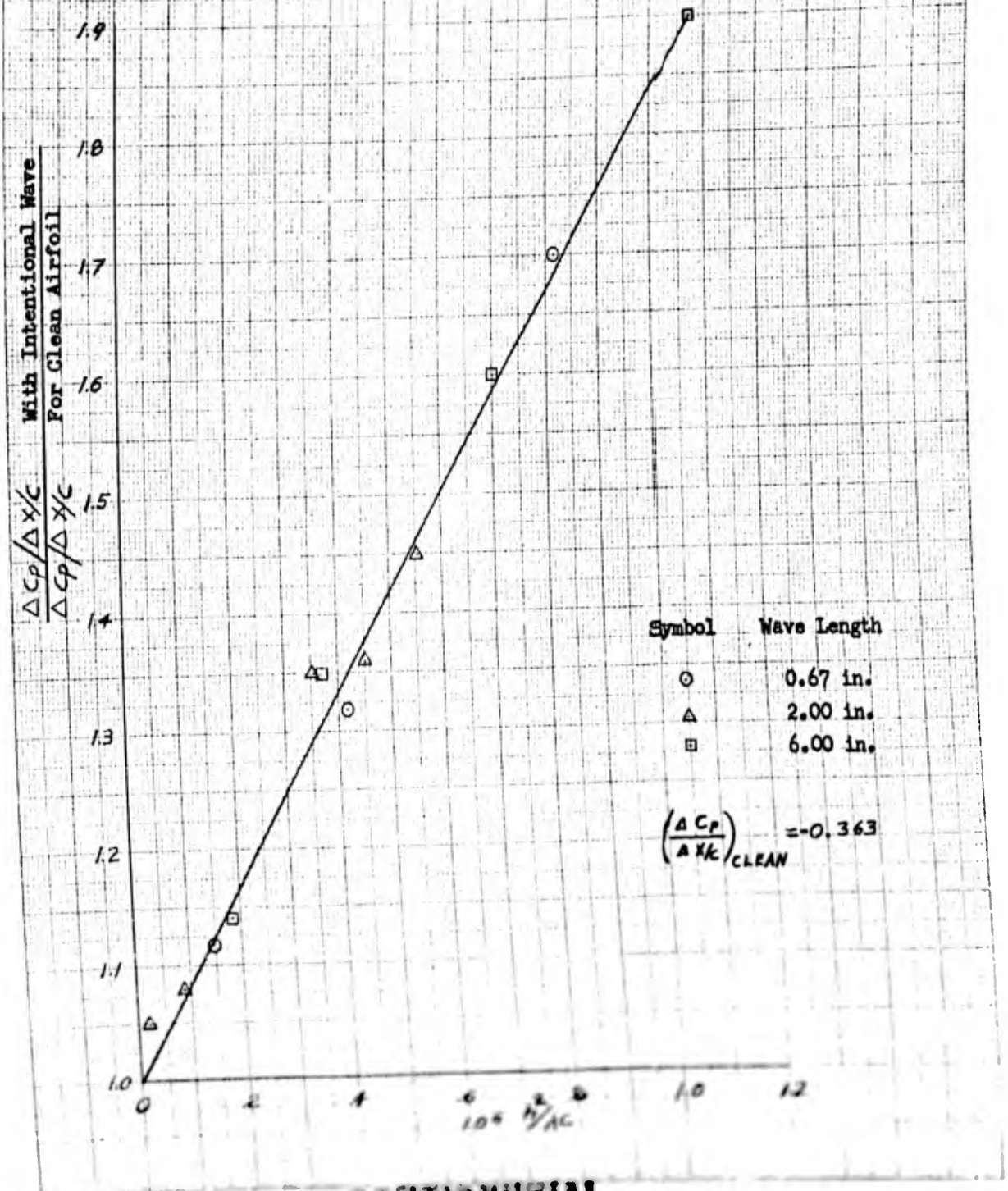

FORM 20-11A (R. 6-51)

ENGINEER: B. Carmichael	NORTHROP AIRCRAFT INC.	PAGE: 30
CHECKER:		REPORT NO.: BLC-101
DATE: August 1957		MODEL:

FIG. 9 SUMMARY OF SINGLE CREST WAVES AT 28% c AND $17 \times 10^6 < R_c < 29 \times 10^6$

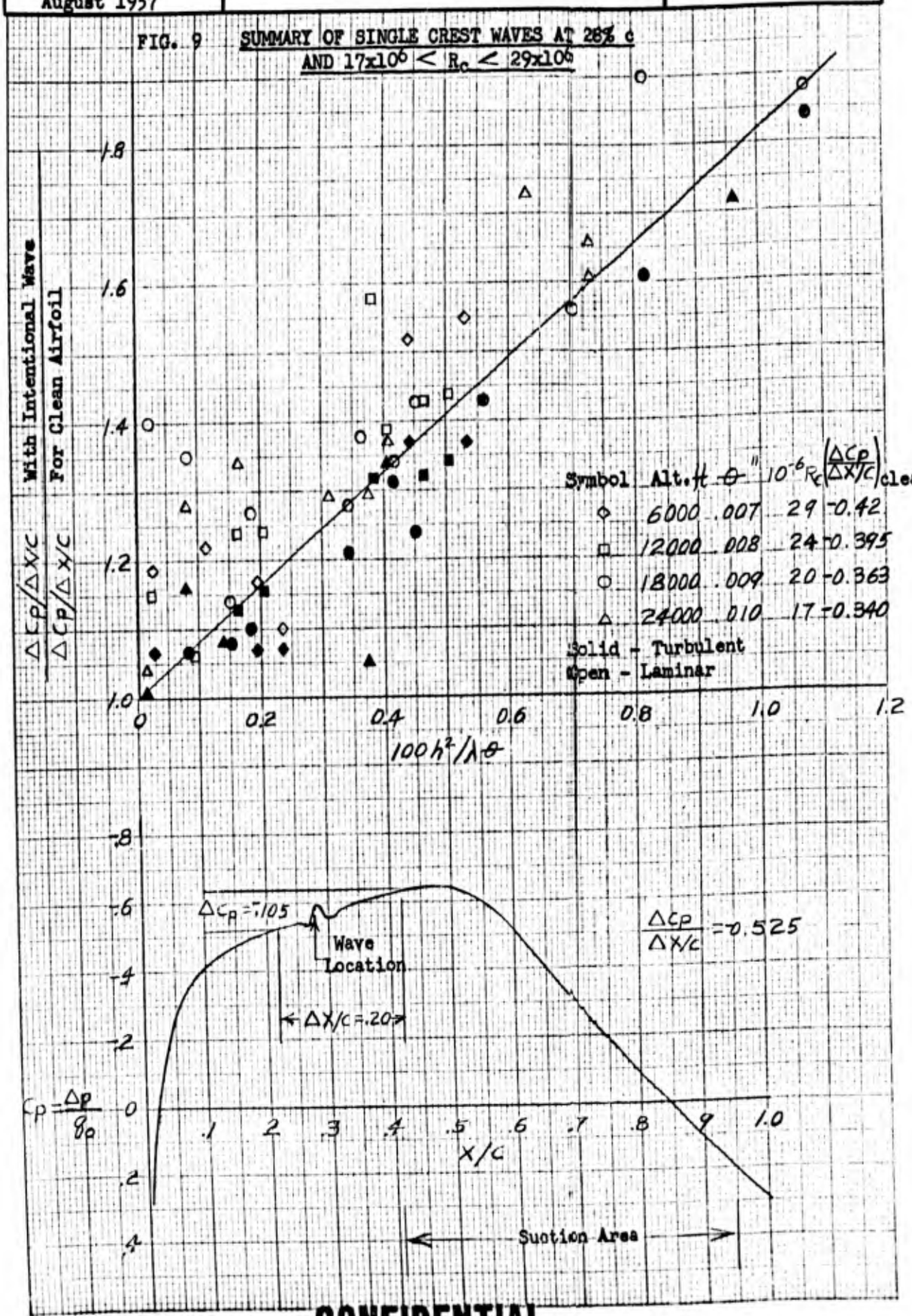

FORM 20-10A (R. 6-51)

ENGINEER	NORTHROP AIRCRAFT INC.	PAGE 31
CHECKER		REPORT NO. BLC-101
DATE		MODEL

FIG. 10 EXAMPLES OF CRITICAL CONDITIONS
(Last Laminar Test Points Preceeding Transition)

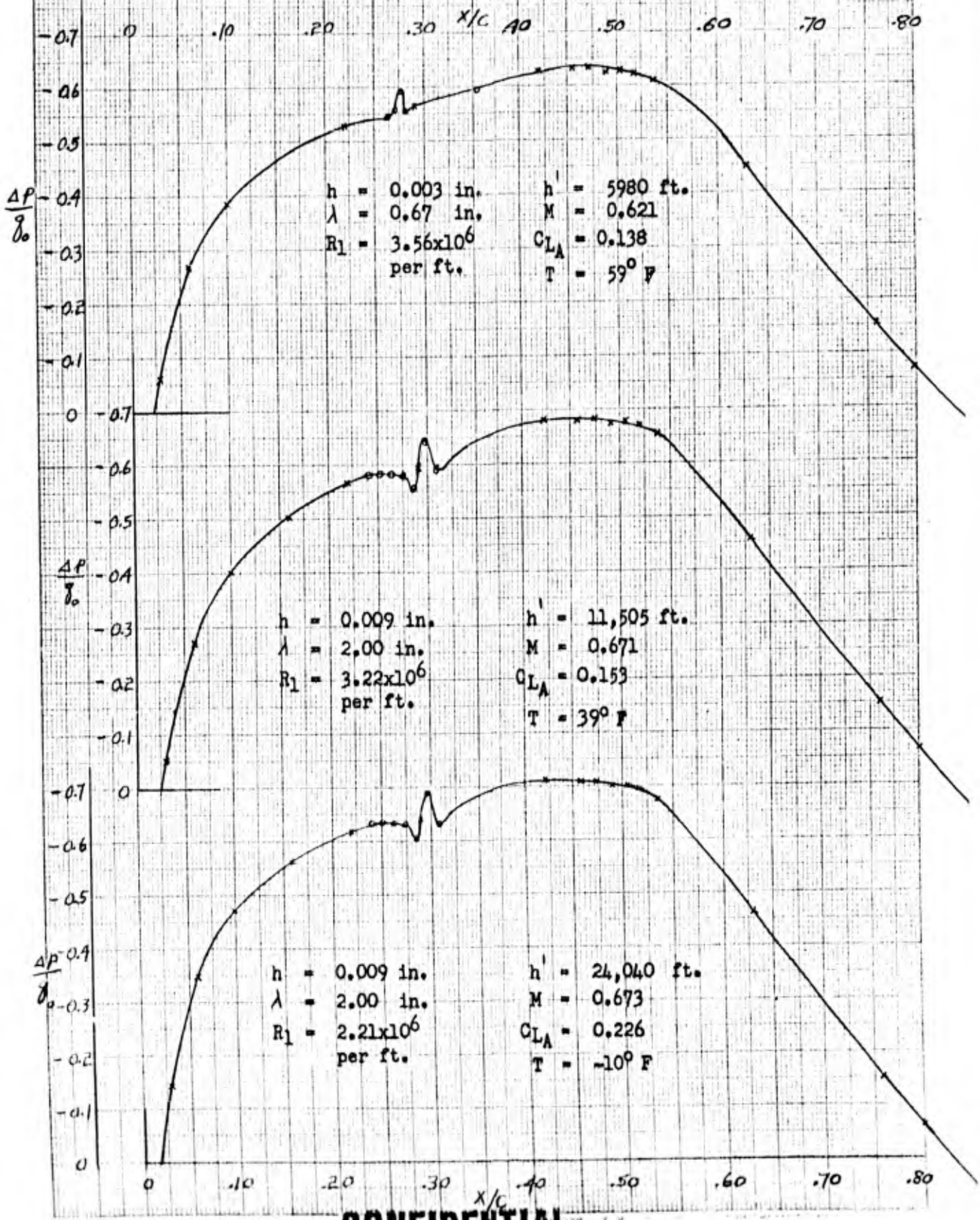

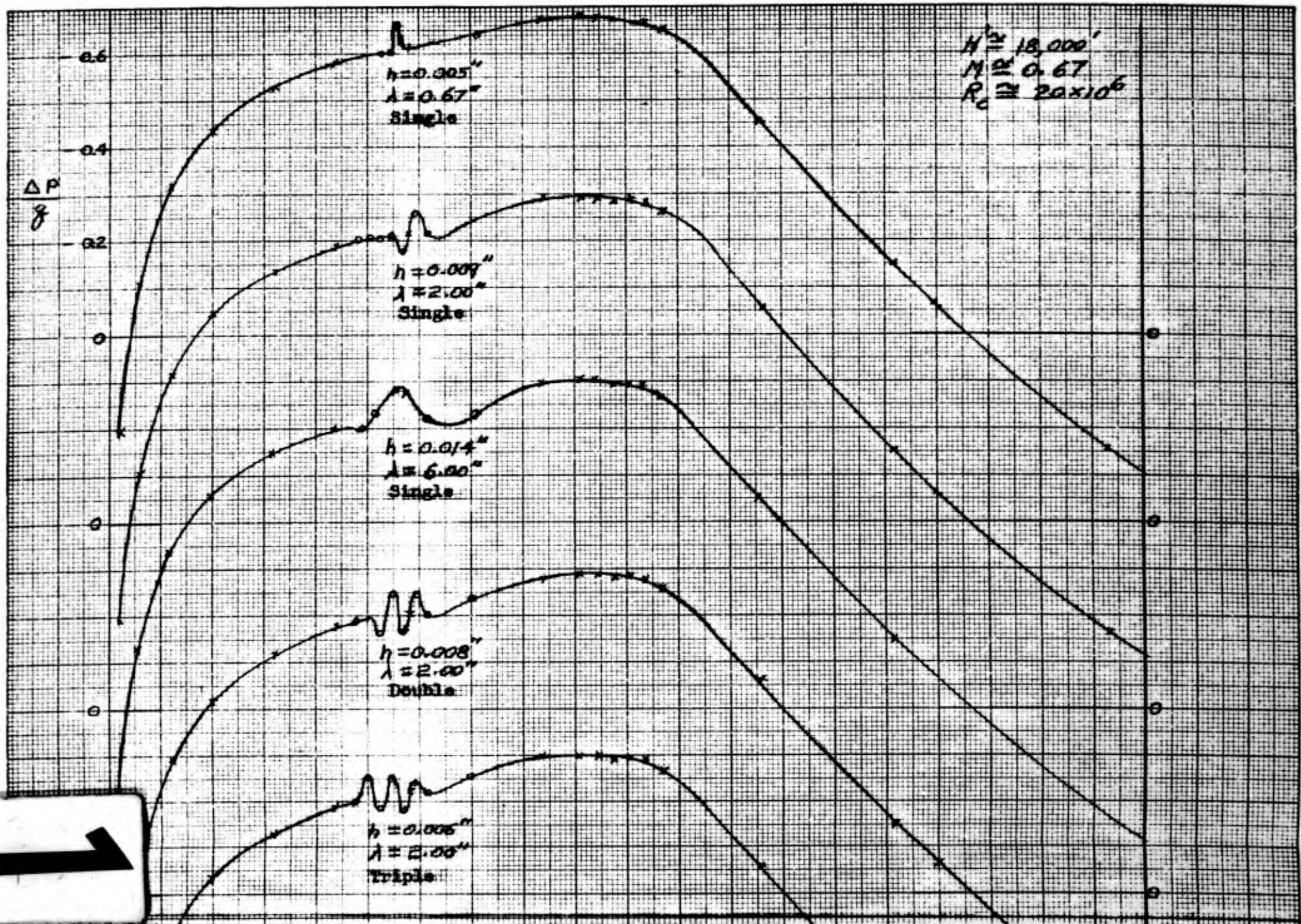
H ≅ 18,000'
M ≅ 0.67
R_c ≅ 20x10⁶
h=0.005"
λ=0.67"
Single
h=0.009"
λ=2.00"
Single
h=0.014"
λ=6.00"
Single
h=0.008"
λ=2.00"
Double
h=0.006"
λ=2.00"
Triple
ΔP/q
0.6
0.4
0.2
0
0
0
0
0

ENGINEER	NORTHROP AIRCRAFT INC.
CHECKER	
DATE	

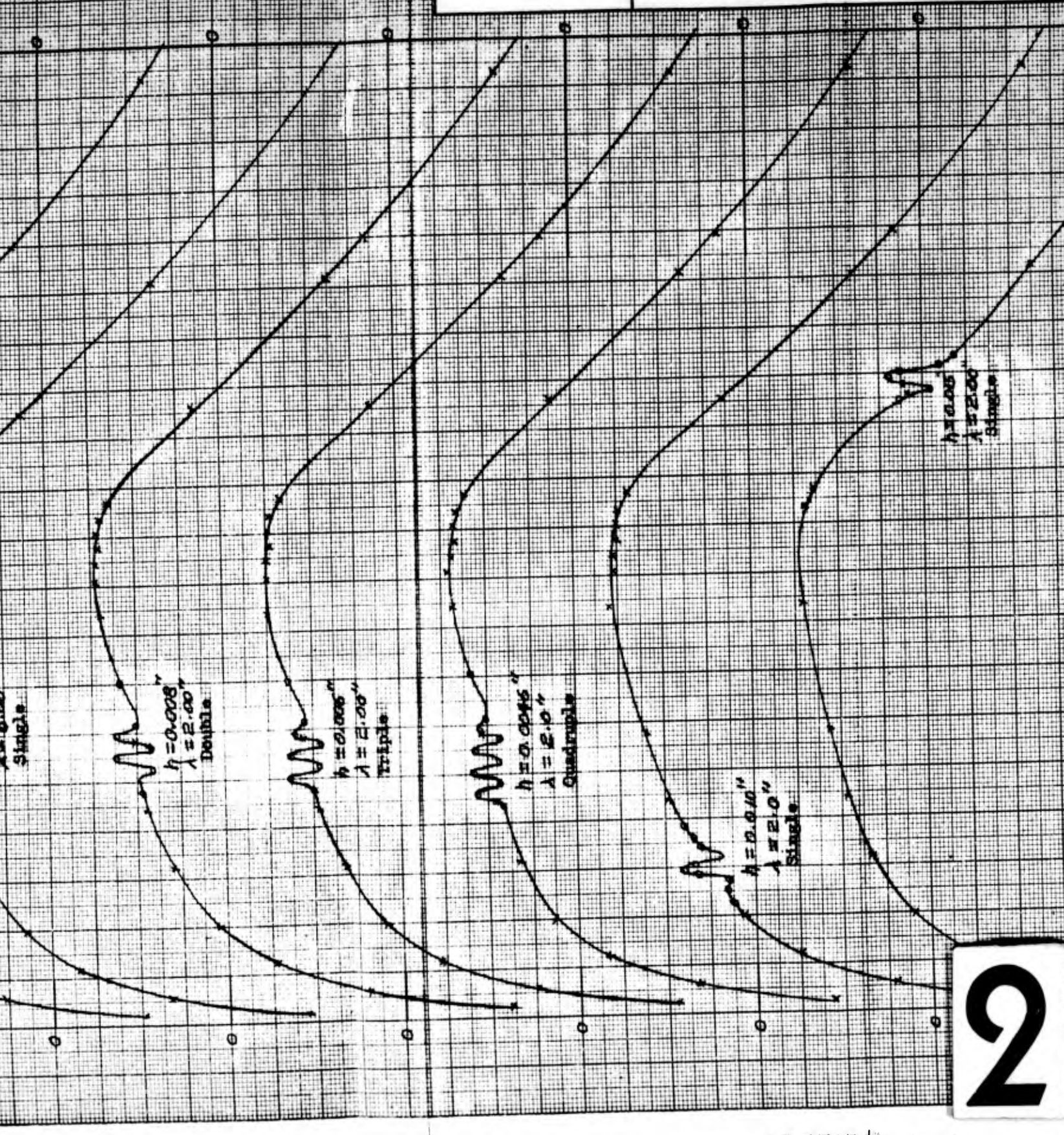

2

Form 20-108 (R. 6-51)

ENGINEER	NORTHROP AIRCRAFT INC.	PAGE 32
CHECKER		REPORT NO. BLC-101
DATE		MODEL

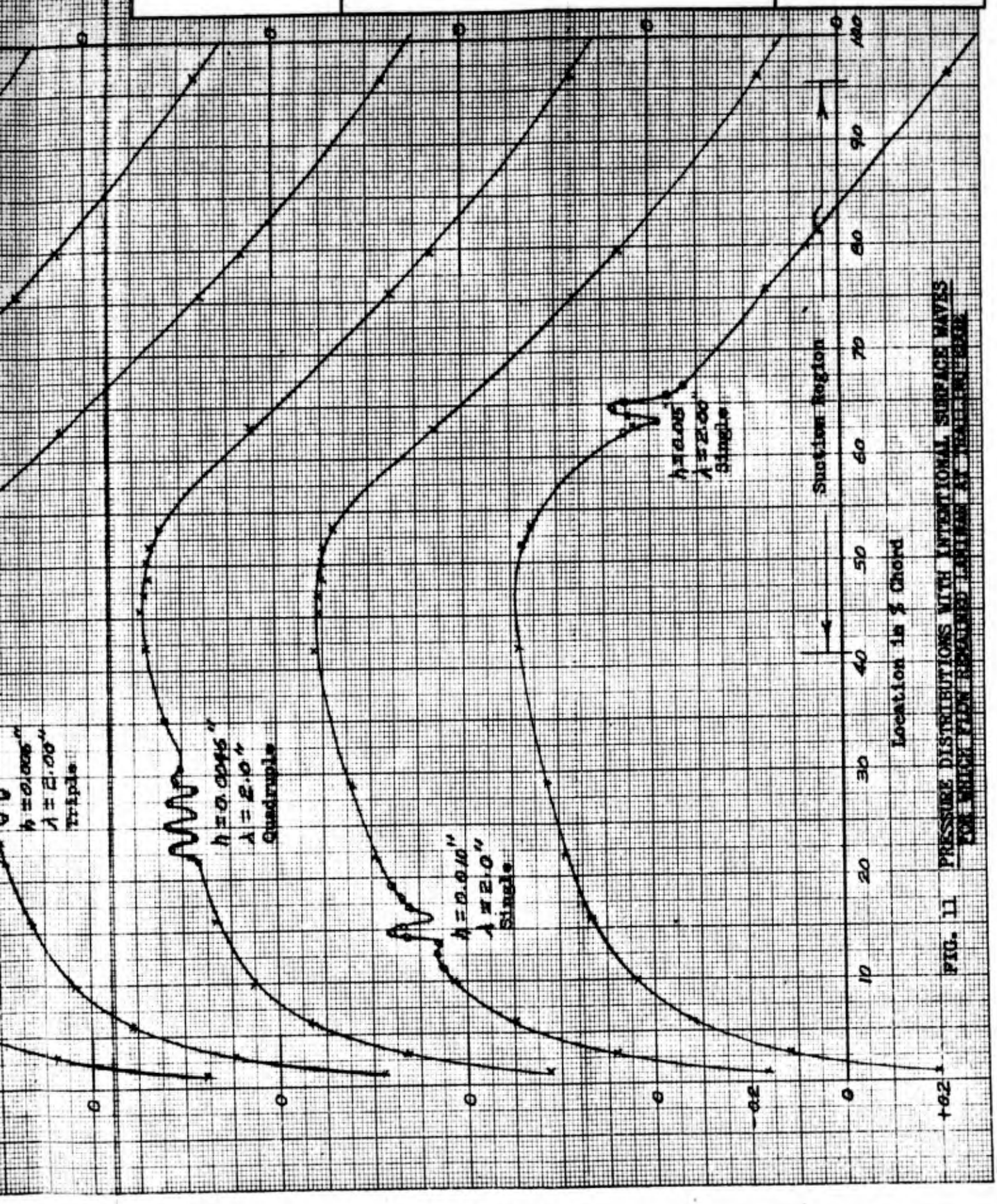

FIG. 11 PRESSURE DISTRIBUTIONS WITH LATERITIONAL SURFACE WAVES ON WING FOR REDUCED LAMINAR AT TRAILING EDGE

3

FORM 20-10A (R. 6-51)

ENGINEER	NORTHROP AIRCRAFT INC.	PAGE
B. Carmichael		33
CHECKER		REPORT NO.
		RLC-101
DATE		MODEL

FIG. 12 EFFECT OF SINGLE SURFACE WAVES ON THE LAMINAR FLIGHT CONDITION BOUNDARY

(Minimum Mach number for required average flow acceleration near wave)

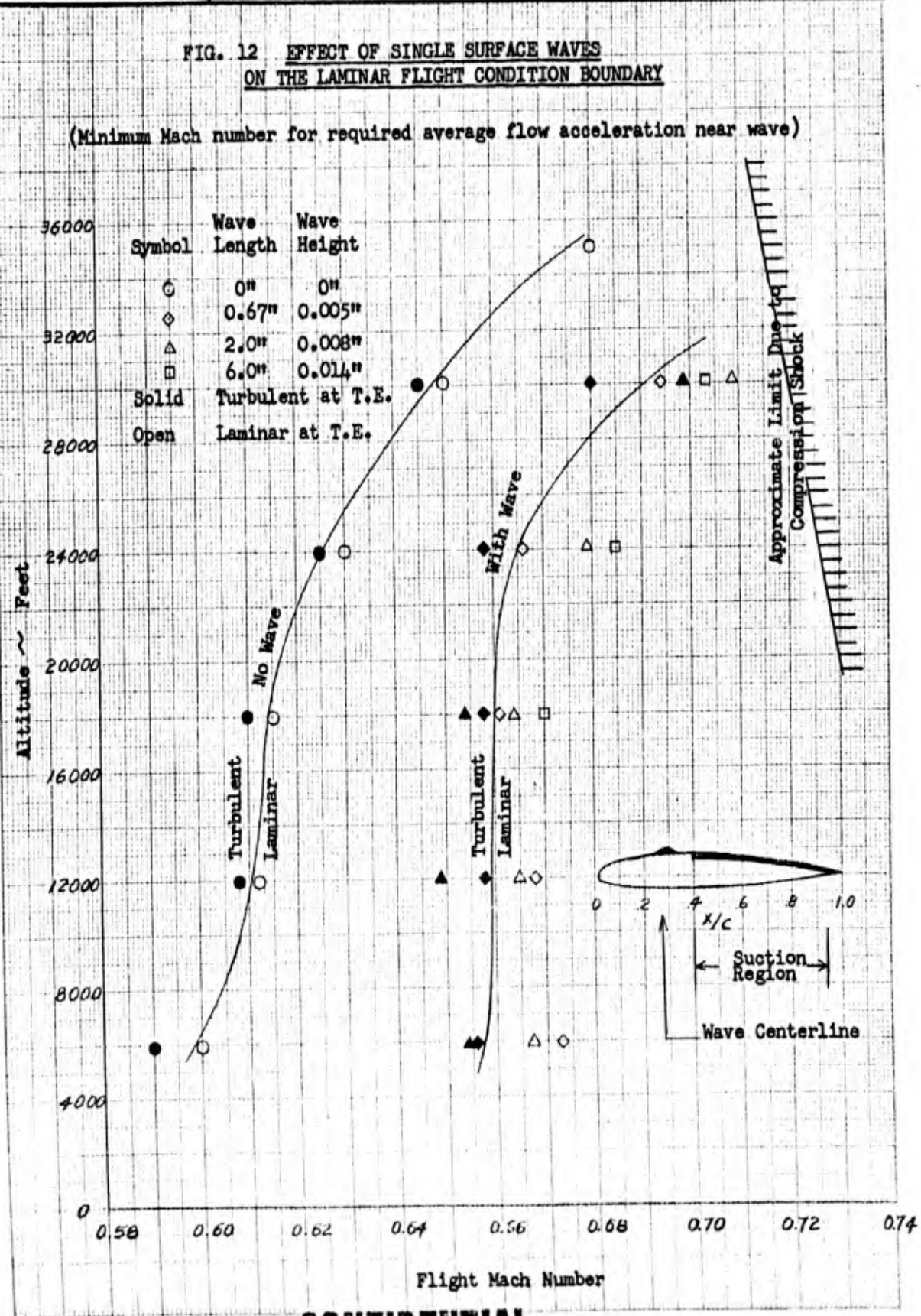

Form 20-11A (R. 6-51)

ENGINEER: B. Carmichael	NORTHROP AIRCRAFT INC.	PAGE: 34
CHECKER:		REPORT NO.: BLC-101
DATE: August 1957		MODEL:

FIG. 13

WAVE INDUCED PRESSURE PEAK AS AFFECTED BY MACH NUMBER

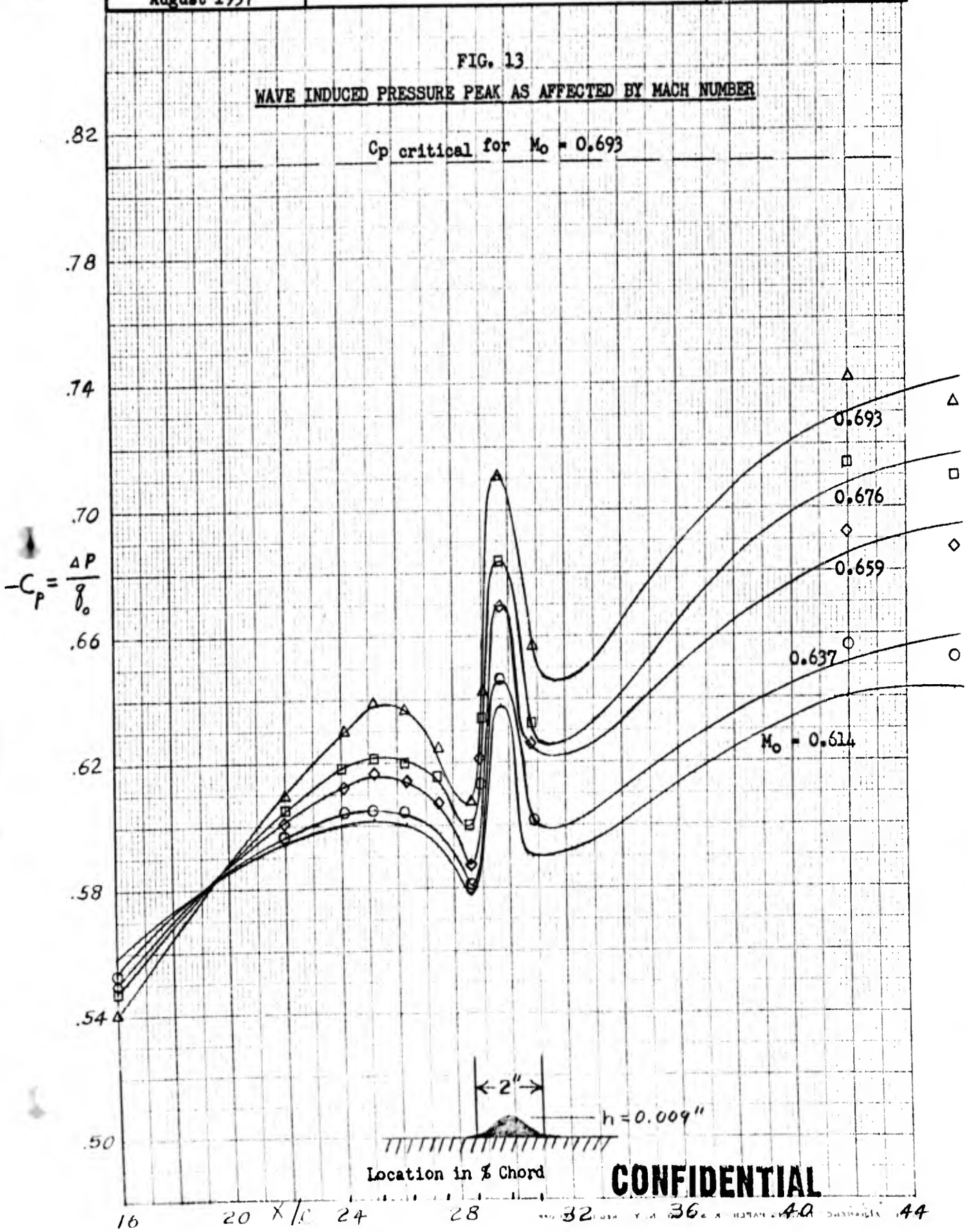

FORM 60-136A (R.8.55)

TABLE I

(A) QUALITATIVE RESULTS FOR SINGLE CREST WAVES

(1) Located at 28% Chord

Wave Length	Wave Height	$\frac{(\text{Height})^2}{\text{Length(Chord)}}$	No.	Boundary Layer Profile Status at Trailing Edge	Required Increase in Chordwise Press. Gradient*	Required Flap Deflection
0.67"	.003"	$.149 \times 10^{-6}$	1	Laminar - all altitudes	12%	0°
"	.005"	.414 "	"	Laminar - all altitudes	32%	"
"	.007"	.815 "	"	Turbulent at 6000, 12000 ft	70%	"
2.00	.002	$.0222 \times 10^{-6}$	1	Laminar - all altitudes	5%	0°
"	.004	.0888 "	"	Laminar - all altitudes	8%	"
"	.008	.355 "	"	Laminar - all altitudes	35%	"
"	.009	.450 "	"	Turbulent at 6000 ft	36%	"
"	.010	.555 "	"	Turbulent at 6000, 12000 ft	80%	"
6.00	.010	$.185 \times 10^{-6}$	1	Laminar - all altitudes	14%	0°
"	.014	.364 "	"	Laminar - all altitudes	35%	"
"	.0194	.700 "	"	Turbulent at 6000, 12000 ft	60%	2° at 18000 to 30000'
"	.024	1.070 "	"	Turbulent at 6000, 12000 ft	90%	7° at 18000 to 30000'
"	.030	1.670 "	"	Turbulent - all altitudes	-	All flap deflections

(2) Located at 15% Chord

2.00	.010	$.555 \times 10^{-6}$	1	Turbulent at 6000 ft	45%	0°
"	.015	1.25×10^{-6}	"	Turbulent at 6000, 12000 ft	90%	8° at 18000 to 30000'
"	.020	2.22 "	"	Laminar only above 30000 ft	145%	15°

(3) Located at 64% Chord - Distributed Suction Region

2.00	.015	1.25×10^{-6}	1	Turbulent at 6000 ft	35%	0°
"	.030	5.00 "	"	Laminar only at h≥24000 ft	50%	10°

TABLE I (cont'd.)

(B) QUALITATIVE RESULTS FOR MULTIPLE CREST WAVES AT 28% C

Wave Length	Wave Height	Number of Waves	Boundary Layer Profile Status at Trailing Edge	Required Increase in Chordwise Press. Gradient*	Required Flap Defl.
2.00	.008	1	Laminar - all altitudes	35%	0°
"	.008	2	Turbulent at 6000 ft	48%	0°
"	.006	2	Laminar - all altitudes	32%	0°
"	.006	3	Barely laminar at 6000 ft	42%	0°
"	.0046	3	Laminar - all altitudes	23%	0°
2.00	.0046	4	Laminar - all altitudes	52%	0°
0.67	.0035	6	Laminar - all altitudes	38%	0°

* Percentage increases averaged over entire Reynolds number range.

(C) EQUIVALENT WAVES (Alt. 18,000 ft. $R_c \cong 20 \times 10^6$) FOR FULL LAMINAR FLOW

Wave Location	Number of Waves	Wave Height	Wave Length	Required Pressure Gradient* $\frac{C_{p_{.42C}} - C_{p_{.22C}}}{(x/c)_{.42C} - (x/c)_{.22C}}$
.28 C	1	0.005	0.67	−0.48
"	1	0.009	2.00	−0.51
"	1	0.014	6.00	−0.50
.28 C	2	0.008	2.00	−0.51
"	3	0.006	2.00	−0.53
"	4	0.0046	2.00	−0.53
"	6	0.0035	0.67	−0.52
.15 C	1	0.010	2.00	−0.55
.64 C**	1	0.015	2.00	−0.49

* No wave value =-0.365 with 100% laminar flow on smooth wing

** In suction area

D. Tolerance to Surface Roughness

1. Experimental Arrangement

The first roughness elements tested were spherical in shape. Glass beads used in the manufacture of movie screens and advertising signs were obtained from the Minnesota Mining and Manufacturing Company under the trade name of "Superbrite". They posessed the advantage of being truly spherical which insured a fineness ratio of 1.0 , and were extremely hard, which prevented damage after installation. They were obtainable in sizes of 0.001 to 0.015-inch diameter and were pre-sorted by the manufacturer. It was necessary to roll them down a smooth incline to eliminate non-spherical beads and those which were fused together. It was also necessary to measure the diameter with a comparator microscope since the original sorting tolerance appeared to be on the order of $\pm$ 0.001 inch. The beads were placed on the metal wing surface and then bonded by letting a fine mist of "Krylon"* fall from the spray can nozzle which was held 18 inches above the surface. The thin bonding film which covered the bead and the surrounding surface was measured as 0.0002-inch in thickness using an Ames dial. It can therefore be stated that the effective height of the bead was not appreciably different from the diameter measured with the microscope. The edge of the Krylon film could also be considered a negligible roughness. Although brisk rubbing with the hand could dislodge the bead, accidental loss after installation did not prove to be a problem. The beads were used for both single and multiple roughness element tests. Quite high density

* Manufactured by Krylon, Inc., Norristown, Pennsylvania.

(approximately 200 beads per square inch) was employed for the latter as indicated full scale in Fig. 15. This imprint was taken by rubbing carbon on thin paper which was placed over the group of beads.

The second type of three-dimensional roughness element tested consisted of discs, die punched from steel shim stock with a Whitney hand punch. The diameter/height ratios varied between 3 and 30 . Krylon bonding was employed as described above. The heights were checked in place with an Ames dial. All elements were mounted at either 22% chord or 2.5% chord.

References 6 through 10 indicate that the natural transition location of a laminar boundary layer is unaffected by the presence of single three-dimensional roughness elements provided that the critical roughness Reynolds number is not exceeded. Once exceeded, transition moves immediately forward to the element.

In the present high Reynolds number experiments, the flight Reynolds number at which the boundary layer at the trailing edge rake became turbulent was noted. The value for which the boundary layer had thickened appreciably at a measuring station one foot behind the roughness element (common to both tests) was found to be identical. The rate of data collection was increased fivefold by spacing elements spanwise across the test section and placing total head probes one foot behind each element and at a height from the surface just outside the laminar boundary layer, as shown in Fig. 14. The total head readings were displayed (together with the freestream total head value) in the photo-observer and also on the flight observer's instrument panel. When transition occurred between the element and the probe, the total head value would fall in response to the rapid thickening of the turbulent boundary layer. Boundary layer velocity profiles were measured at the

(22% c) roughness element station.

2. Experimental Results

a. Roughness Elements at 22% Chord

Figure 15 provides an immediate notion of the maximum allowable roughness dimensions in the flight range bounded by Mach numbers of 0.6 to 0.7 and altitudes of 2000 to 36,000 ft, for roughness elements at 22% chord in a non-suction area. The geometry of the roughness element proved to be a major variable. The spheres of height-diameter ratio of 1.0 required the largest height above the surface to cause transition. The discs with height-diameter ratios less than one, were more critical (see Fig. 16). Critical roughness heights of 0.0105 inch, 0.007 inch, and 0.0055 inch were obtained at 26,000-ft altitude, 0.68 Mach number for a single sphere, a single disc ($\epsilon/d = 0.167$), and a multi-bead band of distributed roughness respectively, at 22% chord.

b. Roughness Elements at 2.5% Chord

As the roughness element location approaches the leading edge, the boundary layer becomes thinner, the potential flow velocity decreases, and the pressure gradient becomes increasingly positive. For thick airfoils at low lift coefficients as employed in these tests, the net result is a moderate decrease in the allowable height of roughness element up to 2.5% chord. Ahead of this location the allowable height again increases as shown in Ref. 7. The single sphere critical height decreased to 0.007 inch and the single disc to 0.004 inch at 2.5% chord at 26,000-ft altitude and 0.62 Mach number as shown in Table II-B.

c. Analysis of the Roughness Experiments

Table II presents the critical condition for each roughness element in three different forms. In the first form, the Mach number and altitude are converted to a freestream Reynolds number per foot U_o/ν_o. These results could only be applied to a very similar situation (e.g., same location, same airfoil thickness, non-suction region, same Mach range). In the second form $R_F = \frac{U \cdot \epsilon}{\nu_s}$ the effects of airfoil thickness and Mach number are also removed by using local potential velocity, and local kinematic viscosity close to the surface. In the third form $R_\epsilon = \frac{u_\epsilon \cdot \epsilon}{\nu_s}$ the effects of location are also removed by bringing in the local velocity at the top of the roughness particle.

This roughness Reynolds number R_ϵ as originally proposed by Schiller (Ref. 11) has been employed in many investigations. In practice, several limitations are found. Reference 6 revealed the dependence of $R_{\epsilon\ critical}$ on the fineness ratio of the projection as confirmed in these flight experiments (Fig. 16). The flow visualization work of References 7 and 12 indicated the complexity of the streamline pattern about a cylindrical projection in a boundary layer and may explain, in part, the limitation of R_ϵ. Reference 8 indicated a 100% increase in $R_{\epsilon\ critical}$ for single roughness elements located in a region of distributed suction under otherwise the same conditions. Reference 9 indicated that, for a non-suction case with roughness elements of a single value of fineness ratio, the R_ϵ value is relatively constant over the major portion of the surface but rises almost

asymptotically near the leading edge where the projection may protrude through the boundary layer. As shown in Table II-B, the values of R_ϵ approach the values of R_F for far forward locations. Employment of the R_F values found at 2.5% c in these experiments will allow rapid determination of critical roughness heights near the leading edge, including the most critical location for the airfoil. For regions other than near the leading edge, use of R_ϵ is preferred. The value should be chosen as a function of roughness fineness ratio from Fig. 16. These critical R_ϵ values might be doubled if the roughness element is in a region of distributed suction through a porous surface.

Form 2G-10A (R. 6-51)

ENGINEER	NORTHROP AIRCRAFT INC.	PAGE
B. Carmichael		42
CHECKER		REPORT NO.
		BLC-101
DATE		MODEL
August 1957		

FIG. 14

GEOMETRIC CHARACTERISTICS OF THE ROUGHNESS TESTS

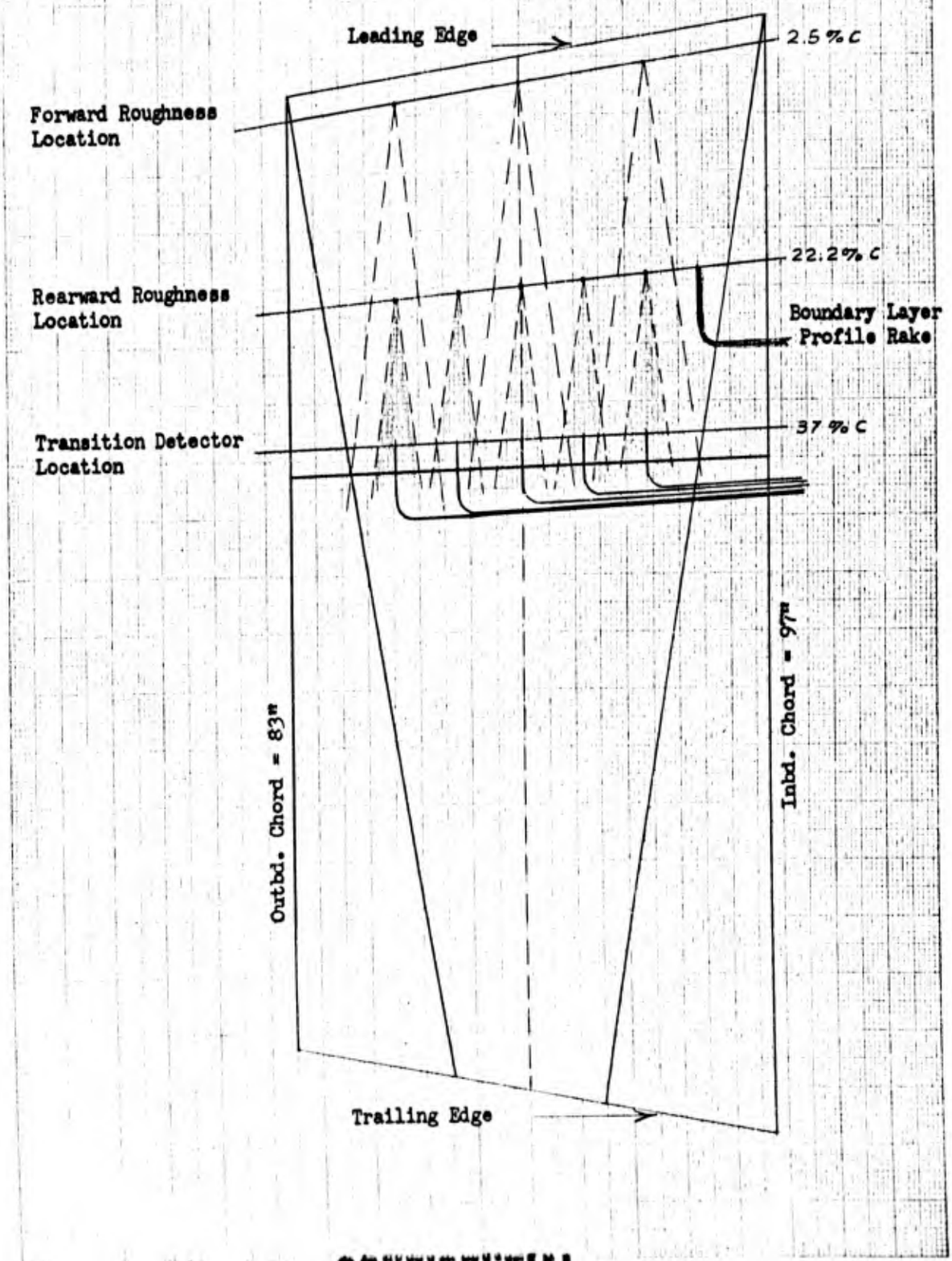

FORM 20-10A (R. 6-51)

ENGINEER: B. Carmichael	NORTHROP AIRCRAFT INC.	PAGE: 43
CHECKER:		REPORT NO.: BLC-101
DATE: August 1957		MODEL:

FIG. 15 DIMENSIONAL RESULTS OF ROUGHNESS TESTS

Location 22% chord
Mach Number increases Linearly from 0.61 at Sea Level
to 0.70 at 36,000 ft

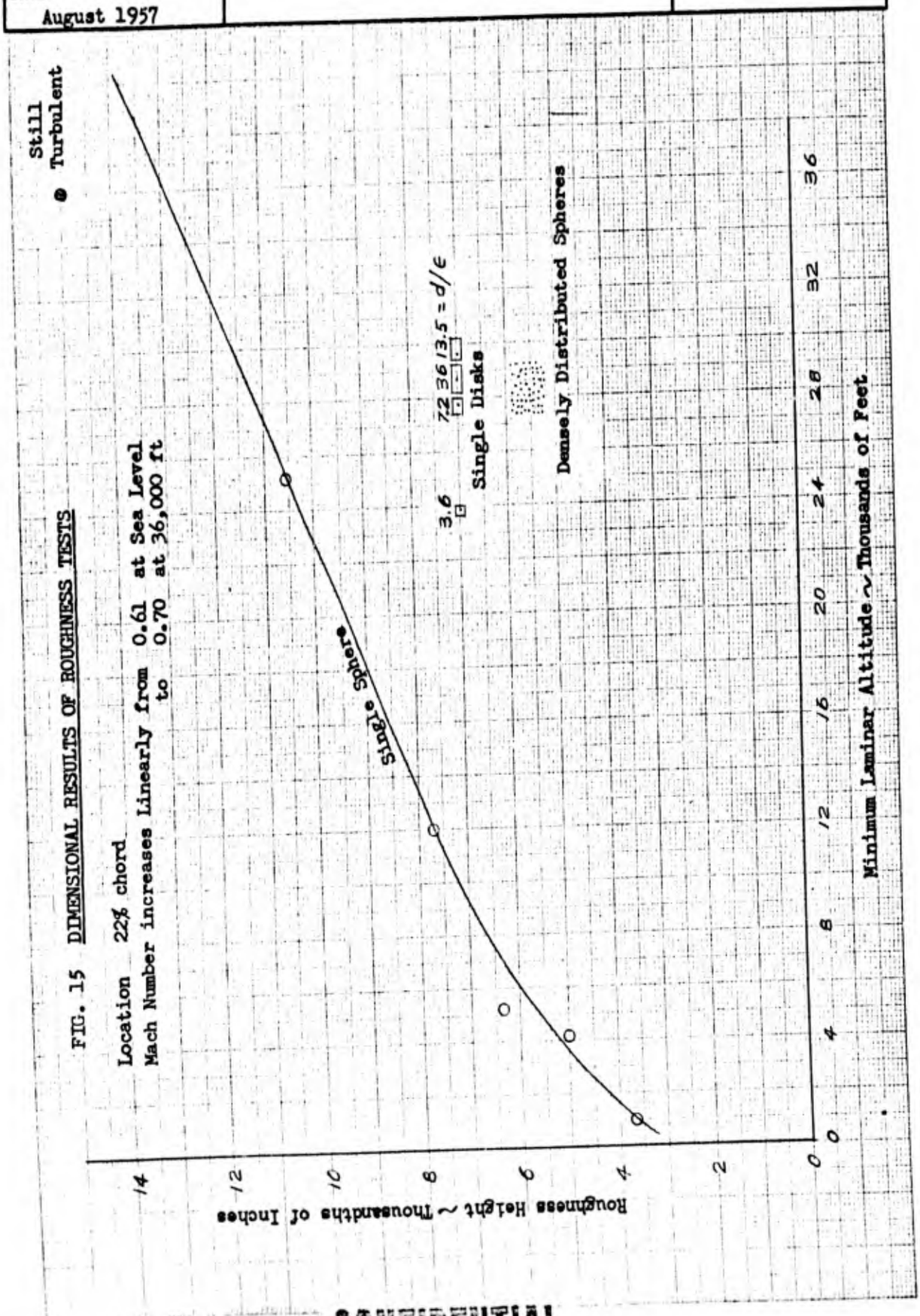

FORM 20-11A (R. 6-51)

ENGINEER: B. Carmichael	NORTHROP AIRCRAFT INC.	PAGE: 44
CHECKER:		REPORT NO.: BLC-101
DATE: August 1957		MODEL:

FIG. 16

EFFECT OF FINENESS RATIO ON CRITICAL ROUGHNESS REYNOLDS NUMBERS AT X/C = 0.22

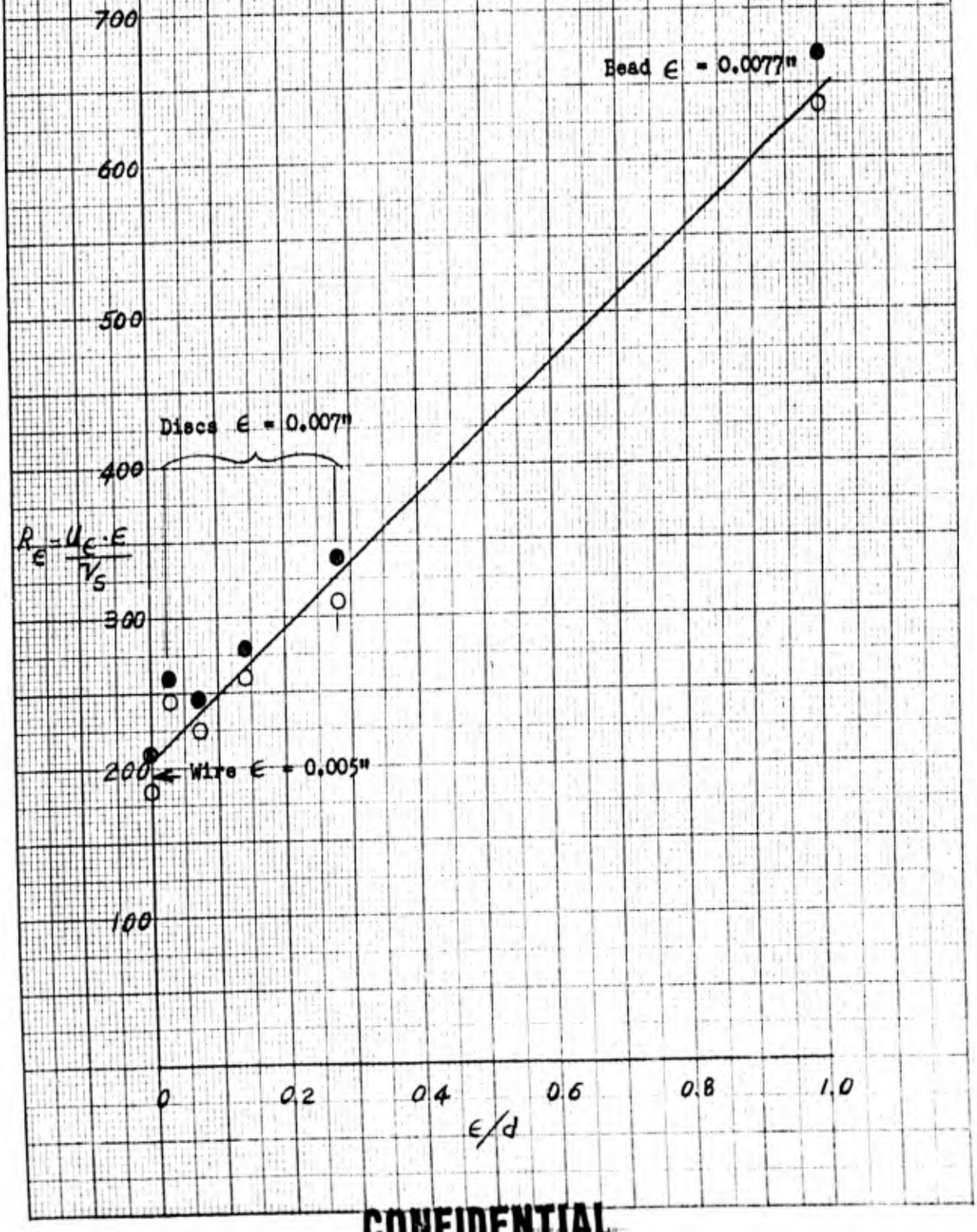

FORM 60-13 (R.6-55)

TABLE II

(A) ROUGHNESS ELEMENTS AT 22% CHORD

Roughness Element			Critical Flight Condition			Roughness Reynolds Numbers	
Type	Height ~ ϵ	Diam. ~ d	Minimum Altitude	Mach No.	$\frac{R.N.}{ft} = \frac{U_o}{\nu_o}$	$\frac{U\,\epsilon}{\nu_s}$	$\frac{u_\epsilon \cdot \epsilon}{\nu_s}$
Single Sphere	.0050"	-	4250	.627	3.74	1495	380
"	.0063	-	5200	.629	3.78	1900	600
"	.0077	-	12000	.646	3.13	1915	666
"	.0105	-	25200	.682	2.22	1770	681
"	.0150	-	Still turbulent at 36,000 ft	.700	< 1.50	< 1960	-
Disk	.0070"	.025"	23,800	.680	2.32	1225	325
"	"	.050	27,800	.691	2.08	1070	272
"	"	.094	29,700	.691	1.91	1020	237
"	"	.250	28,750	.693	1.99	1060	255
Distributed Beads	.005" Ave. .006" Max.	-	28,300	.657	1.94	854	168

(B) ROUGHNESS ELEMENTS AT 2-1/2% CHORD

Sphere	.007"	-	26,350	.621	1.92	1080	1080
Disk	.0033"	.094"	15,260	.654	3.02	719	585

ACKNOWLEDGMENTS

The authors wish to express their appreciation to J. Atkinson, H. Berry, E. Neary (Instrumentation), L. Nelson, J. Wells, and H. Chouteau (Pilots), R. Wisma and E. Seifert (data reading and evaluation) for their valuable contributions in connection with the F94 flight experiments with the sixty-nine slots.

FORM 60-136A (R.8-55)

REFERENCES

1 Pfenninger, W., Groth, E. E., Carmichael, B. H. and Whites, R. C.: Low Drag Boundary Layer Suction Experiments in Flight on the Wing Glove of an F94 Airplane. Phase I - Suction Through 12 Slots (Includes Appendices I, II, and III), Northrop Aircraft, Inc., Report No. BLC-77, April 1955

2 Groth, E. E., Carmichael, B., Whites, R. C. and Pfenninger, W.: Low Drag Boundary Layer Suction Experiments in Flight on the Wing Glove of an F94-A Airplane. Phase II - Suction Through 69 Slots, Northrop Aircraft, Inc., Report No. BLC-94, February 1957

3 Meyer, W. A.: Preliminary Report on the Flow Field Due to Laminar Suction Through Holes, Northrop Aircraft, Inc., Report No. BLC-75, March 1955

4 Goldsmith, John: Critical Laminar Suction Parameters for Suction into an Isolated Hole or a Single Row of Holes, Northrop Aircraft, Inc., Report No. BLC-95, February 1957

5 Fage, A.: The Smallest Size of a Spanwise Surface Corrugation Which Affects Boundary Layer Transition on an Airfoil, British R & M 2120, January 1943

6 Loftin, L. K., Jr.: Effects of Specific Types of Surface Roughness on Boundary Layer Transition, NACA ACR L5J29a, 1946

7 Gregory, N. and Walker, W. S.: The Effects on Transition of Isolated Surface Excrescences in the Boundary Layer, British ARC 13,436, October 1950

8 Schwartzberg, M. A. and Braslow, A. L.: Experimental Study of the Effects of Finite Surface Disturbances and Angle of Attack on the Laminar Boundary Layer of an NACA 64A010 Airfoil with Area Suction, NACA TN 2796, October 1952

9 von Doenhoff, A. E. and Horton, E. H.: A Low-Speed Experimental Investigation of the Effect of a Sandpaper Type of Roughness on Boundary Layer Transition, NACA TN 3858, October 1956

10 Smith, A. M. O. and Clutter, D. W.: The Smallest Height of Isolated Roughness which Affects Boundary-Layer Transition, Douglas Aircraft Company, Inc., ES26344, July 1956

11 Schiller, L.: Strömung in Rohren. Handbuch der Experimentalphysik, Bd. IV 4. Teil, Hydro- und Aerodynamik; Ludwig Schiller, Hrsg.; Akad. Verlagsgellschaft m.b.H. (Leipzig), 1932, p. 191

12 Meyer, W.: Flow Visualization with Smoke in a Laminar Tube. 1956. Moving pictures - obtainable from Boundary Layer Control Research Group, Northrop Aircraft, Inc., Hawthorne, Calif.

UNCLASSIFIED